2007-12-03

One-Dimensional Radial Flow Turbomachinery Performance Modeling

Robert John Pelton
Brigham Young University - Provo

ONE-DIMENSIONAL RADIAL FLOW TURBOMACHINERY PERFORMANCE MODELING

by

Robert J. Pelton

A thesis submitted to the faculty of

Brigham Young University

in partial fulfillment of the requirements for the degree of

Master of Science

Department of Mechanical Engineering

Brigham Young University

December 2007

BRIGHAM YOUNG UNIVERSITY

GRADUATE COMMITTEE APPROVAL

of a thesis submitted by

Robert J. Pelton

This thesis has been read by each member of the following graduate committee and by majority vote has been found to be satisfactory.

Date	R. Daniel Maynes, Chair
Date	Dale R. Tree
Date	Scott L. Thomson

BRIGHAM YOUNG UNIVERSITY

As chair of the candidate's graduate committee, I have read the thesis of Robert J. Pelton in its final form and have found that (1) its format, citations, and bibliographical style are consistent and acceptable and fulfill university and department style requirements; (2) its illustrative materials including figures, tables, and charts are in place; and (3) the final manuscript is satisfactory to the graduate committee and is ready for submission to the university library.

Date

R. Daniel Maynes
Chair, Graduate Committee

Accepted for the Department

Matthew R. Jones
Graduate Coordinator

Accepted for the College

Alan R. Parkinson
Dean, Ira A. Fulton College of Engineering and Technology

ABSTRACT

ONE-DIMENSIONAL RADIAL FLOW TURBOMACHINERY

PERFORMANCE MODELING

Robert J. Pelton

Department of Mechanical Engineering

Master of Science

The Two-Element In Series (TEIS) and Two-Zone models have been used successfully for over twenty years to model test data for radial flow compressors and pumps. The models can also be used to predict the performance of new machines provided that the model inputs can be accurately specified. Unfortunately, use of the TEIS and Two-Zone models as a predictive tool has been limited because an accurate and broadly applicable method of predicting the modeling parameters, η_a, η_b, χ and δ_{2p} does not exist.

Empirical models have been developed to predict the TEIS and Two-Zone modeling parameters based on a large database of centrifugal pump and compressor test results. These test data were provided by ConceptsNREC and have been collected over the past 40 years. The database consists of a wide range of machines including some that were designed and tested by ConceptsNREC and others from the open literature.

Only cases with a vaneless diffuser or volute have been included in the analysis to avoid any possible impeller-diffuser interactions.

From the database, models for all of the TEIS and Two-Zone parameters have been derived using basic regression techniques. Three different models are proposed for each of the two TEIS modeling parameters, η_a and η_b. One model for pumps, another for compressors, and a combined model applicable for all machines is given. For the Two-zone parameters, χ and δ_{2p}, a single set of models was developed to represent the design point performance and another showing how χ and δ_{2p} vary off-design.

The combined models for η_a and η_b are 30% and 70% more accurate than the current state-of-the-art models, respectively. The new models account for the variance in χ and δ_{2p} at off-design flow conditions and further refine the accuracy of the overall prediction by correctly modeling the loss mechanisms in the impeller passage. Validation work has shown that the set of models that predict η_a, η_b, χ and δ_{2p} can be solved to consistently produce sensible results and yield a reasonable "blind" prediction of the performance of a wide range of radial compressors and pumps. These models constitute the first broadly applicable method for predicting the required TEIS and Two-Zone variables and are sufficiently accurate to provide initial performance estimates of new impeller designs.

ACKNOWLEDGMENTS

I would like to recognize several people who has helped with this project and facilitated its completion. First, I wish to thank ConceptsNREC for sharing their vast database of test cases, which the whole project is based upon. I also want to thank ConceptsNREC for providing the software and resources required to update and improve the various codes when necessary. I would also like to thank Dr. Dave Japikse who provided the initial inspiration and continued motivation for this project. His desire for excellence in all aspects of turbomachinery research and development helped produce a high quality result.

I also wish to thanks Dr. Daniel Maynes who patiently supported and guided many aspects of this work. And finally I would like to thank my family, especially my wife, for their patience as I completed this project. Their support provided invaluable encouragement.

TABLE OF CONTENTS

LIST OF TABLES

LIST OF FIGURES

LIST OF SYMBOLS

Roman Symbols	
Symbol	**Definition**
a	Speed of Sound
A_{th}	Impeller Throat Area
A_{in}	Impeller Inlet Area
AK	Impeller Inlet Meridional Velocity Ratio, tip/rms
AR	Area Ratio
AS	Passage Aspect Ratio
b	Passage Width
c_f	Skin Friction
CP	Pressure Recovery Coefficient
C_{pa}	Actual Pressure Recovery, Element "a"; $C_p = \frac{\Delta P}{q}$
$C_{pa,i}$	Ideal Pressure Recovery, Element "a"; $C_{pa,i} = 1 - \frac{1}{AR_a^2}$
C_{pb}	Actual Pressure Recovery, Element "b"; $C_p = \frac{\Delta P}{q}$
$C_{pb,i}$	Ideal Pressure Recovery, Element "b"; $C_{pb,i} = \frac{1}{AR_b^2}$
Clr	Impeller Tip Clearance
D_{Hyd}	Hydraulic Diameter
DF_m	Impeller Disk Friction Multiplier
DR_2	Impeller Diffusion Ratio; $DR_2 = \frac{W_{1t}}{W_{2p}}$
DR_{2I}	Ideal Impeller Diffusion Ratio; $W_{1t}/W_{2p,i}$
g	Gravitational Constant
h	Head Rise
I	Blade Incidence
L	Impeller Passage Length
LC	Loss Coefficient
M	Mass Flow Rate
$M_{rel,1t}$	Inlet Relative Tip Mach Number; $M_{rel,1t} = \frac{W_{1t}}{a_{1t}}$

M_{2M}	Impeller Exit Mach Number
MR_2	Impeller Mach number ratio; $MR_2=M_{rel1t}/M_{rel2p}$
MR_{2I}	Ideal Mach number ratio
N	Shaft speed
NS	Specific Speed; $NS = \frac{2\pi N\sqrt{Q}}{(g\Delta h)^{3/4}}$
P	Static Pressure
PHI_1	Impeller Inlet Inclination Angle
PR	Pressure Ratio
q	Dynamic Head ($\frac{1}{2}\rho W_{1t}^2$)
Q	Volume Flow Rate
R	Radius
rcr_{rms}	Impeller RMS radius of curvature
Re_D	Passage Reynolds Number; $\mathrm{Re}_D = \frac{\left(\frac{W_{1t}+W_{2m}}{2}\right)}{\left(\frac{\nu_1+\nu_2}{2}\right)}\left(\frac{D_{Hyd,Th}+D_{Hyd,Ex}}{2}\right)$
Re_x	$\mathrm{Re}_x = \frac{(C_{2m}+C_5)\cdot s}{2\cdot \nu}$
Re_{R1t}	$\mathrm{Re}_{R1t} = \frac{R_{1t}\cdot W_{1t}}{\nu_1}$
Ri_2	Impeller Exit Richardson Number; $\left(\frac{b_2}{rcr_{rms}}\right)$
Ro_{W2}	Rossby Number (W,2); $\frac{60\cdot W_2}{N\cdot rcr_{rms}}$
Ro_{w2pi}	Rossby Number (W,2pi); $\frac{60\cdot W_{2pi}}{N\cdot R_2}$
$Ro_{C,2i}$	Rossby Number (C,2i); $\frac{60\cdot C_{2i}}{N\cdot Rc_{rms}}$
Ro_{W2i}	Rossby Number (W,2i); $\frac{60\cdot W_{2pi}}{N\cdot Rc_{rms}}$
Rot_{CA}	Rotation Number (C, A); $\left(\frac{(C_1+C_2)\cdot 60}{2\cdot N\cdot rcr_{rms}}\right)$
Rot_{CAI}	Rotation Number (C, Ai); $\left(\frac{(C_1+C_{2i})\cdot 60}{2\cdot N\cdot rcr_{rms}}\right)$
Rot_{W1}	Rotation Number (W,1); $\left(\frac{b_1\cdot N}{60\cdot W_{1t}}\right)$

S	Solidity
W	Relative Velocity
Z_r	Number of Impeller Blades at Exit

Greek Symbols	
Symbol	**Definition**
β	Impeller flow angle
β_b	Impeller blade angle
χ	Secondary mass flow fraction
δ_{2p}	Deviation angle
ε	Secondary flow area ratio
η_a	Inlet effectiveness
η_b	Passage effectiveness
η	Efficiency
v	Wake and Jet velocities
ν	Kinematic viscosity
ρ	Density

Subscripts	
Symbol	**Definition**
0	Inlet
1	Impeller Inlet
2	Impeller Exit
5	Diffuser Exit
t	Impeller Tip (Shroud)
i	Ideal
R	Rear
F	Front
a	Inlet element
b	Passage element
p	Primary zone
s	Secondary zone

1 Introduction

The centrifugal flow impeller is an integral component of many industrial machines. It is used in a wide range of applications including refrigeration, aviation, automotive and the chemical processing industry. Efficient application of centrifugal flow machines has increased as the ability to predict their performance has improved. Accurate performance predictions can be made using a combination of the TEIS (Two Element In Series) and the Two-Zone flow models. Together they form a One-Dimensional, or meanline, modeling system that represents the basic physics of the flow. The models have several input parameters that must be accurately specified to make reliable predictions. These parameters vary for every machine based on the specific geometry and flow conditions. This research presents a set of empirical models that estimate the modeling coefficients required for use with the TEIS and Two-Zone equations. This set of models can be used to predict both on and off-design performance of all radial and some axial flow turbomachines.

1.1 Motivation

Centrifugal flow machines are often used where high levels of performance and reliability are required. Building and testing impellers is both time consuming and expensive. A simple, accurate design process decreases the overall time-to-market and

increases the probability of satisfying the design specifications. The TEIS model used in conjunction with the Two-Zone model has been shown to be able to accurately model test data from many types of turbomachines [1]. However, an accurate method has not previously existed to predict the model input variables and the performance of untested designs could not always be predicted confidently. This work has focused on the development of empirical models that can be used to predict the values of the dependent design coefficients used in the TEIS/Two-Zone modeling system. The models are based on basic geometric and fluid dynamic properties, enabling designers to accurately predict the performance of new machines. Work to develop similar models was conducted in the late 90's [2]. The resulting models were referred to as "Enhanced TEIS", but did not yield results that could be used with confidence in practice. The goal of this study was to improve the accuracy of blind performance predictions by 50% compared to the Enhanced TEIS models.

1.2 Background

The flow through a compressor or pump passes through four basic components, an inlet, rotor, diffuser and a discharge element. The inlet for most machines is axial and directs the flow into the eye of the impeller. An impeller serves to energy to the flow through a set of the rotating blades, or vanes. The impeller inlet, also referred to as the inducer, is designed to get the flow from the inlet into the rotor with minimal losses. In an axial flow machine the impeller exit region, or exducer, is in line with the inducer at a similar mean radius. For a centrifugal flow machine the fluid is turned from axial to radial in the impeller passage. In a radial machine, energy is added both by increasing

the tangential velocity and the mean flow radius of the working fluid. While in axial machines, energy is primarily added by changing the tangential velocity of the fluid.

At the exit of the impeller, the flow contains a significant amount of kinetic energy. A diffuser can be used to recovery this energy and increase the performance of the stage. A diffuser is essentially a passage with an increasing area that will reduce the fluid velocity and recover a fraction of the kinetic energy before it is discharged. In radial flow machines a volute is often used to collect the discharge flow. A volute wraps circumferentially around the discharge of a radial diffuser and channels the flow into an exit pipe oriented perpendicular to the axis of rotation of the impeller. Other discharge elements are used in industry, but they are not studied in this work.

1.2.1 Approach

Flow through the blade passages of a typical radial impeller may include both accelerating and diffusing regions and is subject to the effects of viscous shear, flow path curvature, Coriolis forces due to rotation, etc. Several analytical models, of varying complexity and accuracy, have been developed to aid in the design process. The most basic type of design analysis used is a one dimensional (1-D) or station-by-station analysis, commonly referred to as meanline. 1-D analyses are based on a finite control volume analysis and yield predictions of the mass averaged output conditions without performing detailed modeling of the entire flow path. Detailed 3-D analysis tools, which provide a detailed description of the entire flow, are also being used more frequently as computational fluid dynamic (CFD) packages become more user-friendly and computational power increases. 1-D models will always have a place in the design process, however, since they are efficient to execute, compared to the complex CFD

codes, and can produce accurate first order performance predictions based on basic geometric inputs.

1.2.2 Meanline Design

Several different methods of performing a 1-D analysis exist, and have been divided into three levels of increasing complexity and accuracy. A Level-One design involves direct scaling of an existing design using similitude equations to create a new design. Whitfield & Baines [3], Dixon [4] and Japikse & Baines [5] all provide a description of the application of similitude laws to the scaling of centrifugal machines. Scaling is often employed in industry because it is a fast and accurate method to design an entire family of machines. Although Level-One designs are accurate and simple to use, they are only valid within the limits of the scaling laws, and they don't generally allow designers to improve on past performance.

A Level-Two analysis builds on a Level-One analysis by combining performance correlations for individual machine components, such as rotor efficiency, to yield a prediction of the overall machine performance. This increases the range of designs that may be developed compared to a Level-One design. Rodgers [6] gives a detailed example of a Level-Two analysis using component correlations. A Level-Two design allows for greater flexibility than a Level-One design, but it is still limited by the range and accuracy of the bulk component performance correlations used in the model. Level-One and Two design methods are sufficient for many design applications, but when a new type of machine must be developed or if significant performance improvements need to be made over past designs, only a Level-Three method will suffice.

Level-Three designs use a comprehensive set of models to represent the internal physics of the flow and to predict output conditions. Since a Level-Three analysis models the physics of the flow, new machines can be developed confidently that deviate further from the realm of past experience. For example, many Level-Two flow calculations are based on loosely correlated values of rotor efficiency, whereas by using the TEIS model in conjunction with the Two-Zone model, rotor efficiency can be modeled directly.

Further development and enhancement of the TEIS model, which is the focus of this work, will create a functional Level-Three, 1-D modeling tool that may be used to predict the performance of many radial or mixed flow turbomachines. TEIS model predictions will extend the range and accuracy of previous design procedures while using a basic flow model that is computationally simple, facilitating quick design work and optimization.

1.2.3 Two-Zone Modeling

Detailed flow field analyses by Eckardt [7] and others have shown that the flow through a rotor is often divided into two regions, classically referred to as the Jet and Wake. Dean [8] first proposed a separated flow model in which the Jet was approximated as isentropic, while the Wake was comprised entirely of low momentum fluid and contained all flow losses. Further investigations by Johnson and Moore [9] have shown that the Jet is nearly isentropic, but the Wake is not always stagnant and can carry some of the mass flow. The original Jet-Wake model included many limiting assumptions that hindered the models performance. Japikse [10] increased the accuracy of the Jet-Wake model by refining some of the original modeling assumptions. The

improved model was renamed as the Two-Zone model to reflect the changes made. The Two-Zone model includes a region of primary flow that is isentropic, and a region of secondary flow that is only specified as being non-isentropic. This allows properties in the secondary zone to vary with flow conditions. Japikse [10] also showed statistically that the Two-Zone model yields better performance predictions than those made using similar Level-Two, or so-called Single-Zone modeling techniques.

To complete the Two-Zone model and calculate the change in fluid properties and kinematic parameters, two variables were introduced. First, the ratio of mass flow in the secondary zone to that in the primary zone (χ) must be specified. Second, the exit deviation (δ_{2p}), which is the difference between the exit flow direction and the blade angle, must also be determined. Many correlations have attempted to predict deviation. Wiesner [11] presented a review of several common slip factor correlations that can be used for a wide range of machines. In most Two-Zone models, χ is generally assumed to be a constant in the range of 0.15 to 0.25. Use of a constant χ has been considered to be a good assumption, and Dean [12] showed that performance prediction was not very sensitive to the specified value of χ. Frigne and van den Braembussche [13] suggested using the ratio of Wake and Jet velocities (ν) instead of χ to better understand the extent of the wake.

The Two-Zone model provides designers with an accurate method to predict thermodynamic state change through a radial impeller. To completely specify the output state of the rotor, the kinetic properties of the fluid must also be found. This is accomplished using the TEIS model that provides a simple flow diffusion model of the

fluid. By coupling the TEIS model kinetics with the Two-Zone flow thermodynamic calculations, the complete outlet conditions can, in theory, be accurately predicted.

1.2.4 TEIS Model

Japikse [5] developed the TEIS model by recognizing several similarities between impeller flow and the performance of conventional diffusers and nozzles. This lead to the development of a conceptual model based on diffuser or nozzle geometry (Figure 1-1).

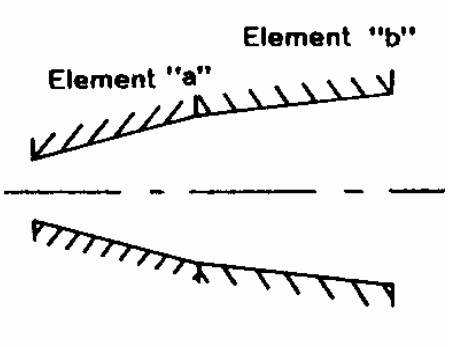

Figure 1-1: Conceptual representation of the TEIS model showing the series arrangement of the two flow elements [1].

In the TEIS model, the blade passages of an impeller are modeled conceptually as two nozzles or diffusers in series, referred to as Elements "a" and "b" (Figure 1-1). Element "a" represents the inlet portion of the blade passage and is considered a variable geometry element which may either accelerate or diffuse the flow depending on geometry and mass flow rate. Figure 1-2 shows the basic geometry of Element "a" as it is used in the TEIS model. In Element "a", the throat area (A_{th}) is constant as defined by the impeller geometry, but the inlet area (A_{in}) changes with flow rate. The inlet area is a

maximum at high flow rates and a minimum at low flow rates, as show in Figure 1-2. Therefore, at high flow rate fluid must accelerate through the inlet and the element acts as a nozzle. Conversely, at low flow rates the inlet actually diffuses the flow. Element "b" models the passage portion of the impeller from the throat to the exit of the rotor. For incompressible fluids, Element "b" acts as a fixed geometry diffuser or nozzle. For compressible flows the passage portion may function as a variable geometry diffuser due to the change in density. Figure 1-3 details the geometry of the passage region.

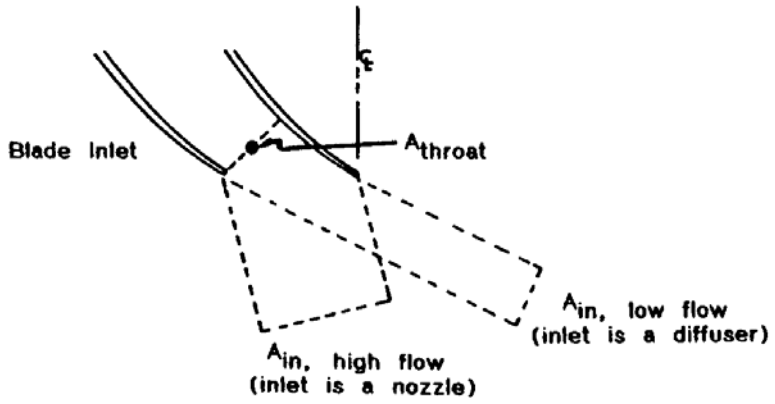

Figure 1-2: TEIS model inlet portion (Element "a") showing variable geometry characteristic of the model [1].

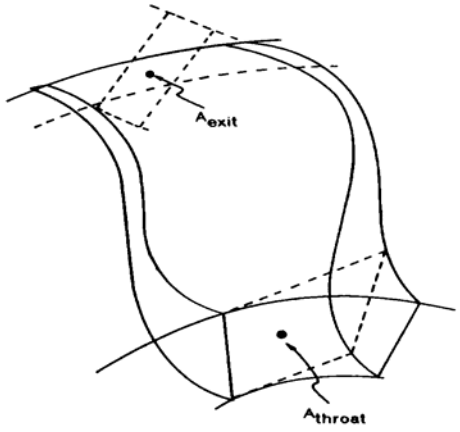

Figure 1-3: TEIS model passage portion, element "b" [1].

As with diffuser design, the performance of each element may be specified using a corresponding effectiveness value, called η_a and η_b for the inlet and passage elements, respectively. The effectiveness of each element is defined according to a typical diffuser or nozzle effectiveness as shown in various turbomachinery texts, such as Whitfield & Baines [3] and Dixon [4]. The effectiveness of Element "a" is calculated using Equation 1.

$$\eta_a = \frac{C_{pa}}{C_{pa,i}} \tag{1}$$

In the above expression C_{pa} and $C_{pa,i}$ are the actual and ideal pressure recovery coefficients, respectively. For Element "a" the pressure recovery terms are calculated as follows [1].

$$C_p = \frac{\Delta p}{q} \tag{2}$$

$$C_{pa,i} = 1 - \frac{1}{AR_a^2} = 1 - \left(\frac{\cos\beta_1}{\cos\beta_{1b}}\right)^2 = 1 - \left(\frac{\cos(\beta_{1b} - I_{1t})}{\cos\beta_{1b}}\right) \tag{3}$$

where q is the dynamic head ($\frac{1}{2}\rho W_{1t}^2$) calculated using the density, ρ, and inlet velocity, relative to the impeller tip, W_{1t}, and Δp is the change in static pressure through the element. AR_a is the area ratio of the inlet to the throat, β_1 is the relative flow angle at the inlet and β_{1b} is the inlet blade angle and I_{1t} is the inlet tip incidence, defined as blade angle minus flow angle.

The ideal pressure recovery coefficient shown in Equation 3, is typical of those used in the design of channel diffusers. Japikse [14] comments further on the derivation of this coefficient using Bernoulli's equation, conservation of mass, and its application to diffuser technology. Although in Japikse's derivation, the fluid was assumed to be locally incompressible, the TEIS model has proven accurate in representing both incompressible and compressible fluid systems. Adding compressibility directly to the model has only shown to complicate the calculations without significantly increasing the model's accuracy [15].

For the passage portion, η_b is calculated in a similar fashion as η_a, equation 4. C_{pb} is also computed in the same manner as C_{pa} except across element "b", and $C_{pb,i}$ is given by the following Equation [1]:

$$\eta_b = \frac{C_{pb}}{C_{pb,i}} \tag{4}$$

$$C_{pb,i} = \frac{1}{AR_b^2} = 1 - \left(\frac{A_{th}}{A_{exit}} \right)^2 \tag{5}$$

AR_b is the passage area ratio, A_{th} is the throat area and A_{ex} is the impeller exit area as shown in Figure 1-3. To complete the TEIS model, it is necessary to define the diffusion relative velocity ratio (DR_2) for the overall machine:

$$DR_2 = \frac{W_{1t}}{W_{2p}} \tag{6}$$

where W_{2p} is the relative velocity of the primary flow zone at the impeller exit. To extend the range of the TEIS model, the affects of stall must also be accounted for. The onset of stall in a radial compressor effects component performance and can be difficult to accurately predict. In practice, there are many different modes of stall that combine to affect to the overall performance and onset. In general, stall can be roughly approximated using knowledge of the diffusion or pressure loss characteristics of an impeller. In the TEIS model, a constant value of diffusion ratio DR has been used to approximate the effects of stall.

Japikse [1] derived the following equation for DR_2^2 to relate the performance model to the output thermodynamic state:

$$DR_2^2 = \left(\frac{1}{1-\eta_a C_{pa,i}}\right)\left(\frac{1}{1-\eta_b C_{pb,i}}\right) \tag{7}$$

Using Equation 7 in conjunction with Equation 6, the change in fluid velocity through a rotor can be predicted using η_a and η_b. Furthermore, when η_a and η_b are known the results can be combined with those from the Two-Zone model and the complete output state of any machine can be modeled.

Since accurately predicting η_a and η_b for a new design has previously been impossible, use of the TEIS model has been challenging. Although η_a and η_b could not be predicted in advance, they can be determined after the fact based on machine test data. Using impeller test data, actual effectiveness values are derived by varying η_a and η_b to yield the best match of the model prediction to the test results. Values of η_a and η_b have

been determined for a variety of machines and have consistently yielded rational numbers, typically between 1 and -1. Following this procedure, the TEIS model has been used to represent test results for many machines with excellent accuracy.

Matched results are unique to each specific machine and cannot be applied to another geometry or at another flow condition. Early matching results showed a general dependence of η_a and η_b on parameters such as rotor diameter, rotation number, etc. These types of relations suggest that a correlation exists, relating the values of η_a and η_b to the geometry and flow conditions of an arbitrary machine. Japikse [1] proposed that a correlation would likely be a function of several geometric and flow parameters, including Reynolds number, a Rotation number, inlet clearance and possibly blade thickness, etc.

1.2.5 Current State-of-the-Art

Early work by ConceptsNREC [2] focused on the development of both linear and non-linear regression models to predict η_a and η_b. At that time the database of test cases only consisted of about 25 cases. This regression work produced high order models that could accurately represent the test data. These models are referred to as the Enhanced TEIS models. The Enhanced TEIS model calculates a single value of η_a and η_b, based on geometric and flow parameters, that is applied to all speedlines. These values are then used with user-defined value of χ, δ_{2p}, and c_f to predict the stage performance.

Figure 1-4 [2] shows the reduced test data for a centrifugal compressor, dashed lines, compared to performance predictions made with the older Enhanced TEIS model, solid lines. A 2-D cartoon of the compressor is shown in the lower right. The rotating

impeller is light red and the blue regions represent the stationary vaneless diffuser and collector. The plot in the lower left shows the rotor efficiency against mass flow rate, *M*. Each line is a different color and corresponds to one of the different test speeds, in rpm, shown just above the plot (i.e. N = 10000, etc.). Total-to-static stage pressure ratio is plotted in the upper left panel. The upper right panel shows the actual Mach number ratio, $MR_2 = M_{1t} / M_{rel2p}$, calculated at the inlet and exit of the impeller, compared to the ideal Mach number ratio, $MR_{2I} = M_{1t} / M_{2mi}$.

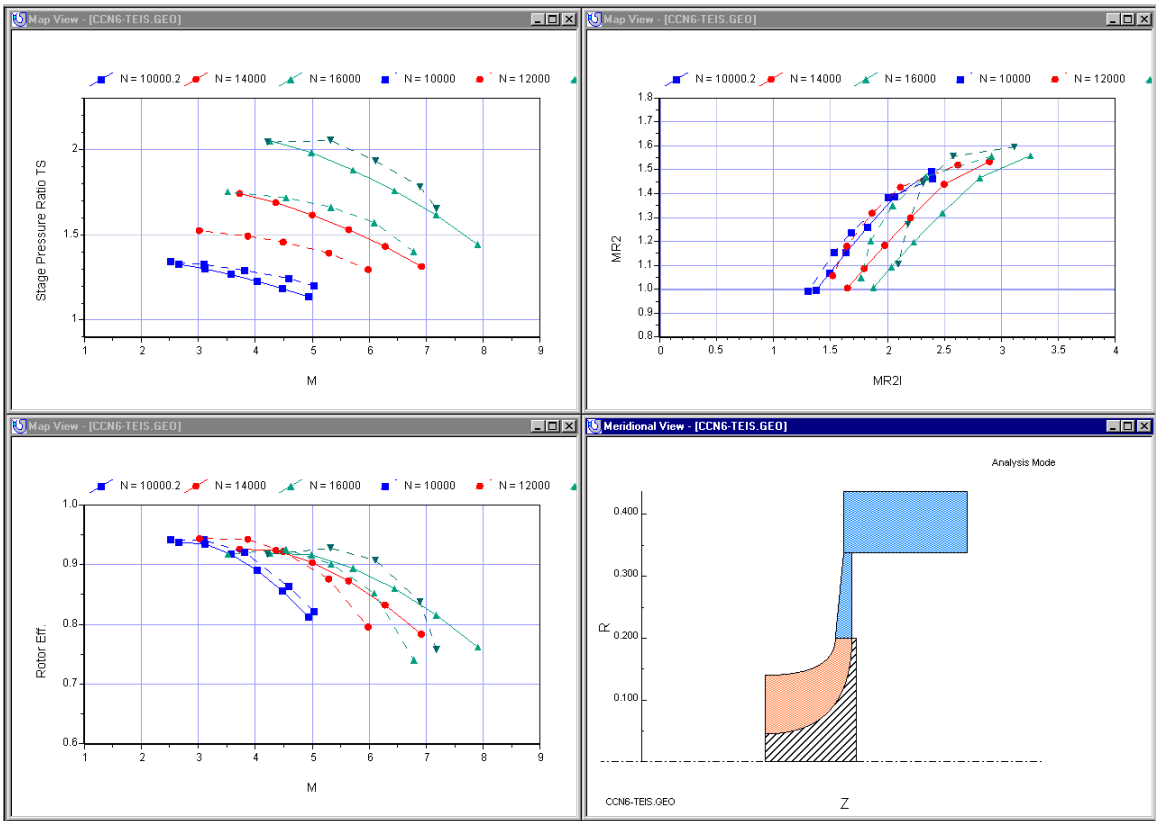

Figure 1-4: Enhanced TEIS model predictions for a centrifugal compressor [2]

At the lowest speedline the predicted trend in rotor efficiency is very close to the measured data. At the higher speedlines, the error in predicted rotor efficiency is as high

as 10% at off-design flow rates. The variation in the stage pressure ratio with flow rate (top left panel) is well matched in the stable operating range, but the overall magnitude is in error by several percent. At low flow conditions the impeller begins to stall and the pressure rise profile becomes flat; this is not captured with the TEIS models.

Continued testing of these models has shown that the underlying equations are very "stiff" and often give irrational results for cases outside the range of those included in the development. Since the database that the models were built upon was so small, none of the final models were broad enough to be used for general engineering purposes. These early models will be used as a benchmark for comparison to the refined models developed over the course of this project.

1.3 Contributions

Use of the TEIS and Two-Zone flow models as an accurate one-dimensional modeling tool has been frustrated since an accurate method to predict the design variables η_a, η_b, χ, δ_{2p} and c_f does not exist. Currently only experienced engineers can set these values with a high degree of confidence. Through this research, a procedure was developed to predict a priori the values of the design variables (η_a, η_b, χ, δ_{2p} and c_f) used in the TEIS and two-Zone models based on basic machine geometry and flow conditions. This procedure will enable even inexperienced engineers to sensibly predict the performance of many new designs. This will both speed up the design process and help accelerate the development of higher performance machines.

1.4 Delimitations

TEIS modeling has proven to be very robust and facilitates accurate modeling of most types of turbomachines. The majority of the cases examined in this study are radial flow machines, although several mixed and axial flow machines have also been included to provide a broader range to build correlations on. All axial flow machines included in this work are single stage pumps. Although the models are equally valid for multi stage axial compressors, none have been examined in this work.

Many modern machines employ a diffuser at the exit of the impeller to recover excess kinetic energy from the fluid. Both vaned and vaneless diffusers are used in industry. Vaned diffusers are typically used to maximize the performance of a machine at specific operating conditions, but may reduce the overall operating range of the machine. The presence of diffuser vanes alters the overall performance of the machine making it more difficult to quantify the actual performance of the rotor itself due to the coupling effects. Consequently, machines tested with a vaned diffuser have been excluded from this study.

Two types of exit element are considered in this study. The first most basic design is that of a collector. Collectors are often used in testing since they eliminate nearly all circumferential variation in the diffuser, as compared to other exit elements. In this work collectors are modeled as a sudden expansion, which is an approximate representation of their geometry. Volutes are the second type of exit element that will be included in this research. Volutes are common in many commercial applications since they direct the discharge fluid into a duct. The losses though a volute must be modeled to completely specify the stage performance. An estimate of volute losses is calculated

assuming all meridional component of velocity is lost, in addition to radial conservation of momentum [1].

There are some flow conditions where the TEIS/Two-Zone model cannot predict performance, including regions of choke or stall. Steady flow usually occurs where the design point is found and where the machine is designed to operate. Since most machines are designed to operate only under conditions of steady flow, it is important to accurately model these conditions. The TEIS model was developed using locally incompressible flow assumptions that work well in stable flow regions even with moderate compressibility. Stall is still a poorly understood phenomenon and in general performance modeling in this realm is not attempted.

2 Procedure

The goal of this work is to develop empirical correlations to estimate the meanline modeling coefficients required for use with the TEIS and Two-Zone models. Figure 2-1 presents the general method used in achieving this goal. The first phase of the project, represented by the upper left block, involved identifying and classifying a large collection of test data. From this data the TEIS and Two-Zone modeling coefficients were calculated, upper right block.

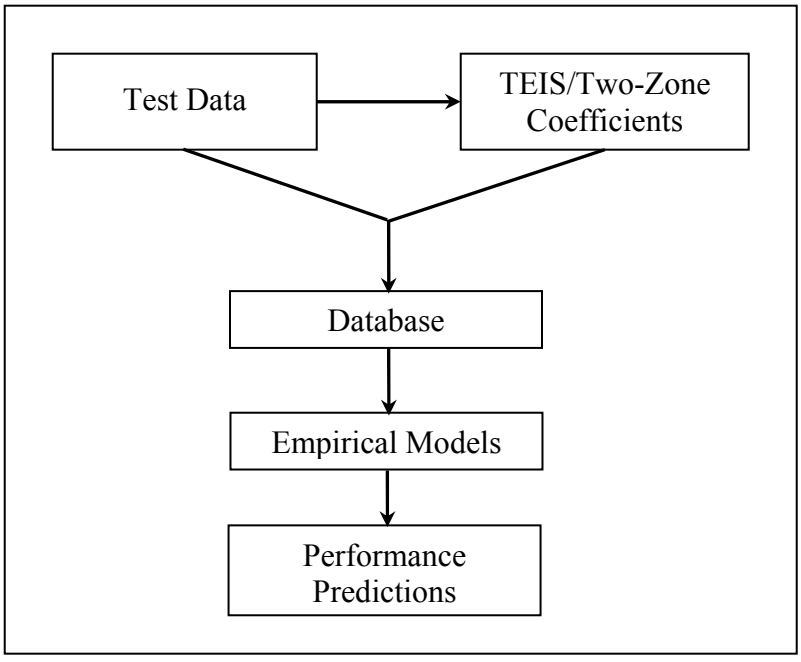

Figure 2-1: Overview of project approach

The test data was then combined with the deduced modeling coefficients to create a large database. This database included the measured performance, geometry and the associated TEIS and Two/Zone modeling coefficients that best matched the performance of each case. From this database empirical correlations were developed to relate the modeling coefficients to the geometry and flow conditions. These models can now be applied to calculate the meanline modeling coefficients and used estimate the performance of machines during the design process.

2.1 Database Development

The first phase of research involved the development of a large database of turbomachines. All of the data used in this research was provided by Concepts NREC and has been collected over the past 35 years. The database includes test results for a wide range of centrifugal flow machines, including pumps and compressors. Industrial machines, and cases from the open literature, where test data is publicly available, have also been included in the database. The final database contains approximately 125 different machines, including 50 pumps and over 75 different compressor designs. This equates to about 300 speedlines and over 1000 discrete data points. Although this study does not focus on axial machines, the TEIS/Two-Zone models are applicable for axial geometries and can be used to accurately model their performance as well. Consequently, several mixed flow and some axial machines have also been included in this study to increase the range of the resulting correlations.

This database constitutes one of the largest compilations of test data ever available for a comprehensive study of this type. Japikse [16] estimated that if this data

were taken today it would cost over 50 million dollars to compile. A large database was necessary to ensure that any correlations deduced from the data would be statistically significant and broad enough for use in general engineering. This research is therefore an attempt to glean further knowledge out of the test data by considering the ensemble set of results. Any additional data that could be used to increase the size or range of the database would also be valuable.

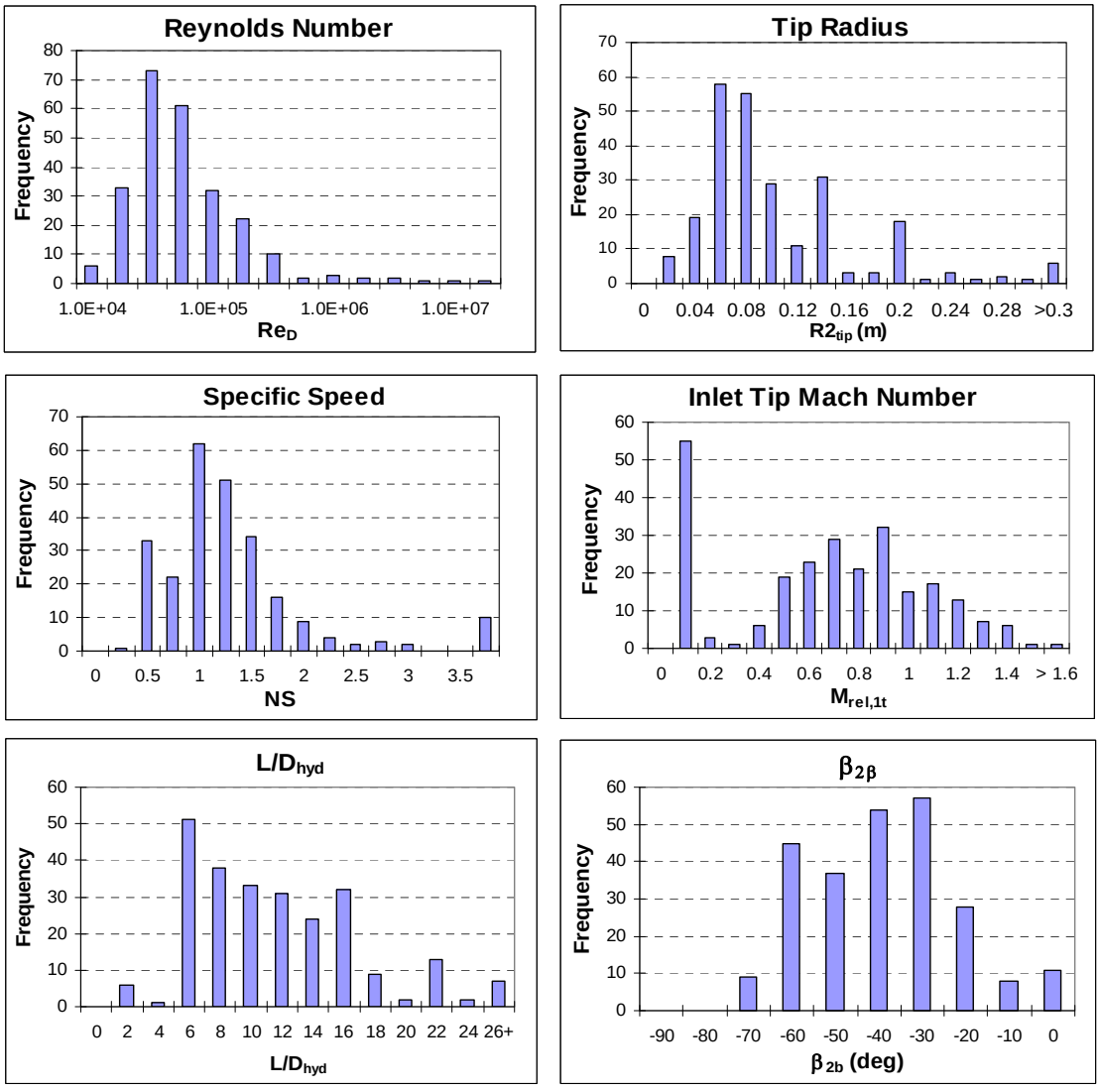

Figure 2-2: Range of cases represented in the database

Figure 2-2 shows histograms of six different impeller parameters represented in the database; impeller tip radius (R_2), dimensionless specific speed (NS), average Reynolds number (Re_D), inlet relative tip mach number ($M_{rel,1t}$), the ratio of impeller passage length to hydraulic diameter (L/D_{hyd}) and the exit blade angle (β_{2b}). Re_D, $M_{rel,1t}$ and NS are defined in Equations 8 – 10, respectively, with relevant variables defined in Table 2-1.

$$\mathrm{Re}_D = \frac{\left(\frac{W_{1t} + W_{2m}}{2}\right)}{\left(\frac{\nu_1 + \nu_2}{2}\right)}\left(\frac{D_{Hyd,Th} + D_{Hyd,Ex}}{2}\right) \quad \textbf{(8)}$$

$$M_{rel,1t} = \frac{W_{1t}}{a_{1t}} \quad \textbf{(9)}$$

$$NS = \frac{2\pi N\sqrt{Q}}{(g\Delta h)^{3/4}} \quad \textbf{(10)}$$

Table 2-1: Definition of variables associated with equations 8 - 10

Name	Definition
$D_{Hyd,Th}$	Impeller inlet hydraulic diameter (m)
$D_{Hyd,Ex}$	Impeller exit hydraulic diameter (m)
υ_1	Kinematic viscosity, impeller inlet (m2/s)
υ_2	Kinematic viscosity, impeller exit (m2/s)
a	Inlet speed of sound (m/s)
N	Shaft speed (rpm)
Q	Volume flow rate (m3/s)
g	Gravitational constant (m/s2)
Δh	Head rise (m)
W_{1t}	Inlet relative velocity, tip (m/s)
W_{2m}	Exit relative velocity (m/s)

Very small impellers as well as large industrial stages have been included. The smallest machine has an impeller exit radius of 1.4 cm while the largest has a radius greater than 30 cm. A wide range of specific speed machines is also covered in the database, where the high values represent axial pumps. The data spans approximately three orders of magnitude of Reynolds number with the bulk of the cases between $5 \cdot 10^4$ and 10^5. The inlet tip Mach number ranges from 0 to 1.5, with the large clustering of cases at low mach numbers being pumps. Exit blade angle, β_{2b}, ranges from –75º to 0º, and L/D varies from 2 to more than 26. This range of machines spans the vast majority of commercial machines in service today. Some early historical designs of pumps and compressors have also been included in the database for completeness.

Because this data was gathered from a variety of sources, the exact type and quality of the measurements vary from machine to machine. Much of the data has been taken in a laboratory test facility. Laboratory tests usually have high quality detailed data collected at multiple measurement locations. Several sets of laboratory data have been included that contain flow measurements from inlet and exit traverses. In contrast to controlled laboratory tests, data for some machines have been gathered at on-site industrial settings where it was only possible to obtain data concerning the overall stage. Although more detailed internal data is desirable, it is necessary to include some low quality test data when developing models because for some classes of machine there is little, or no other data available.

2.1.1 Data Classification

A simple classification procedure, based on the outline proposed by Japikse [1], was used to organize all of the data used in this study. Table 2-2 details how a particular

set of test data is classified based on both the quality and type of measurements made. The highest quality laboratory test data, where detailed inlet and exit traverses were preformed, is classified as 1a data. Very little class 1a data exists, but several class 1b tests have been included in the database. It is much more common and cost effective for researchers to compile class 1b and 2a data. Class 4 is reserved for the lowest quality data, usually pumps and blowers, where only basic measurements of the head, speed and flow rate are available. All other test data can be assigned to an intermediate class and is also useful in model development. The final database contained approximately 50 class 1, 70 class 2, 60 class 3 and 10 class 4 cases.

Table 2-2: Data classification used to organize the test cases

Data Classification	
1	Internal static pressure data with traverses, plus overall pressures and temperatures
	a. Static pressures at all stations, traverses at the inlet and exit of each element, power input to 1% or better
	b. Static pressures at all stations, partial traverses, power input to 2% or better
	c. Static pressures at all stations, occasional traverses, power input to 3% or better
2	Internal static pressure data without traverses, plus overall pressures and temperatures
	a. Static pressures at all stations, power input to 1% or better
	b. Static pressures at all stations, power input to 2% or better
	c. Static pressures at all stations, power input to 3% or better
3	Overall pressures and temperatures only
	a. Overall pressure and temperature rise, power input to 1% or better
	b. Overall pressure and temperature rise, power input to 3% or better
	c. Overall pressure and temperature rise, power input to 6% or better
4	Overall pressures only

2.2 Data Reduction Tools

2.2.1 Modeling Tools

Two commercially available software packages were used to process the test data and evaluate the model performance for each machine. These programs are COMPAL® and PUMPAL® used for compressors and pumps, respectively, and are referred to as the meanline code. The programs were supplied by ConceptsNREC and are configured to run on a WINDOWS® based operating system. Each program is designed to operate in three different modes; analysis, data reduction, and design, the last of which was not used in this work.

The first mode, analysis, is used to predict the performance of a given geometry. The TEIS and Two-Zone models are built into the code and can be used to make a meanline performance prediction based on the modeling coefficients input by the user. The basic geometry and operating conditions of the machine are also required inputs to the meanline code. Other loss models are included in the code to account for additional stage losses. These losses may include factors such as disk friction, seal leakage and diffuser skin friction.

When the code is used to process measured test data, such as temperatures and pressures, it is operating in data reduction mode. Data reduction mode is used to convert the raw measured data into results that are easier to interpret and present graphically such as efficiency, pressure rise, loss coefficient, etc. The accuracy of the reduced test results is directly related to the quality and type of data collected. If internal static pressure measurements are available then the performance of the individual stage elements can be

accurately deduced. When only flange-to-flange data are available the component losses cannot be correctly separated from each other. In these cases, assumptions about the performance of one or more of the components must be made to complete the analysis. Any error in modeling one component will force a corresponding error in another component to match the stage data.

2.2.2 The Modeling Approach

Using both the data reduction and analysis mode in the meanline code allows for the model coefficients to be determined for each machine. A simple overlay and compare (OC) procedure is used to determine the coefficients that best represent each machine. First, test results from a given machine are reduced to yield complete stage performance details including, pressure ratio (*PR)*, diffusion ratio (DR_2), impeller efficiency (η_{rotor}), diffuser pressure recovery (*CP)*, etc. These results are then compared to the performance predictions made in analysis mode. A graphical comparison is made to examine how well the stage performance has been predicted based on various parameters deduced from test data including pressure rise, efficiency, loss coefficient, etc. Figure 2-3 shows an example of the quality of match that can be achieved using the TEIS and Two-Zone meanline models in a sample compressor case. The test data is shown as blue squares connected with a dash line and the model is shown as a solid red line and triangles. The TEIS and Two-zone modeling coefficients have been manually adjusted, following the overlay and compare method, to visually match the predicted performance to the measured test data.

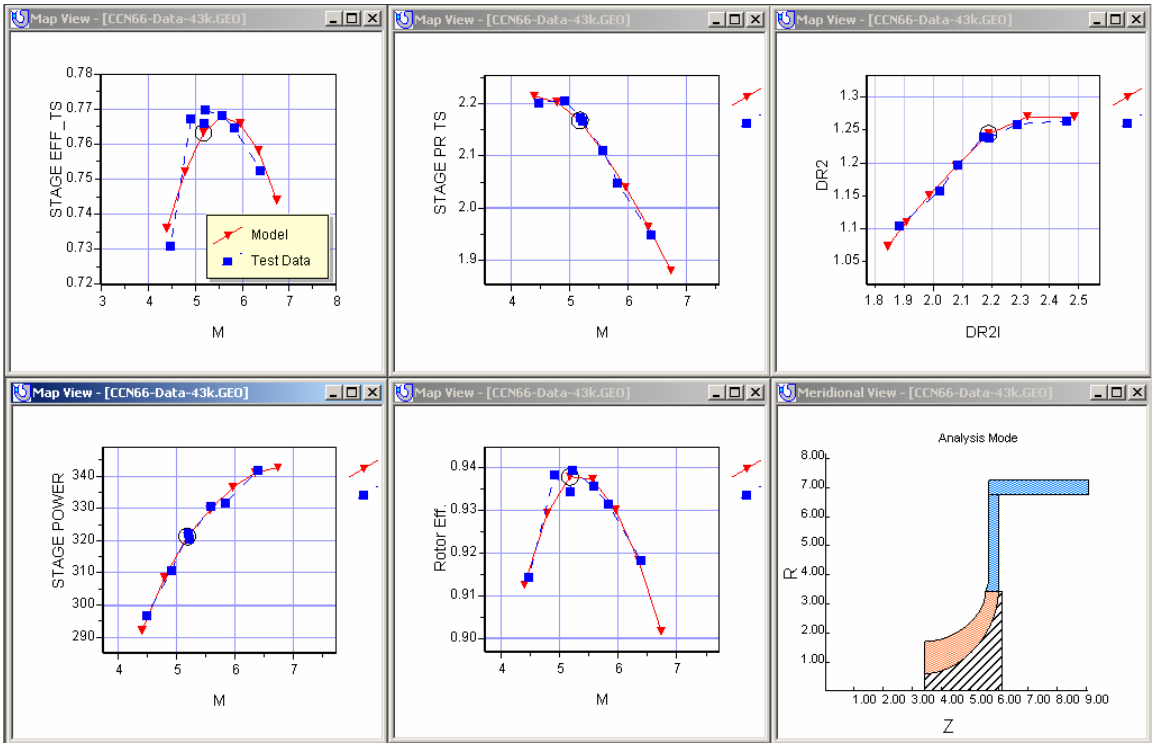

Figure 2-3: Typical overlay and compare method for comparing test data to model predictions

2.2.3 Impeller TEIS Matching

Achieving a good match of test data requires that an accurate prediction of the diffusion characteristics (DR_2) of the impeller can be made, as shown in the top right panel of Figure 2-3. Matching the impeller diffusion profile specifies the TEIS model parameters. Figure 2-4 shows a typical plot of the actual diffusion ratio (DR_2) compared to the ideal diffusion ratio (DR_{2I}), $W_{1t}/W_{2p,i}$. This plot provides a baseline for determining η_a and η_b for a machine. DR_2 is calculated using Equation 6 and the ideal diffusion ratio, DR_{2I}, is calculated assuming ideal flow with zero deviation. Solid boxes connected by a dashed line represent the reduced test data. The analysis results have been overlaid using a solid line.

If the impeller exit static pressure (P_2) has been measured, then the diffusion characteristics of the machine are fixed. For these cases, η_a and η_b can be identified by adjusting the TEIS parameters to reduce the residual error between the model prediction of DR_2 and the test data. The η_a setting essentially changes the slope of the diffusion curve, pivoting around $C_{pa,I} = 0$, or the point of zero incidence ($I_{1t} = \beta_{1b} - \beta_1$), Equation 3. η_b shifts the entire curve up or down and does not affect the slope of the curve. Some stall may appear in compressor test data and is identified as the region where DR_2 stops increasing and the curve becomes flat. A simple first order approximation has been used to model stall which forces the predicted diffusion curve to be horizontal.

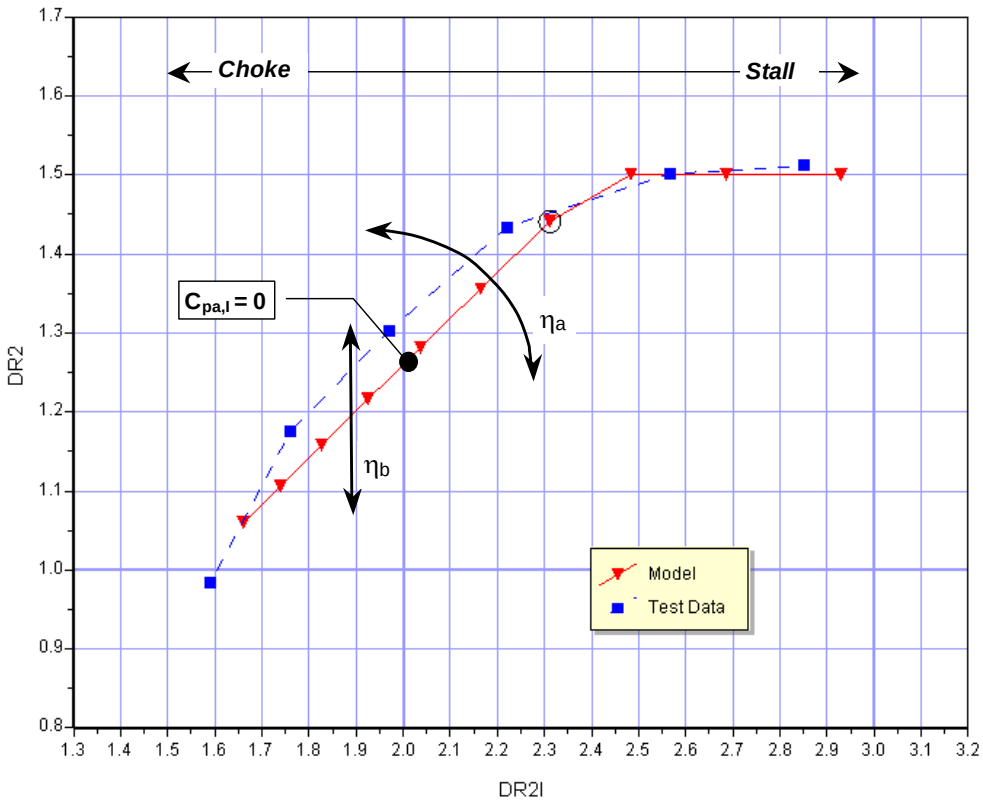

Figure 2-4: Influence of the TEIS parameters, η_a and η_b, on matching the diffusion ratio curve

Cases with tip static pressure measurements, data classes 1 and 2, are the simplest to match, but this data it is not always available. Without a measured tip static pressure, the diffusion characteristics can change slightly as the Two-Zone modeling parameters are adjusted. Therefore, values of η_a and η_b must be identified iteratively as χ and δ_{2p} are set. η_a and η_b have the strongest impact on the shape and position of the overall head characteristic of the stage, while χ and δ_{2p} have a much lesser effect. Therefore, when using the TEIS and Two-Zone models, η_a and η_b can be deduced with good accuracy, even for stages with low quality test data, since these parameters dominate the overall stage performance prediction.

2.2.4 Impeller Two-Zone Matching

The Two-Zone modeling parameters χ and δ_{2p} must also be specified to define the performance of a machine. Traditionally, χ and δ_{2p} have been set based on their values when the impeller recirculation loss (IRL) is at a minimum. This was achieved by adjusting the modeling parameters, χ and δ_{2p}, until the point of minimum loss is at, or slightly above, zero. Zero *IRL* indicates that there is little or no recirculation at the inlet or exit of the impeller. This is generally a good assumption for a well-designed rotor.

IRL includes losses due to flow recirculation as well as all other unmodeled losses. Impeller recirculation losses are most evident in the power measurement where losses cause a rise in the required power to drive the machine. Recirculation losses are adjusted to set the point of minimum loss equal to zero, and never below. At off-design flow rates the recirculation increases with leading edge incidence, I_{1t}, as stall occurs and backflow is engendered, and typically assumes a "bucket" shape over the full operating

range. Figure 2-5 shows a typical loss variation with I_{1t} for a radial machine showing a characteristic bucket shape. The data for this case and most others does not give a perfectly smooth profile to the loss bucket. This is likely due to uncertainly in the data or an artifice of the complicated secondary flows that constitute recirculation.

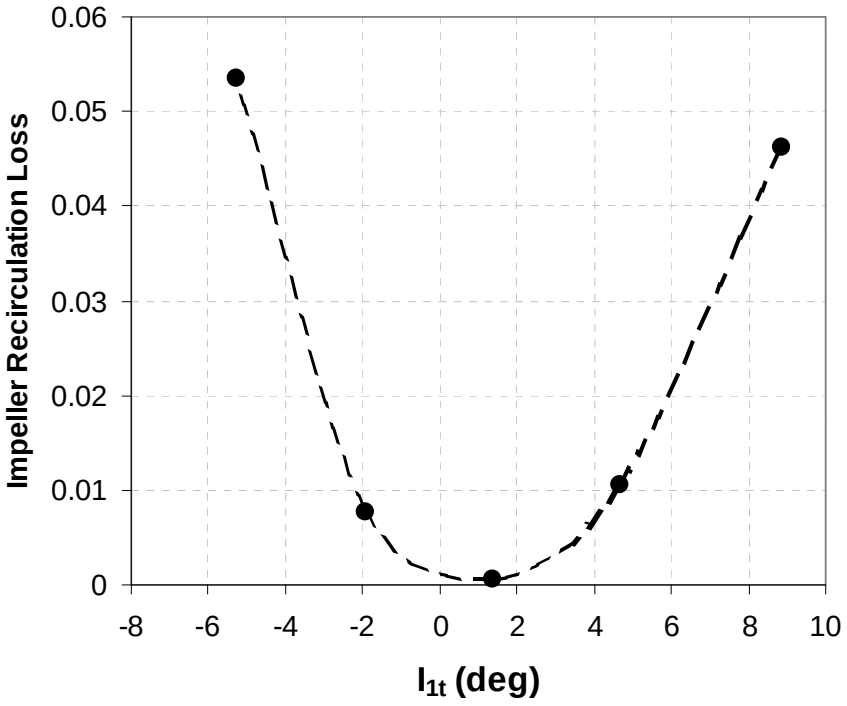

Figure 2-5: Typical impeller recirculation loss profile over a range of inlet blade incidences

The position of the loss bucket is controlled by the specific values of χ and δ_{2p}. Increasing the value of χ will shift the entire *IRL* bucket lower, while assuming more deviation shifts it higher. In the past, engineers set these values based on historically observed trends. Figure 2-6 shows a set of simple empirical correlations for χ and δ_{2p} [17] that were developed to provide some guidance in setting these parameters for new designs. The correlation on the right proposes that primary flow deviation increases with

decreasing backsweep angle, β_{2b}. The correlation on the left suggests that χ is typically near 0.2 for average to high specific speed compressors and may rise for low specific speed machines. While these correlations provide a baseline for selecting sensible values for modeling purposes, they are not accurate enough for use in blind modeling.

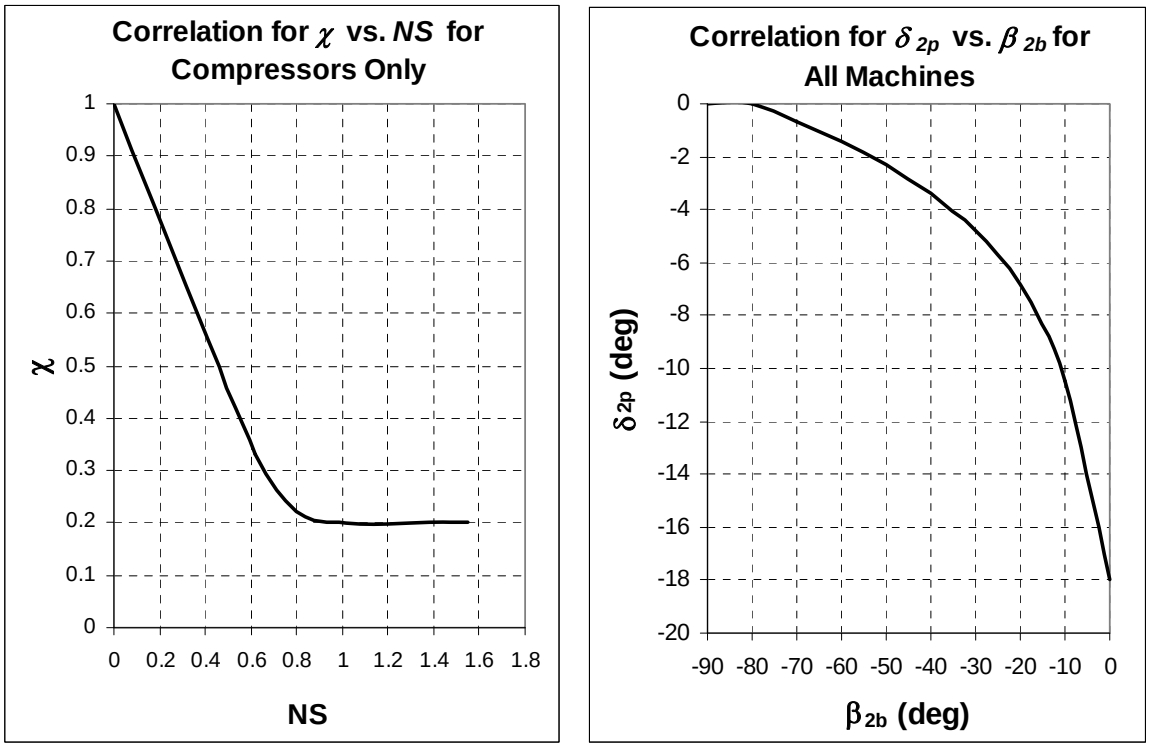

Figure 2-6: Historical guidelines for selecting two-zone model coefficients [17], χ and δ_{2p} as a function of *NS* and β_{2b}, respectively.

In the two-zone modeling system the secondary flow deviation (δ_{2s}) can also vary. Traditionally, δ_{2s} has been set to zero since no method existed for predicting the complicated secondary flow regime. Laser velocimetry data exists for a few select cases and suggests the actual δ_{2s} may vary from +20˚ to -5˚. However, several sensitivity studies were conducted over the course of this study that showed that δ_{2s} has only a slight

effect on the overall stage performance. Performance is most sensitive to δ_{2s} when χ is large, but these cases make up only a small fraction of the total database. For this work δ_{2s} was set to zero for all cases unless specific information indicated that another value was more appropriate.

Some uncertainty exists in determining the recirculation losses because an estimate of the disk friction and leakage power must be made. The leakage path includes the cavities between the rotating impeller and the casing, and some variety of mechanical seal. In the case of shrouded impeller there is both a front face leakage path, typically from the impeller exit to the inlet. Estimates of the leakage flow and losses are made using simple meanline models that account for the individual seal type and the specific cavity geometry.

Disk friction is a measure of the heat that is generated and may be added to the flow due to viscous dissipation in the cavity between the back face of the impeller and the machine casing. Disk friction may also occur in the region between the shroud and the blades. Basic models exist to estimate the total heat generation in these areas [18]. Assumptions must be made, however, regarding the fraction of heat that is transferred into the working fluid and the portion that is lost to the atmosphere. The actual values are dependent on the quality of insulation and the layout of the test rig.

A basic disk friction model, based on equations proposed by Daily and Neece [18], is implemented in the data processing code. This estimate can be varied by the use of a multiplier, DF_m, if deemed necessary. For an insulated compressor it is generally assumed that the loss multiplier would be within the range 0.7 to 1.1. Increasing the DF_m, or the assumed fraction of heat added to the flow, shifts the *IRL* profile up, while

assuming less heat is added to the fluid shifts the profile down. For the cases included in the database, the DF_m was always set to 1 unless specific testing details were available to indicate another value was more appropriate.

2.2.5 Two-Zone Design Space

A careful study of the design space revealed a weakness in the traditional data matching procedure used with level 2 or lower data, cases where only static pressure measurements are available. In these cases a unique solution for χ and δ_{2p} cannot be identified based only on static pressure data. Figure 2-7 shows a 3D contour plot comparing the match quality using the overlay and compare (OC) approach for various settings of χ and δ_{2p} in a typical centrifugal compressor. The objective function, on the z-axis, is the sum of the actual residual error between the model prediction and the test data for the following variables; efficiency, power, pressure ratio, DR_2, and others. The residual error is calculated as the square root of the difference between the square of the data and the model value. Maintaining the impeller recirculation loss near zero was also added as an objective to ensure that the resulting solution was rational.

In Figure 2-7 it is clear that a unique solution for χ and δ_{2p} cannot be determined based on minimizing these objectives alone. Instead of finding a clear minimum point, where the model best matched the data, a valley appears. This valley traverses the design space and identifies a wide range of χ values where a corresponding δ_{2p} exists, and their combination produces a good match between the model and the test data. But there is no unique minimum.

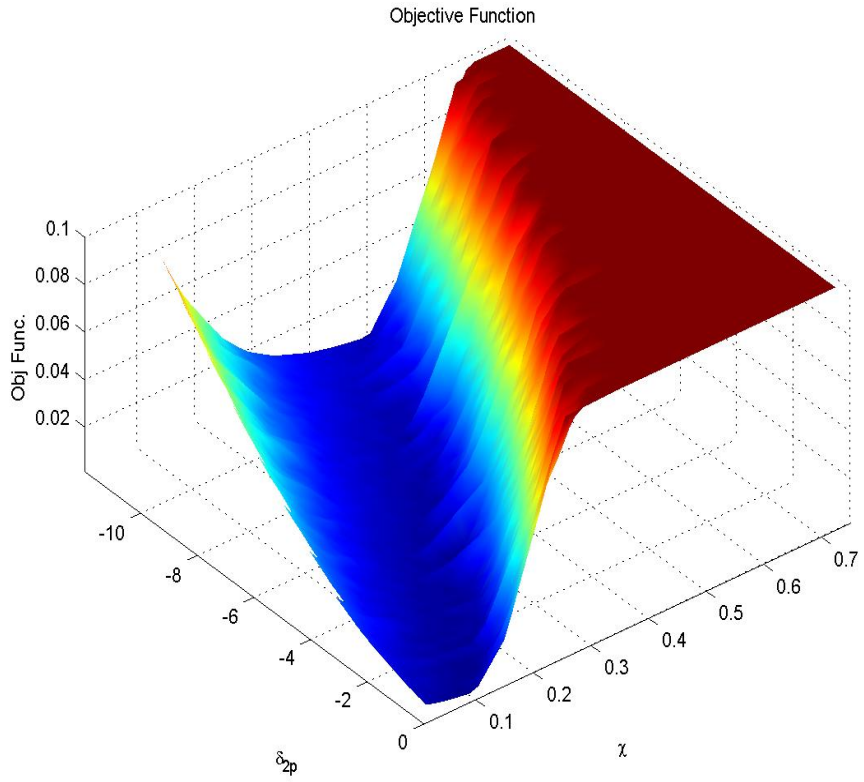

Figure 2-7: Two-Zone design space for a sample centrifugal compressor data reduction case

To identify the minimum point, additional information about the flow state at the exit of the impeller is required. This type of information can be derived from point-wise traverse measurements made just downstream of the impeller exit in a vaneless diffuser, as will now be described. Since class 2 data does not contain adequate information to derive the actual two-zone values exiting an impeller, class 1 data, where traverse information has been measured, must be used to make a unique determination. Although the bulk of the database is comprised of class 2 or lower data, several cases of high quality class 1 data are available. For class 1 data, traverse measurements are taken near the impeller exit, typically within R/R_2 = 1.05-1.10. Traverse measurements include the spanwise distribution of static and total pressure measurements, and the associated flow

angle at a given radius in the diffuser. Since the meanline code only predicts bulk flow parameters, the spanwise data is mass-averaged to produce a single representative value. These measurements provide significant insight into the flow conditions at the exit of the impeller and can be used to uniquely identify the appropriate values of δ_{2p} and χ.

Although different values of χ and δ_{2p} can produce similar predictions of impeller performance, based on a bulk flow analysis, each set will result in different flow structure at the inlet of the diffuser. In cases where traverse data have been collected, the diffuser flow structure is completely defined and can be used to identify a single value of χ and δ_{2p} that best matches the mass averaged traverse data. Because the flow continues to evolve through the diffuser, χ and δ_{2p} can be determined with the greatest certainty when traverse data at multiple radii are available.

Using traverse data, in conjunction with the basic static pressure measurements at the impeller tip, the valley seen in Figure 2-7 is eliminated and a unique set of modeling parameters can be identified. Figure 2-8 shows the same design space as seen in Figure 2-7 except the objective, the z-axis, has been modified to include the residual error in matching the mass average traverse data, collected in the vaneless diffuser, as well as the bulk performance parameters considered previously. With this additional constraint, the open ended valley evident in Figure 2-7 has vanished and an optimum point can be identified from the data. The design space show in Figure 2-8 appears uneven because a relatively small number of sample points was calculated to minimize processing time. If more data points are evaluated than the representation of the design space is smooth and the global optimum can be readily identified without the existence of false minimums.

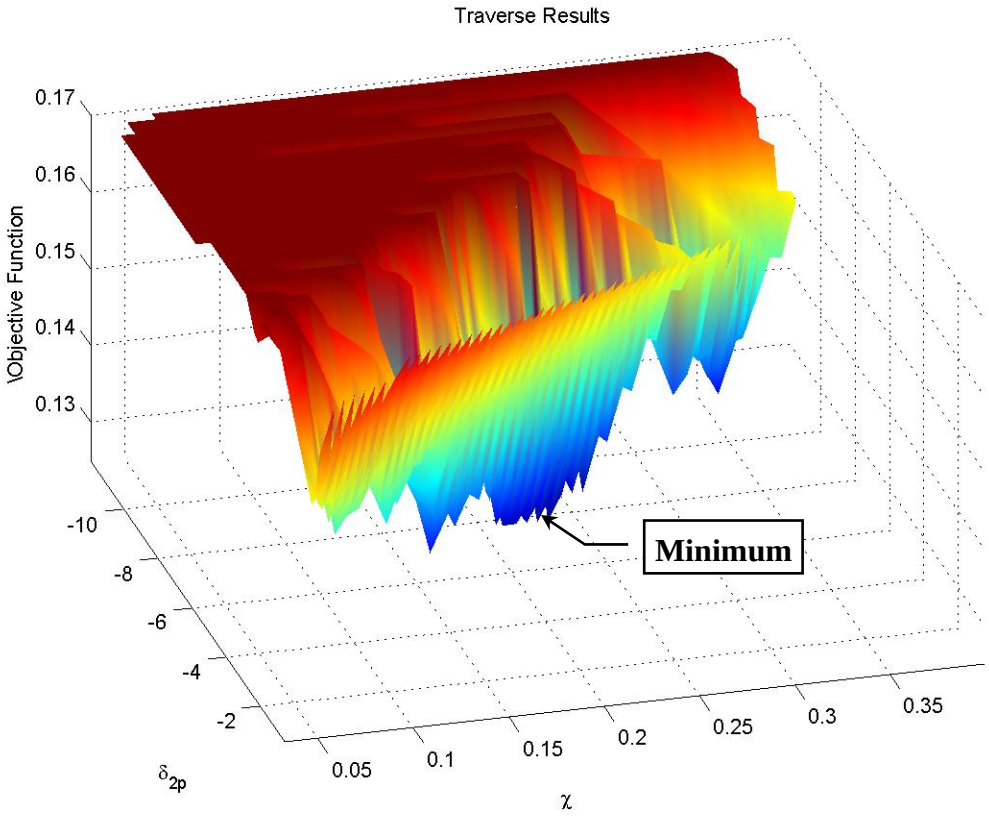

Figure 2-8: Two-Zone design space for a sample centrifugal compressor data reduction case using traverse data to help identify the minimum model settings

2.2.6 Vaneless Diffuser Processing

Traverse data cannot be used effectively without an accurate model of the vaneless diffuser loss. The Stanitz model [19] has been an industry standard in evaluating vaneless diffusers for the past 50 years. The Stanitz model evaluates the vaneless space using a control volume approach. The control volume is comprised of infinitesimal differential elements that are integrated from the impeller exit to the diffuser exit. The Stanitz model assumes the flow in the diffuser is fully mixed at both the diffuser inlet and exit. It can be applied most accurately to diffusers that are sufficiently

long to allow the primary and secondary flow to fully mix. At a radius ratio of 1.5, the flow is usually fully mixed and the Stanitz model is valid. In reality, at the inlet to the diffuser, the jet and wake structure that developed in the impeller still exists. A separate mixing calculation is made to account for the losses due to the jet and wake when using the Stanitz model. In the meanline code, the impeller exit radius is used as a mixing plane. Using the primary and secondary flow properties at the impeller exit, a simple mixing calculation is made according to basic conservation laws [1].

An average skin friction, c_f, is used to calculate the losses in the passage. When static and total pressure measurements are available at the inlet and exit, the performance of the diffuser can be accurately calculated and an average value of c_f can be determined. In cases without test data, a correlation for c_f is used to close the system of equations that model the control volume. Equation 11 shows a simple model used to predict the average c_f based on inlet Reynold's number [1].

$$\overline{c_f} = 0.1\left(\frac{1.8*10^5}{\mathrm{Re}_D}\right)^{0.2} \tag{11}$$

2.2.7 Time Cyclic Vaneless Diffuser

Initial attempts to derive χ and δ_{2p} using traverse data (Class 1) were frustrated because use of the Stanitz model would not allow the test data to be matched for traverses near the impeller exit. The assumption of instantaneous mixing results in large errors when processing traverse data collected near the impeller. To accurately model the flow at the diffuser inlet, an improved model was needed that removed the mixing plane assumption. The Traupel model [20], although slightly more advanced than the Stanitz

model, still struggles to model the vaneless space near the impeller exit where mixing losses dominate the flow.

Dean and Senoo [21] recognized the shortcomings of the Stanitz model and outlined a periodic mixing model that allows mixing to occur gradually. Their proposed solution was not sufficiently well developed for broad application in a meanline code. This forced the development of an advanced time-cyclic diffuser model. In the time-cyclic model, proposed by Dubitsky and Japikse [22], the mixing plane assumption is eliminated and the jet and wake structure is allowed to mix out gradually through the diffuser. This substantially improved the modeling of both pressure and flow angle near the impeller exit and allowed much better matching of the traverse test data.

Figure 2-9 illustrates the modeling improvement that was achieved using the time-cyclic diffuser model compared to the standard Stanitz model. The pressure and flow angle distribution are shown compared to radius ratio, R/R_2, in the diffuser. Figure 2-9 corresponds to a single operating point from one compressor test, but the results are typical of the improvement achieved. The Stanitz model can predict the diffuser exit conditions reasonably well ($R/R_2 \approx 1.7$), which has kept the model in use for more than 50 years, but performs very poorly near the impeller exit ($R/R_2 \approx 1.0$). In fact, the Stanitz model produces a rising trend in total pressure, shown with a dashed line and open circles, near the inlet due to the mixing plane assumption (n.b. the measured static pressure is forced as an input in this treatment giving an implied or deduced c_f). The improved Time-Cyclic model, represented with a solid line and open circles, corrects this problem and produces a good prediction in the entry region and at the exit.

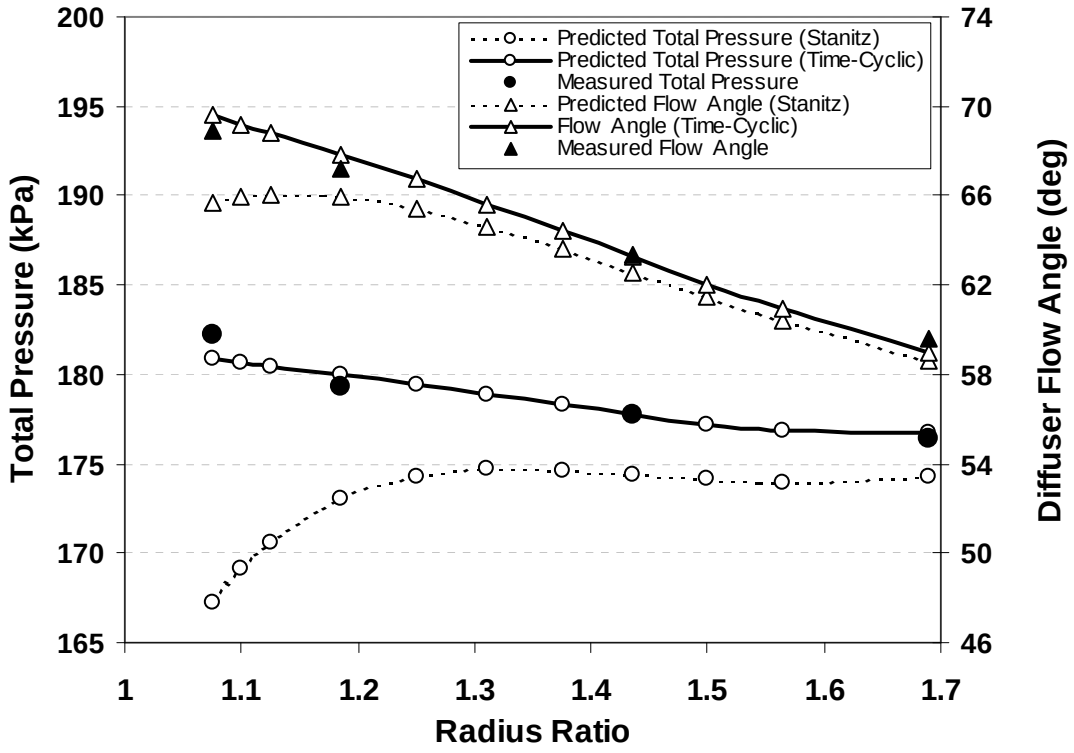

Figure 2-9: Performance of the Time-Cyclic diffuser model compared to a Stanitz calculation in a vaneless diffuser using measured static pressure as an input

A comparable improvement in the predicted flow angle is also evident with the Time-cyclic model. The improved fidelity at the inlet is crucial to accurately processing traverse data. The time-cyclic model was tested on several dozen sets of traverse measurements and was able to consistently match the measured test data. The entire set of traverse data in the database was processed to determine the associated values of χ and $\delta_{2p.}$

The time-cyclic model also improved the accuracy of the deduced diffuser skin friction. Since a differential control volume analysis is used to characterize the diffuser, with matching to the local static pressure, any losses that are otherwise unaccounted for in the diffuser will increase the resulting c_f calculation. Figure 2-10 compares the

calculated skin friction variation though a constant area ratio diffuser using the advanced time cyclic mode and the traditional Stanitz approach. The Stantiz model produces artificially inflated values of c_f since the mixing losses are not properly handled in the model.

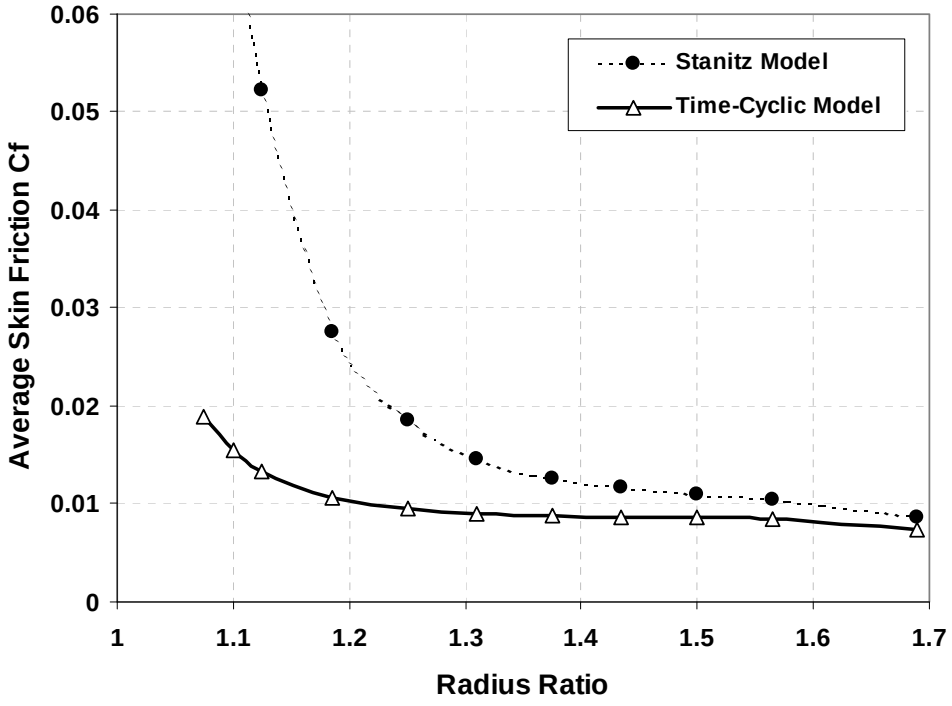

Figure 2-10: Deduced skin friction as a function of radius ratio in a vaneless diffuser calculated with the Time-Cyclic diffuser model compared to a Stanitz calculation.

The discrepancy between the c_f values predicted by the two models is greatest at the inlet of the diffuser where mixing of the primary and secondary zones discharging from the impeller dominate the losses in the flow. The time-cyclic (*TC*) model produces a much more realistic prediction of the skin friction development through the diffuser, with values that follow a more classical trend. The predicted values of total pressure and flow angle are also more accurate with the time cyclic model since the mixing losses are more correctly accounted for and the thermodynamic state is more precisely predicted.

2.2.8 Level 2 Data Processing

Since class 2 and lower data sets do not contain sufficient information to uniquely determine χ and δ_{2p}, it cannot be processed accurately without an additional constraint. In this situation, knowledge gained from processing the high-level traverse data can be applied. It is only necessary to constrain one of the two variables since they are linearly dependent. An empirical correlation for $\delta_{2p,}$ based on the processed traverse data, has been used to bound the problem. The correlation was developed using manual curve fitting and basic linear regression analysis to set the modeling coefficients.

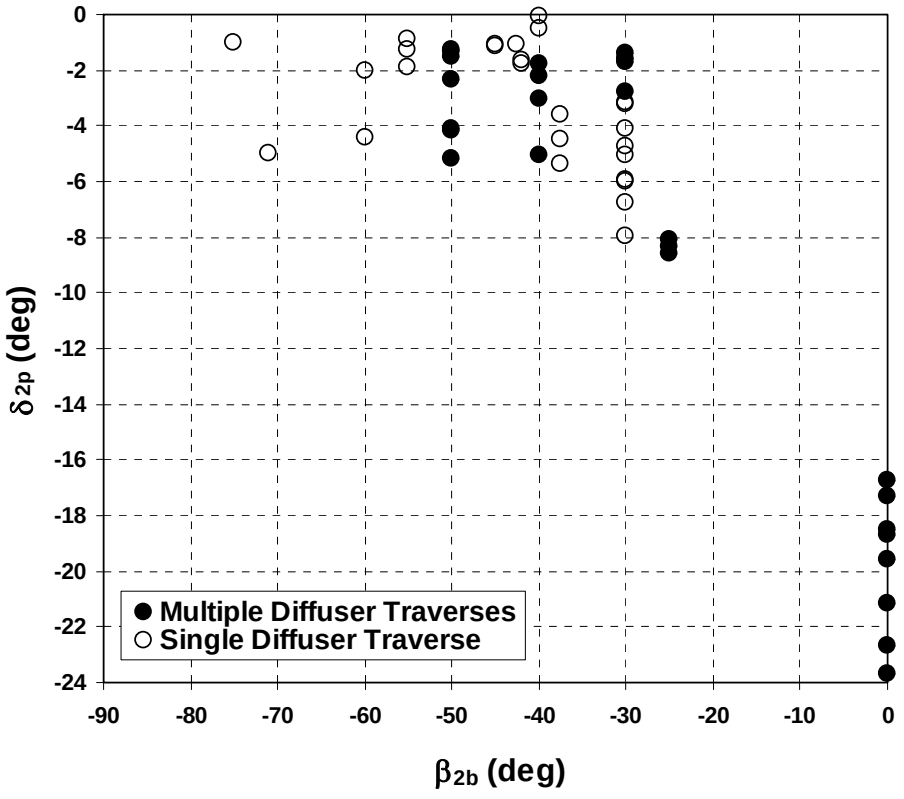

Figure 2-11: δ_{2p} calculated from traverse data as a function of exit blade angle

Historically good correlations for deviation have been developed based on exit blade angle (β_{2b}), and a strong dependence is seen in the data. Figure 2-11 shows how the magnitude of the blade backsweep corresponds to the level of primary flow deviation. The solid black dots represent data where more than one radial traverse location was measured. The open circles indicate cases only with a diffuser inlet traverse. The values of δ_{2p} less than –15° are associated with impellers without backsweep and the other data points correspond to cases with backsweep. A significant amount of scatter exists in Figure 2-11, suggesting that deviation depends on more than just exit blade angle.

An empirical model for δ_{2p} was developed using the 53 data points shown in Figure 2-11. The model, Equation 12, uses only two geometric variables, β_{2b} and exit solidity, S_2. The variables in the equations have been replaced with constants, k_1, k_2, etc. to preserve the proprietary value of this work and the data upon which the equations were based. S_2, defined in Equation 13, is based on β_{2b} and exit blade count, Z_R. This model was developed using simple regression techniques to match observed trends in the data. In the first term, sine was used to scale the value of β_{2b} and in the second term, an exponential was employed because it produced the best match of the data.

$$\delta_{2p} = -k_1 \exp\left[-k_2(-\sin(\beta_{2b}))^{k_3}\right] - k_4 \exp(-k_5 \cdot S_2) + 1 \qquad (12)$$

$$S_2 = \frac{Z_R}{2\pi \cos(\beta_{2b})} \qquad (13)$$

Figure 2-12 compares the prediction of δ_{2p} using Equation 12 to the measured values for these 53 points. The quality of the model can be assessed by calculating the

coefficient of determination [23]. The coefficient of determination is a measure of the variability in the data that is captured by the model. A perfect model would represent the data with an $R^2 = 1$, while a model that does not represent the data will have a significantly lower value. An $R^2 \sim 0$ would imply that the model does not predict the data at all. In this case, the model represents the test data with a coefficient of determination, or R^2, accuracy of 0.92. Although only geometric variables are used in the model, it is believed that some fluid dynamic parameters are important in determining the exit deviation. The data set is insufficient, however, at this point to reveal any fluid dynamic dependence at a statistically significant level. This model was tested against the entire database and has shown to produce reasonable results for all cases. For no cases were any positive or extremely large negative values of deviation predicted.

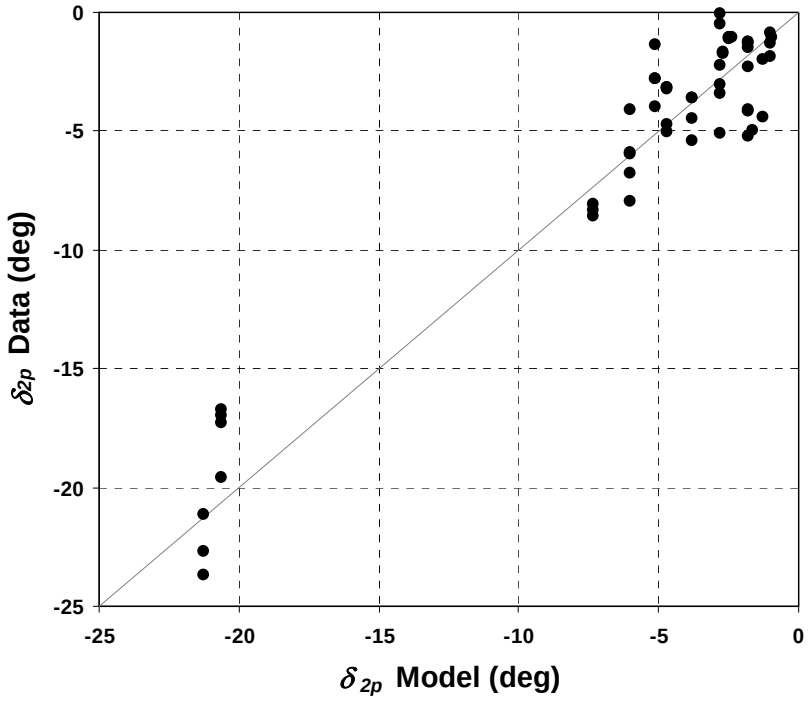

Figure 2-12: Predicted δ_{2p} compared to measured values obtained from traverse data

2.3 Variation in Two-Zone Modeling Parameters With Flow Rate

2.3.1 Variation in χ

Using traverse data, the appropriate values of χ and δ_{2p} were found for multiple points on an individual speedline. The resulting values of χ and δ_{2p} are different, however, at each flow rate along the speedline. Traditionally the values of χ and δ_{2p} had been assumed to be constant across a speedline for meanline modeling. Figure 2-13 shows the deduced values of χ calculated using traverse data for several speedlines in a centrifugal compressor.

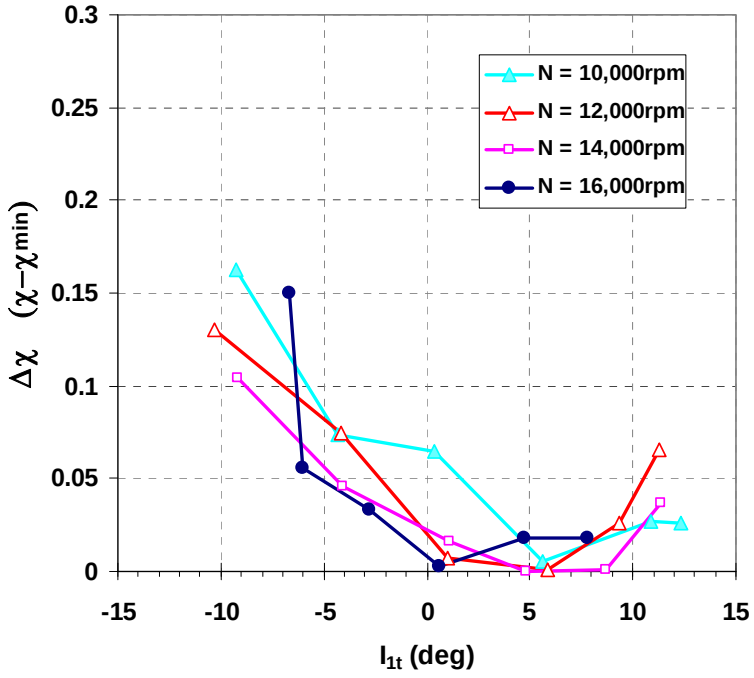

Figure 2-13: χ values for Eckardt rotor "O"[24] as a function of incidence calculated from traverse data

A clear trend is evident in the plot showing that χ increases as the flowrate changes from a nominal incidence. In this case the minimum value of χ exists for each speedline at about 5º incidence. Several other cases were examined, and they all showed the same characteristics as seen above, except the minimum point was slightly different for each case. A simple parabolic function was used to model the change in χ at off-design operating conditions. The parabola is centered on the incidence angle where the minimum χ occurs. This point of minimum impeller recirculation loss is hereafter referred to as the Benign Incidence Point (BIP).

2.3.2 Off-BIP δ_{2p} Variation

The traverse data was also used to examine the variance in δ_{2p} across a speedline. Japikse [1] suggested that Mach number ratio, MR_2 ($MR_2=M_{rel1t}/M_{rel2p}$), might substitute as a type of loading coefficient and showed that δ_{2p} varies with this parameter. Figure 2-14 shows the deviation angle calculated by Japikse, based on the class 2 data, compared to MR_2 for the three Eckardt rotors, A, B and O. Figure 2-15 shows the same plot of δ_{2p} as derived from traverse data for the same three rotors as in Figure 2-14. Using the traverse data and through careful control of the data reduction procedure a significant amount of error has been removed from the resulting calculation of δ_{2p}. In the updated plot, the deviation of rotor B was calculated to be less than zero for all points, while in Figure 2-14 most of those points showed positive deviation which is not rational since there is no physical mechanism to enable the primary to lead the blade since it is modeled as near isentropic. Although it is possible that the secondary zone may show positive deviation since it is non-isentropic.

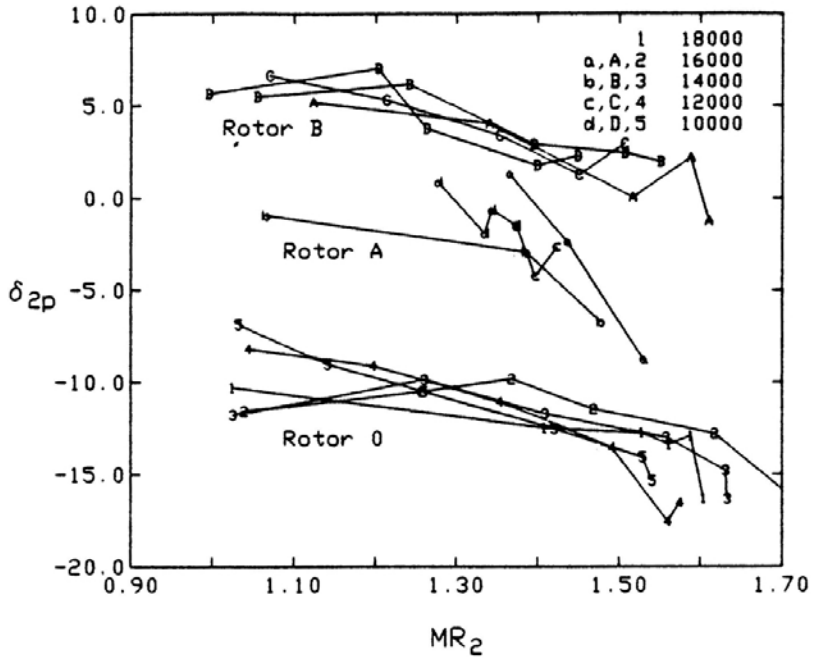

Figure 2-14: Calculated flow deviation for the three Eckardt rotors made by Japikse [1]

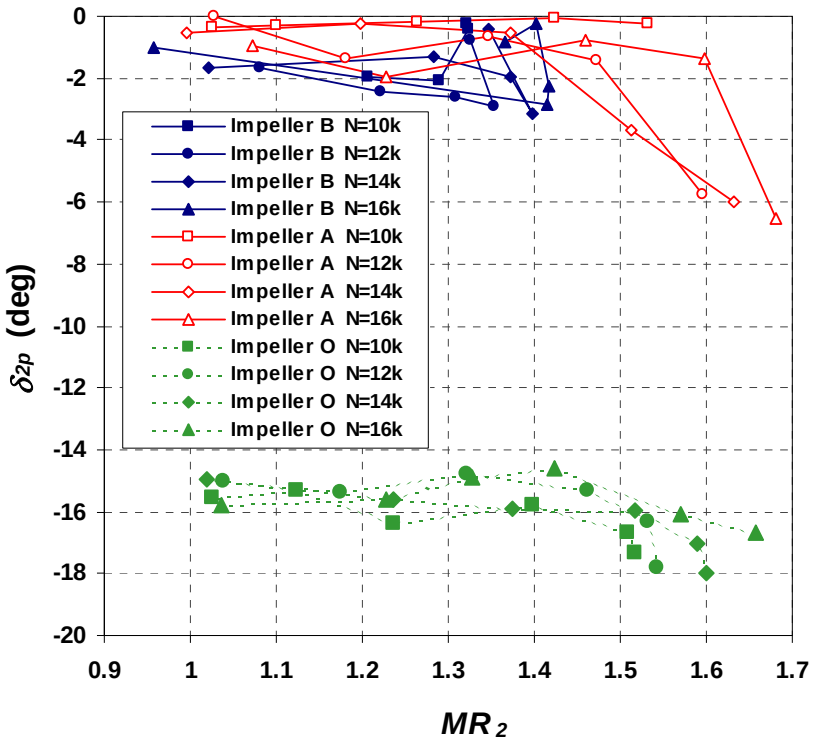

Figure 2-15: Deduced δ_{2p} for Eckardt rotor O, A and B [24,25,26] calculated from traverse data

The calculations made with the traverse data show that δ_{2p} is fairly constant across each speedline below $MR_2 \approx 1.45$. At $MR_2 > 1.45$, however, or at low flow conditions, the magnitude of the deviation begins to increase rapidly. This variation was modeled with an exponential function based on MR_2 and a baseline, or BIP, δ_{2p} value. Equation 14 shows the proposed off-BIP model for δ_{2p}. The model reproduces the uniform distribution as seen from the test data for an $MR_2 < 1.45$, and allows the deviation angle to increase rapidly, following an exponential profile above $MR_2 \approx 1.45$. The Off-BIP value of δ_{2p} was constrained to differ by no more than six degrees from the BIP value of the deviation.

$$\delta_{2p(Off-BIP)} = -\exp\left(k_1 \cdot MR_2^5\right) + \delta_{2p(BIP)} + 1 \quad \textbf{(14)}$$

2.3.3 Two-Zone Model Coupling

When using the proposed data reduction procedure detailed earlier, χ and δ_{2p} are coupled parameters, so variations in one influence the other. Figure 2-16 illustrates this dependence, as evidenced in data deduced from the Eckardt A impeller traverse measurements [25]. The plot on the left in Figure 2-16 shows δ_{2p} compared against inlet tip incidence, which is proportional to flow rate. The plot on the right shows the corresponding values of χ for the same data also compared to incidence. For the lowest speedline, 10,000rpm, δ_{2p} is nearly constant for the entire tested range, which results in a parabolic variation in χ. For the three higher speedlines, the value of δ_{2p} begins to increase rapidly with increasing incidence while at the same time the corresponding value of χ also begins to increase dramatically. Three points that exhibit this trend have been highlighted in Figure 2-16.

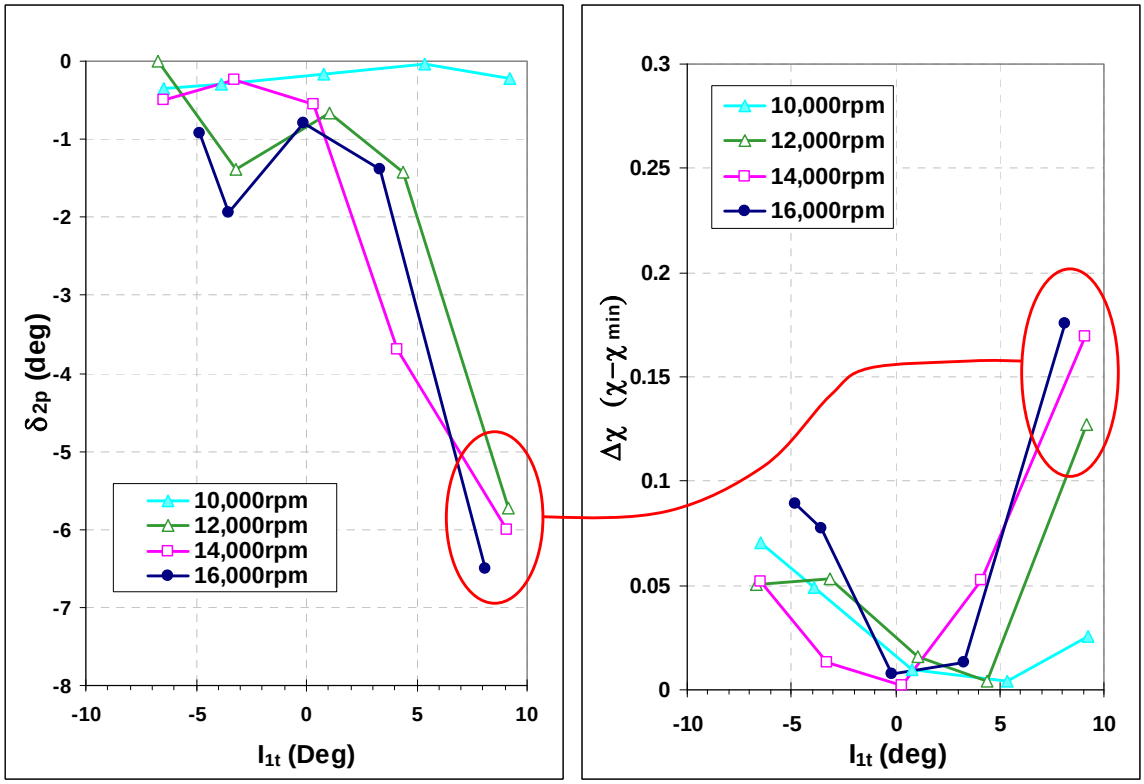

Figure 2-16: Two-zone parameters calculated for Eckardt rotor A [25], illustrating the coupling between χ and δ_{2p}

Equation 15 was developed to model the off-BIP variation in χ. It contains four separate variables, χ_{BIP}, I_{1t}, I_{BIP} and MR_2. I_{BIP} is the tip incidence at the Benign Incidence point and χ_{BIP} is the corresponding value of χ at this point.

$$\chi = \chi_{BIP} + k_1 (I_{1t} - I_{BIP})^2 - k_2 \left(\exp\left(k_3 \cdot MR_2^5 \right) - 1 \right) \qquad (15)$$

Both I_{BIP} and χ_{BIP} must be estimated using an empirical model; a model for each has been created from the database and will be presented later. The second term in the model, $(I_{1t} - I_{BIP})^2$, defines the nominal parabolic increase in the value of χ as the

incidence increases from the BIP point. The third term, containing MR_2, accounts for the increase in δ_{2p} that occurs far off-design as MR_2 becomes large, following the same form as in Equation 14 and effectively couples the off-BIP χ and δ_{2p} predictions.

2.3.4 Impeller Recirculation Loss

The impeller recirculation loss (IRL) measures all unaccounted losses through the impeller, principally due to recirculation, but perhaps others as well. Consequently, the shape of the impeller recirculation loss bucket also changes when χ and δ_{2p} are allowed to vary off-BIP. Traverse data showed that both χ and δ_{2p} can vary significantly along a speedline. Assuming they are constant leads to artificially high levels of IRL to compensate for losses that are actually due to changes in χ and $\delta_{2p.}$ When the off-BIP models are applied a more realistic level of IRL can be found. In many cases, the deduced level of impeller recirculation losses may be reduced by a factor of two or more when using the off-BIP models for χ and δ_{2p}. The difference between the deduced IRL with and with out the assumption of constant two-zone parameters, χ and δ_{2p}, is shown below in Figure 2-17. When the off-BIP models are used, the losses are reduced dramatically suggesting that earlier models were somewhat inaccurate and bookkeeping needed improvement. At BIP the losses calculated with the traditional and off-BIP models are comparable. As the flow rate increases from the BIP the reduction in IRL becomes more significant as χ and δ_{2p} increase from their BIP values.

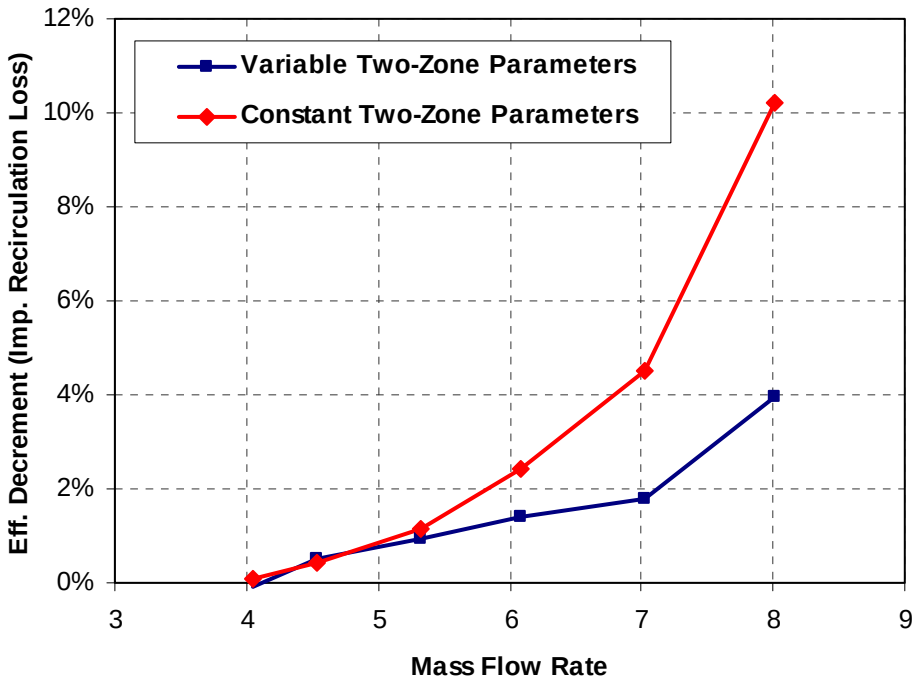

Figure 2-17: Impeller recirculation loss for a typical centrifugal compressor calculated within COMPAL using both constant two-zone values and with the variable off-BIP models.

2.4 Processing Various Classes of Data

When class 1a data is available, all of the relevant modeling parameters can be accurately deduced from the data. When lower quality data is processed a unique set of modeling parameters cannot be identified and supplemental information deduced from the higher level data can be used to close the system of equations. Although it would be desirable only to work with high quality, class 1a data, this is not often possible. Full flow field traverses are expensive to conduct and they are rarely performed in certain industries, such as in most pump and blower companies. Fortunately, several sets of class 1a data were available to guide this work.

The flowchart shown in Figure 2-18 is broken up into three branches that represent different classes of data and show how each class can be processed to yield the maximum amount of useful information. The branch on the left, micro-database 1, represents the highest quality data, class 1, where all of the pertinent modeling parameters can be determined. Class 1 data includes cases with full internal measurements and inlet and exit traverses. From class 1 data the two-zone modeling coefficients χ and δ_{2p} can be accurately deduced.

From this subset of the database three important models have been developed. One model to predict the BIP value of δ_{2p}, and the other two predict the off-BIP variation in χ and the δ_{2p}, respectively. The model for $\delta_{2p,BIP}$, Equation 12, is required when processing the lower class data in order to bound the design space. Recall that without this model a valley in the design space exists and χ and δ_{2p} cannot be uniquely determined. The second set of models, Equations 14 and 15, define how χ and δ_{2p} vary off-BIP, and are applied when processing lower class data. Without these additional constraints, a sensible and consistent match of class 2 - 4 data cannot be made. The branch on the right is comprised of a second subset of the main database, micro-database 2, which contains cases with traverses and a string of static pressures through the diffuser. From this data, detailed information about the skin friction development, c_f, in the diffuser can be gathered. This information can than serve as a guide in estimating the frictional influences on diffuser performance in cases were internal pressures were not measured.

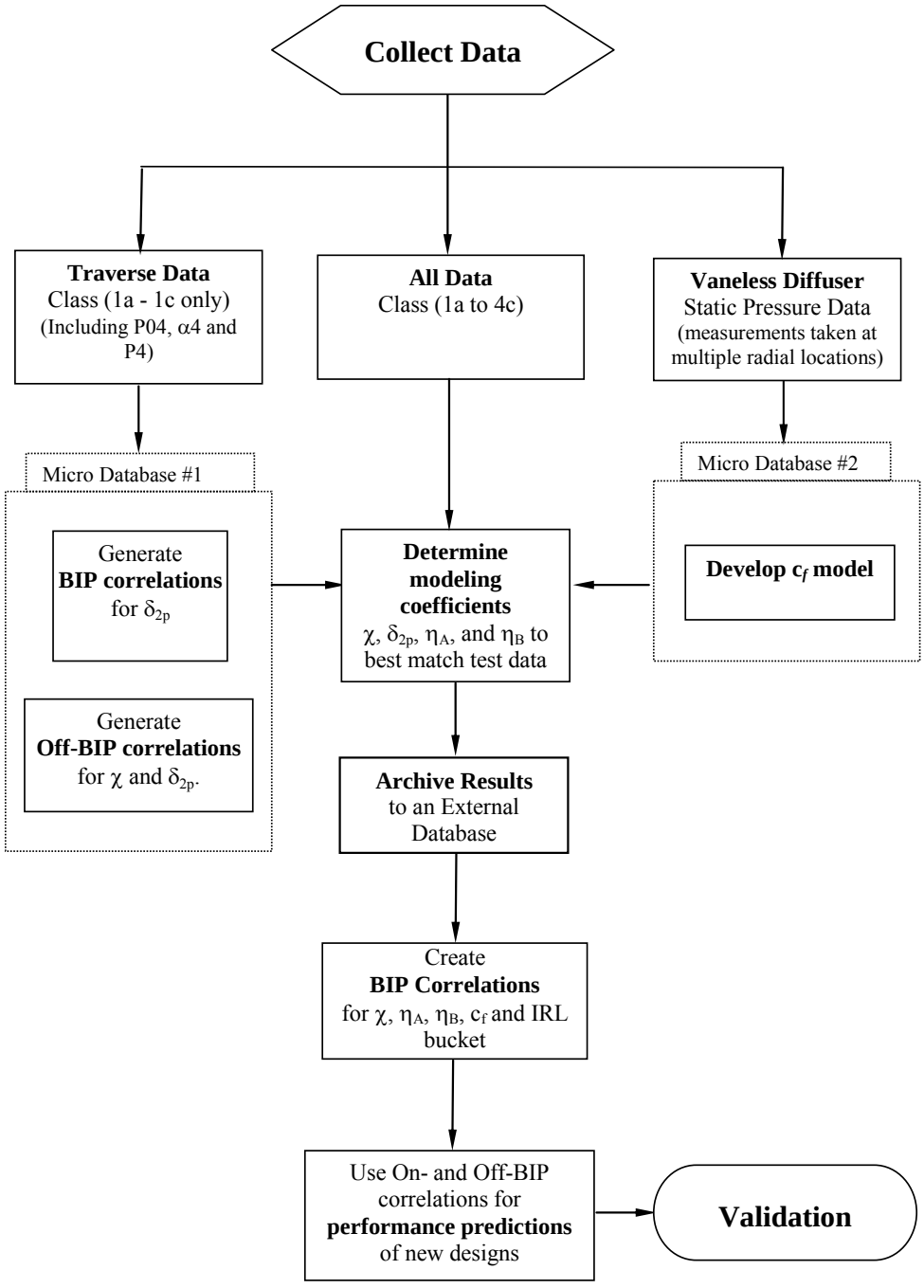

Figure 2-18: Data processing flowchart detailing use of various data levels

2.5 Automatic Data Reduction

2.5.1 Easy Control

Historically, all test data were processed manually to determine the values of η_a, η_b, χ and δ_{2p}. These values were determined by matching the model prediction to the reduced test data. Manually matching the data required an individual to compare predicted performance plots generated using the TEIS/Two-Zone models to those of the test data. The modeling coefficients were then adjusted to produce the most accurate match of the test data. Manual data processing was used for many years and proved that sensible values for the TEIS and Two-Zone model variables could be found to match test data for virtually all machines.

Manual data processing produced many useful insights and illustrated the validity and effectiveness of the TEIS model for representing a wide range of machines. Manual data reduction had several drawbacks, however. First, it is a very time consuming, iterative process that could be difficult for an inexperienced engineer. Second, different users would often model the same test case using slightly different settings. In these cases, each individual user incorporated some personal bias when setting the TEIS and Two-Zone model variables. This bias was not uniform and often based on historical modeling assumptions or personal preference. This bias created noise in the data that was difficult to quantify and hindered modeling efforts.

ConceptsNREC developed an automatic data-matching program, EasyControl, in parallel with this work, to address the problems associated with manual data matching. The final version of the software was designed specifically by ConceptsNREC to meet the needs of this project, and is now commercially available. The software was designed

to eliminate user bias and increase numerical accuracy by automating and standardizing the overlay and compare (OC) procedure. The program automatically runs the meanline codes, COMPAL or PUMPAL, and iterates on the setting of the modeling parameters while monitoring the OC match quality. It was designed to function following the same basic procedure that was used in manual data reduction. Specific procedures and constraints were applied to match the physics of the modeling system and incorporate the practical knowledge gained from years of experience with manual data matching.

EasyControl determines the best data match by iterating on the dependent variables using a simple optimization algorithm. The optimization routine functions by minimizing a user-defined fitness function that represents the quality of the models match of the data. The fitness function used in EasyControl is a weighted sum of the residual error between the test data and analysis prediction for eight different performance measures.

Table 2-3 contains a list of the objectives and constraints that constitute the objective function that ConceptsNREC developed to be optimised by EasyControl. Each of the eight parameters has been assigned a weighting factor. The weighting factor is representative of the relative importance that each factor would receive if the data had been processed manually. In cases where the impeller tip static pressure has been measured the weighting applied to the rotor performance parameters is increased by a factor of two because the performance of the impeller can be calculated independent of the other stage components. Correctly setting the weighting factors is critical to help the solver converge quickly and consistently to an optimum.

Table 2-3: Weighting values and constraints used by EasyControl

EasyControl Objectives and Constraints		
	Weights	
Objective	**Pumps**	**Compressors**
Stage Efficiency	10%	10%
Stage Power	10%	10%
Impeller Recirc. Loss	10%	10%
Rotor Efficiency	20%	20%
Minimum Delta Recirc.	10%	10%
Stage Pressure Ratio (TDH)	20%	20%
P02m/P00	10%	10%
DR2 (MR2)	10%	10%
	Bounds	
Constraint	**Lower**	**Upper**
Min. Impeller Recirc. Loss	0	0.05
δ_{2p}	None	0
DF_{mult}	0	2
χ	0.01	1
Diffuser C_f	0	None

Several design constraints, shown on the bottom half of Table 2-3, must also be satisfied to keep the solution in a physically rational domain. Constraints are applied using penalty functions that increase the objective value when a constraint is violated. One of the parameters that is set using a penalty function is the point of minimum impeller recirculation loss. The impeller recirculation loss (IRL) can never be less than zero, which would signify that energy had been added to the flow. At the design point, a well-designed impeller will have little or no recirculation. Although in some situations, such as off design speeds or poorly designed impellers, it is possible to have some recirculation at all flow rates. The penalty function was set to increase gradually to allow the point of minimum impeller recirculation loss (MIRL) to be slightly greater than zero if a significant improvement to the overall match could be made.

The two-zone modeling parameters are also constrained to be within physically rational bounds. δ_{2p} is constrained to be less than zero because the primary zone flow cannot lead the blade. χ is constrained to within the range of past experience, between 0.05 and 0.95. It was also necessary to impose a constraint to keep the skin friction, c_f, above zero. Using these constraints and the listed objectives, EasyControl is able to automatically determine a value of η_a, η_b, χ, δ_{2p}, and all other modeling variables, which results in the best match of the given test data.

2.5.1 Design Space Search

The first task that EasyControl must accomplish is to identify a valid start point for the optimization routine where IRL is close to zero. The starting place must be close enough to the global optimum so that the solution does not converge to a local minimum. Three different methods have been included in EasyControl to evaluate the design space and select a starting point. Each method systematically searches a portion of the design space by evaluating the model predictions compared to the test data made using various Two-zone parameter settings. The location with the minimum valued fitness function is selected as the starting point for the optimization.

The most time consuming, but most thorough analysis, is a Latin Hyper Cube (LHC) search. This method is commonly employed in optimization cases to evaluate the design space and select a starting point. A LHC search covers the entire design space by sampling at least 200 randomly distributed points. If the density and the range of the LHC search are sufficient, then a starting point can be found that will lead to the global

optimum. To perform a full LHC search of the entire domain is very time consuming and often unnecessary.

A Gaussian Hypercube (GHC) search was developed to reduce the number of sample points required to identify an adequate starting point. The GHC search starting point is based on historical guidelines in setting values of χ and δ_{2p}. Instead of performing a full LHC search, sample points are selected that follow a classical Gaussian distribution around the predictions of χ and δ_{2p}, made following the trends shown in Figure 2-6. This approach greatly decreases the number of search points that must be tested to determine a starting point, but relies on the accuracy of the historical χ and δ_{2p} correlations. Typically the models for χ and δ_{2p} are sufficiently accurate to position the search region over a valid starting point. A typical GHC search requires 75 samples to find a start point, or less than half the time of an LHC search.

The simple χ search is the third search method in EasyControl and requires the fewest sample points. The χ search assumes that the design space for χ and δ_{2p} is similar for all machines and forms a valley, as seen in Figure 2-7. If this assumption is correct, then for any value of δ_{2p} a corresponding value of χ exists that would yield a starting point that is along the valley floor. To identify such a point, a single value of δ_{2p} is selected as a starting point and χ is varied until $IRL \approx 0$. Following this logic a valid starting point can be identified in fewer than ten iterations as opposed to 200 with a LHC search.

Once a starting point is selected, EasyControl uses a hill climb method to optimize the full set of design variables to yield the best match of the data. The hill climb algorithm (method of steepest accent or descent) calculates the gradient of the objective

function based on changes in the design variables. At each iteration, all design variables are adjusted in the direction of steepest descent to minimize the objective function. This method is very robust and will always proceed toward a minimum. Hill climb algorithms work best on smooth design spaces, and require a starting point that is near the global optimum.

Since the design space for level 2-4 data forms a valley instead of a unique optimum point, an additional constraint must be used when processing these cases. The model for δ_{2p}, developed from the traverse data, has thus been included in EasyControl. The overall OC match is penalized as it deviates from the value of δ_{2p} predicted by Equation 14.

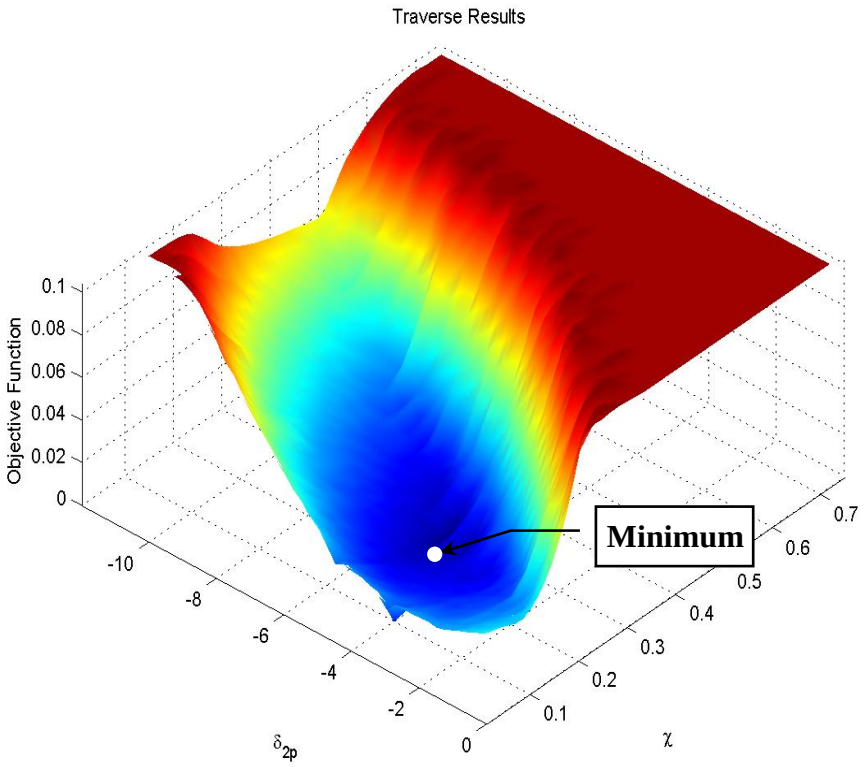

Figure 2-19: Two-zone design space with δ_{2p} constrained to produce an optimum

The penalty function applied for δ_{2p} is relatively small compared to the other constraints so that final match may use a slightly different value of δ_{2p} if a significant improvement to the overall match can be made. The addition of δ_{2p} as an objective creates a clear optimum that EasyControl can readily identify. Figure 2-19 shows the same design space as seen in Figure 2-7, evaluated with the addition of the δ_{2p} constraint. The resulting objective function produces a smooth design space with unique optimum near δ_{2p} = -4º and a χ = 0.25.

2.6 Data Archiving

After the data have been processed the results are added to a database for further review and use in model building. Only a single representative point from each speedline is included in the database. Each entry in the database includes the complete meanline geometry of the machine, a wide variety of fluid dynamic variables and the associated modeling parameters that were used to match the test data. Careful consideration was made in selecting what point should be included in the database. The performance of a stage or machine is often referenced to a "Design Point" that corresponds to a specific operating speed and flow rate that the machine was designed for. The design point is not a good value to add to the database because it is arbitrary and inconsistent between different designs and designers. The Best Efficiency Point (BEP) is also commonly used to describe performance, and typically occurs at the design speed near zero incidence. Unfortunately, the BEP can only be determined from testing and can not be known in advance so it would be difficult to use in the database.

To avoid the problem associated with the BEP and design point positioning, the database was selected to be at $C_{pa,i} = 0$ because it is near zero incidence where losses are typically low. At this point the values of η_a and η_b are independent of each other, which reduces the interaction effects between the two parameters and improved the model fidelity. It is also a point that can be readily calculated based on geometry and flow, unlike the BEP, which cannot be accurately predicted. In most cases a data point does not exist exactly at the point of $C_{pa,I} = 0$ so EasyControl is designed to interpolate to this point. At the selected database point, $C_{pa,I} = 0$, all of the relevant flow and geometric variables are calculated and written to a data file. This data file contains information on the final dependent variable settings and approximately 1000 corresponding independent variables calculated by the meanline code. The data file can be easily read into a spreadsheet to facilitate further analysis and model development.

3 Model Development

Initial attempts to develop models to predict the meanline coefficients were frustrated due to a relatively small number of quality datasets that were available. The current database, with over 300 points, has reduced many of the statistical limitations encountered in earlier modeling attempts. As the size of the database grew it became increasingly necessary to have robust tools to help process and model the data. A variety of model building tools were evaluated during this project to determine which would be most applicable. Initial efforts were focused on developing the most accurate models possible for each coefficient using powerful regression tools. Two fully automatic modeling tools, neural networks (NN) and genetic algorithms were tested, but both failed to produce models that fully satisfied the objectives of this project.

3.1 Advanced Regression Tools

Use of neural networks and genetic algorithms were explored because of their ability to automatically capture complex variable couplings. A neural network is comprised of a series of basic mathematical operators that are linked together. Training the model sets the exact order of the operators and their coefficients. Training is accomplished by tuning the model to use the provided inputs, or dependent variables, to match a given set of data, independent variables. Although neural network solutions

produced accurate models of the TEIS and Two-zone parameters, the formulation of the solution could not be reviewed to identify weaknesses such as unusual asymptotes or singularities.

Genetic algorithms were developed [27] for solving complex problems where an exact solution form was unavailable. Genetic algorithms are similar to neural networks in their capability to model complex phenomena, but they produce solutions in the form of mathematical models that can be easily evaluated. Genetic Programming (GP) mimics nature by creating a solution based on natural selection and evolution. Genetic algorithms begin with an initial population of randomly generated solutions for the specified problem. In this case each solution, or individual in the population, is expressed as a mathematical equation comprised of a unique arrangement of several independent variables included in the database. The performance of each individual is evaluated based on how well it predicts the dependent variable. Equations that perform poorly are eliminated from the population. A group of the best performing models are identified and reordered into new equations, based on terms from two separate models. These new equations are added to the population to replace the poor performing models that were removed and the entire population is re-evaluated. This process is continued until no further improvement is noticed and a solution is found that best matches the data.

Although models developed using Genetic Programming produced mathematical expressions, they were often very large and complex. A GP solution usually appeared as very unconventional equation that incorporated diverse terms and frequently failed to satisfy known physical trends and avoid singularities. In some instances these problems could be corrected manually, but the final equation form was still too large and

cumbersome to use with confidence. Both NN and GEP demonstrated that accurate models of the dependent variables could be developed from the database. They also illustrated that the most desirable solutions needed to be both accurate and simple to understand. Ideally the user should control which variables are used in the model and evaluate their application to ensure that the resulting model is both physically rational and accurate. The most practical tool to achieve this goal proved to be stepwise linear regression.

3.2 Linear Regression

After evaluating the automatic modeling tools it was decided that manual linear regression offered the necessary control over the model form, with minimal compromise in accuracy. Stepwise regression is advancement over simple linear regression techniques. In stepwise regression an initial linear regression is preformed using a base set of variables. Once a basic regression model has been created the P-Value [23], and other statistical measures are reviewed to determine the relevance of each variable in the model. Any insignificant variables are removed from consideration and another regression model is created. In subsequent iterations additional independent variables are added to the base set and evaluated. If the additional variable improves the resulting model then it is retained or eliminated if it does not contribute. One of the weaknesses associated with linear regression is that it cannot identify important variable couplings or automatically capture non-linear trends. Since the models for η_a, η_b, χ and δ_{2p} are both coupled and non-linear, these effects must be manually added to the models.

3.3 Variable Selection

The basic database contains nearly 1000 independent variables for each speedline. Past experience suggested that only a small fraction of those variables had any effect on dependent variable. So, before any modeling was done this data set was reduced to include only those variables that had a significant effect on the dependant variable in question. Some basic statistical tools were used to filter the full set of nearly 1000 variables, and identify the primary dependencies for each model coefficients.

First, a correlation matrix, including all 1000 variables, was constructed to determine if any linear dependencies exist to represent the dependent variables. The correlation value is calculated by scaling the covariance by the standard deviation [23] to normalize the result. The correlation value ranges between –1 and +1. Positive values suggest that an increase in one variable is associated with an increase in the other. Negative values indicate that a rise in one parameter results in a decrease in the other. The correlation statistic can be used to analyze a very large array of parameters and easily identify linear relationships between any two variables.

Table 3-1 shows a sample correlation analysis for η_a and η_b. The correlation analysis for η_a and η_b identified many variables that are linearly dependent on the TEIS modeling parameters. Non-linear relations were also evaluated by calculating the correlation matrix on the database with the independent variables raised to various powers, such as 0.5 and 2. Couplings were determined in a similar manner by calculating the correlation statistic on the product of different variables. The important linear, non-linear and coupled terms were then introduced to the stepwise regression model. In the

regression analysis both the coefficients and exponents on individual variables were allowed to vary, but the structure of the equation was fixed.

Table 3-1: Correlation values for η_a and η_b vs. various independent variables in the database

Correlation Statistics for η_a		Correlation Statistics for η_b	
Variable	**Correlation**	**Variable**	**Correlation**
MREL1T	0.4870	ARa	-0.4877
ZI	0.4559	I1T	-0.4006
AS1	0.4506	CpA Ideal	-0.3978
Specific Speed(NSUS)	-0.4429	CpB Ideal	0.3456
B2/R2	-0.4349	ZI	0.3372
AS1 Tip	0.4341	E	-0.3031
Rossby Number (W,2)	-0.4212	AS1	0.2509
Richardson Num (2)	-0.4182	AS1 Tip	0.2492
Rossby Number (W,A)	-0.3917	MREL1T	0.2363
Richardson Num (A)	-0.3714	M2M	0.2323
AR2 Pure	-0.3455	Rotation Number (W,1)	-0.2296
Rot. Num. (C,A)	-0.2959	Rot. Num. (C,A)	-0.1902
CpA Ideal	0.2683	Clr/B2	-0.1811
Area 2	-0.2511	R2	0.1773
Specific Speed(NS)	-0.2481	ETAa	0.1673
ARa	0.2292	ARb	0.1575

Not all of the variables identified via the correlation analysis were used in the final models. Rather, some were removed from consideration because they may not be independent of other important parameters. For example, several different calculations of Rossby number (*Ro*), which are all related, appear to be important factors controlling η_a. It would only add redundancy to the final model to include multiple variables that are directly related.

Different data classes required different processing during regression to ensure that the models did not include any unnecessary noise or uncertainty. To avoid biasing the regression model with the low quality or low performance data, a weighting function was used. The different data classes, 1a – 4, were assigned a multiplier of 1 to 0.1

respectively. This multiplier was applied to the calculated residual for each case included in the regression. Linear regression fits the model to the data by minimizing the sum of the squares residual error for the sum of all cases. By reducing the calculated residual on the low class data cases, the model puts more weight on matching the higher quality data, where the modeling parameters are known with more certainty.

4 Results and Model Performance

4.1 η_a Models

Three separate models for η_a were developed: a combined model appropriate for all types of machines, a model for pumps only, and a model for compressors only. The combined model is the least accurate, but the most broadly applicable. The individual models for pumps and compressors alone results in more accurate prediction and uses simpler mathematical expressions than for the combined model. However, the scope of the subset models is smaller and the statistical confidence is lower because it is based on fewer data points. To increase the statistical confidence in the pump and compressor models, the combined model was used as a starting point from which the basic equation form was set for the pump and compressor models.

When building models for η_a it proved to be difficult to achieve high R^2 values, although acceptable levels of standard error, calculated as the standard deviation of the difference of the model prediction and the data, have been achieved. This difficulty suggests that some of the important parameters that control η_a may not be captured yet in the meanline geometry. Some of these additional parameters may include inlet blade turning or the effects of tip recirculation.

4.1.1 η_a Combined Model

The combined model is the broadest of the three models developed for η_a. It is applicable for all types of turbomachines included in the database, including radial and mixed flow machines and axial flow pumps. Since the majority of the database consists of radial compressors, the model will be most accurate for similar machines. The final model, Equation 16, consists of nine separate independent terms. The model was developed using the stepwise regression techniques detailed previously.

$$\eta_a = k_1\sqrt{\mathrm{Re}_{R1t}}\left(B_1/R_{1t}\right)^{1.5} + k_2 \cdot OC - k_3 \cdot L/D - k_4 \cdot Ro_{W2} - k_5\left(Clr_R/B_2\right)^2 - k_6 \cdot \cos(I_{1t}) - \frac{k_7}{AK \cdot \cos(\beta_{1t} - I_{1t})} - k_8 \cdot Z_R + k_9 \quad \textbf{(16)}$$

The terms in the model include both geometric and flow based variables. The individual non-dimensional variables used in the model are defined in Table 4-1.

Table 4-1: Definition of non-dimensional variables used in the combined pump and compressor model for η_a

Name	Definition
Re_{R1t}	Density * Inlet tip radius * Inlet Relative Velocity / Kinematic viscosity
B_1/R_{1t}	Inlet blade height / Inlet tip radius
L/D	Impeller passage length / Impeller passage hydraulic diameter
Ro_{W2}	Impeller exit relative velocity / (Impeller radius of curvature*shaft speed)
Clr_R/B_2	Clearance / Exit blade height
I_{1t}	Inlet blade tip incidence
β_{1t}	Inlet relative velocity, Tip / Absolute inlet velocity
Z_r	Exit blade count
AK	Impeller inlet meridional velocity ratio, tip/rms

The terms in the equation are arranged in order of decreasing statistical significance, as measured by the P-value. The first and most important term in the model shows that the inlet effectiveness is strongly related to inlet Reynolds number and the relative inlet blade height, B_1/R_{1t}. The next most important parameters are non-dimensional passage length, L/D, and the shroud type, OC. Rossby number, Ro_{W2}, relative tip clearance, Clr_R/B_2, and inlet blade incidence, I_{1t}, also appear in the model, but are less important. Exit blade number, Z_R, is also included in the model, but has a very modest effect on the result. Since the bulk of the cases in the database are small to medium centrifugal compressors, the model gives the best prediction for similar types of machines. The database value of η_a is plotted vs. the prediction made with Equation 16 in Figure 4-1.

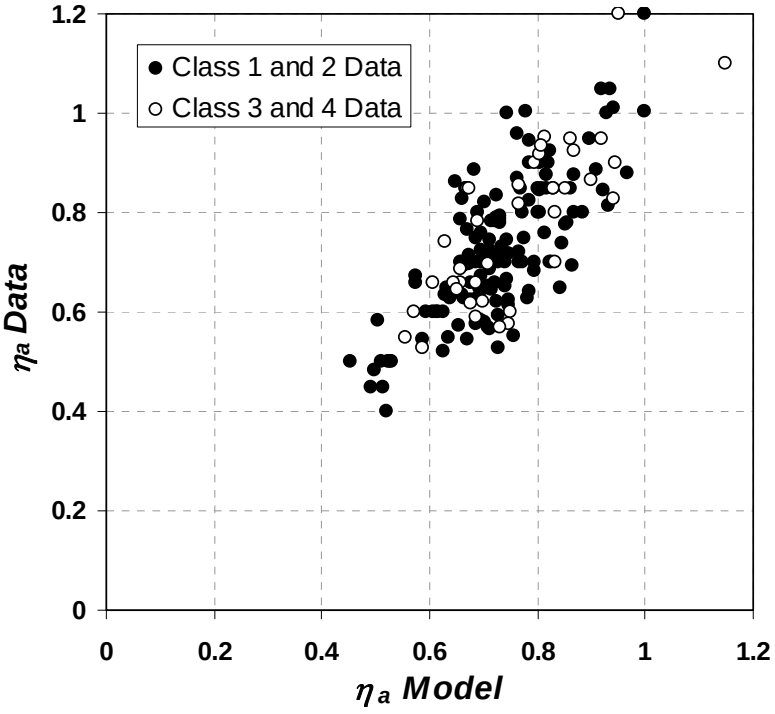

Figure 4-1: Regression results for the combined η_a model

The combined η_a model represents the test data with an R^2 of 0.54 and a standard error of 0.08. The value of R^2 is lower than would be desired; however the standard error is at an acceptable level. The η_a model was constrained to be within the range of 0 to 1.2 since values outside this range are irrational and do not represent a valid solution. Although none of the model predictions, for the validation cases shown in Figure 4-1, were limited by these constraints

4.1.2 η_a Model for Compressors Only

The final expression derived from a stepwise linear regression approach is given in Equation 17. The model for compressors contains eight separate terms, one fewer than the number used in the combined model. As fewer cases are included for model building, as with the compressor or pump only models, the data can be represented more accurately with fewer terms, but the applicability of the model is reduced. The most important variables are again the inlet Reynolds number (Re_{R1t}) and the relative blade height at the inlet, B_1/R_{1t}. The compressor model includes three additional terms that were not included in the combined model, inlet aspect ratio (AS_1), inlet solidity (S_1), and DR_{2i}. Several variables were used in the combined model that did not appear in the compressor only model including, L/D and Ro_{W2}, which were both moderately significant in the combined model. A broader range of data would likely help bridge the gap between the pump, compressor and combined models and result in a more uniform set of variables in each subset model. Overall, the η_a model for compressor only performs similar to the combined model, although it more accurately predicts the performance of certain types of

compressors. For example, the performance of process compressors, which are not well represented with the combined model, are modeled much better by Equation 17.

$$\eta_a = k_1 \cdot \ln\left(\mathrm{Re}_{R1t}\right) / \left(B_1 / R_{1t}\right)^{k_2} + k_3 \cdot OC - k_4 \left(Clr_R / B_2\right)^{k_5} + k_6 \cdot AS_1 + k_7 / S_1 + k_8 \cdot DR_{2I} + k_9 \left(\frac{B_1}{R_{1t}}\right) \cdot OC - k_{10} \quad \textbf{(17)}$$

The results of the regression analysis are shown in Figure 4-2 where the actual database values of η_a are presented vs. the predicted value of Equation 17.

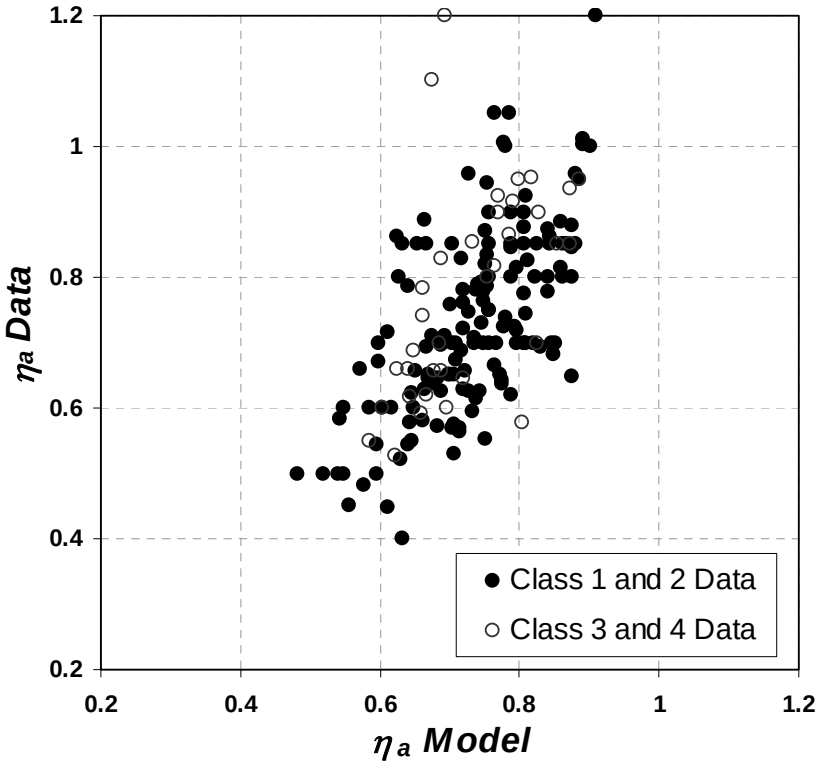

Figure 4-2: Regression results for the η_a compressor specific model calculated at the BIP point

The regression analysis yields an R^2 match of approximately 0.5 and a standard error of nominally 0.069. Although the R^2 value is comparable to the combined model, the standard error is approximately 15% lower. The model appears to yield the largest error when η_a is large. Specifically when η_a is larger than approximately 0.75 the model tends to yield an under-prediction in the magnitude of η_a. Below a value of 0.75 the model slightly over-predicts the data.

4.1.3 η_a Model for Pumps Only

Modeling pumps alone presents some challenges since the range of machine types is so broad. The database consisted of some very low-tech industrial pumps that perform poorly, as well as high performance rocket turbopump impellers. It also contains the widest range of machine type, with many mixed and axial cases along with the basic radial flow impellers. The values of η_a deduced from test data of pumps are much broader than those found for compressors, ranging from 0.1 to 1 for pumps, compared to 0.5 to 1 for compressors. The η_a model for pumps only, Equation 18, uses nine different variables. The form of the equation is significantly different from the combined model for η_a. Although the combined model was used as a baseline, significant improvements in performance prediction were realized by including additional variables. The additional non-dimensional variables that we used in this model are defined in Table 4-2.

$$\eta_{a,pump} = -k_1 \cdot Rot_{CA}^2 + k^2 \cdot (Ri_2)\left[-k_3(OC) - 1\right] - k_4 \cdot \cos(PHI_1) + k_5 \cdot \ln(\mathrm{Re}_{R1t}) \\ - k_6(DR_{2I})^2 + k_7(DR_{2I})^4 + k_8(AS_1)(AS_2) - \left(\frac{Clr_R}{B_2}\right) - k_9(OC) + k_{10} \quad \textbf{(18)}$$

Table 4-2: Definition of non-dimensional variables used in the pump only model for η_a

Name	Definition
Ri_2	Exit blade height / Impeller radius of curvature
Rot_{CA}	Average blade height *Shaft speed / Average meridional velocity at the inlet and exit
PHI_1	Impeller inlet inclination angle
AS_1	Blade aspect ratio at inlet
AS_2	Blade aspect ratio at exit

Figure 4-3 shows the model prediction of η_a compared to the values of η_a deduced from the test data. The model accurately captures the performance of most class 1 and 2 data in the range of 0.4 to 1.0.

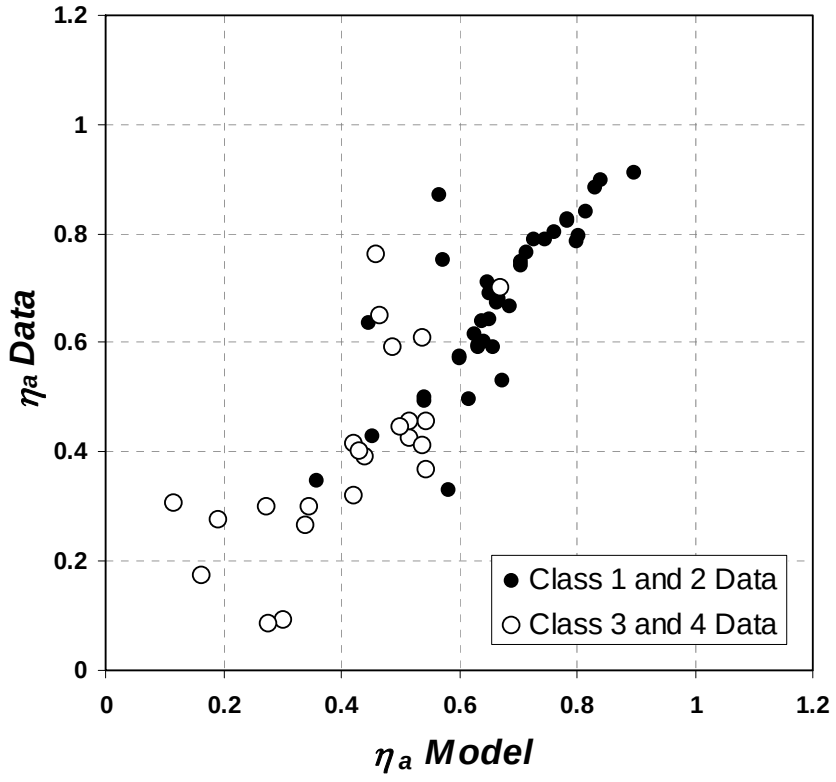

Figure 4-3: Regression results for the η_a pump specific model

The outliers that are under-predicted correspond to several different turbopumps and inducers. There is more scatter as η_a becomes small, but this is not a serious concern since most modern designs achieve higher values of performance. The final model matched the test data with an R^2 of nominally 0.74 and a standard error of approximately 0.11.

4.2 η_b Models

4.2.1 η_b Model for all Machines

An accurate model for η_b that can be applied to all machine types was developed using seven different independent variables. Equation 19 shows the final expression developed to model all types of machines. Table 4-3 defines the variables not previously defined in the text including two different calculations of Rossby number. The variables exerting the greatest influence in the prediction of η_b are the passage length to hydraulic diameter ratio, *L/D,* and the passage area ratio, $AR=A_2/A_1$, terms traditionally used in mapping diffuser performance. *L/D* and *AR* both appear multiple times in the expression, producing a coupled, non-linear affect. Two separate Rossby numbers also appeared to be significant. In each case the Rossby number was calculated based on ideal parameters. Traditionally Rossby number is defined using the actual flow velocity at the rotor exit. When using the TEIS/Two-Zone modeling system, the actual impeller exit state is closely related to the assumed value of η_b. A model of η_b should not be built on variables defined by the actual impeller exit state since these values are unknown when making a prediction. Using ideal parameters ensures that the result of the η_b model is independent

of the model inputs. Equation 19 shows the final model for η_b and is based only on 5 different geometric parameters and two different ideal flow parameters.

$$\eta_b = k_1\sqrt{{}^{L}\!/_{D}} - k_2\sqrt{A2/A1} - k_3\frac{\left(Ro_{W2i,R2}\right)}{\left({}^{B2}\!/_{R2t}\right)^{k_4}} - k_5\left(\frac{\left({}^{L}\!/_{D}\right)}{\left({}^{A2}\!/_{A1}\right)^{k_6}}\right) + k_7\cdot\ln\left(k_8 + Ro_{C2i}\right) \qquad \textbf{(19)}$$

$$- k_9\cdot{}^{ClrR}\!/_{B2} + k_{10}\cdot MT\cdot{}^{Clr}\!/_{B2} - k_{11}\cdot MT - k_{12}\cdot\frac{\left(Ro_{W2i,R2}\right)}{\left({}^{B2}\!/_{R2t}\right)}\left(\frac{\left({}^{L}\!/_{D}\right)}{\left({}^{A2}\!/_{A1}\right)}\right)^{k_{13}} - k_{14}$$

Table 4-3: Definitions of the non-dimensional variables not previously defined used in the η_b combined model

Name	Definition
$Ro_{C,2i}$	Absolute impeller exit velocity, ideal / (Shaft speed * Impeller radius of curvature)
Ro_{W2i}	Relative impeller exit velocity, ideal / (Shaft speed * Impeller radius of curvature)
MT	Machine type (1 Comp; -1 Pump)

The final model matched the class 1 and 2 test data with an R^2 of approximately 0.79 and a standard error of 0.149. Figure 4-4 compares the model prediction of η_b to the test data for values within the range of –1.5 and 1. Class 1 and 2 data are well represented by the model. The residuals for the low class data were reduced by a factor of four during the regression analysis to focus the model on the high class, level 1 and 2 data. This resulted in a larger error on average for the low class and low performance test data but this is not a concern since there is much greater uncertainty in actual values of η_b for the lower class data. Some of the low class data for pumps show significant error between the data and the model prediction, such as the point shown in the lower right of

Figure 4-4. Low class pump data typically contains the most uncertainty of all the cases in the database. Much of the low class pump data was collected from industrial machines where the quality of the design, manufacturing, and test procedure may be far below that of a typical laboratory test case. Therefore little attention was paid to these outliers since there was so much uncertainty in the data itself.

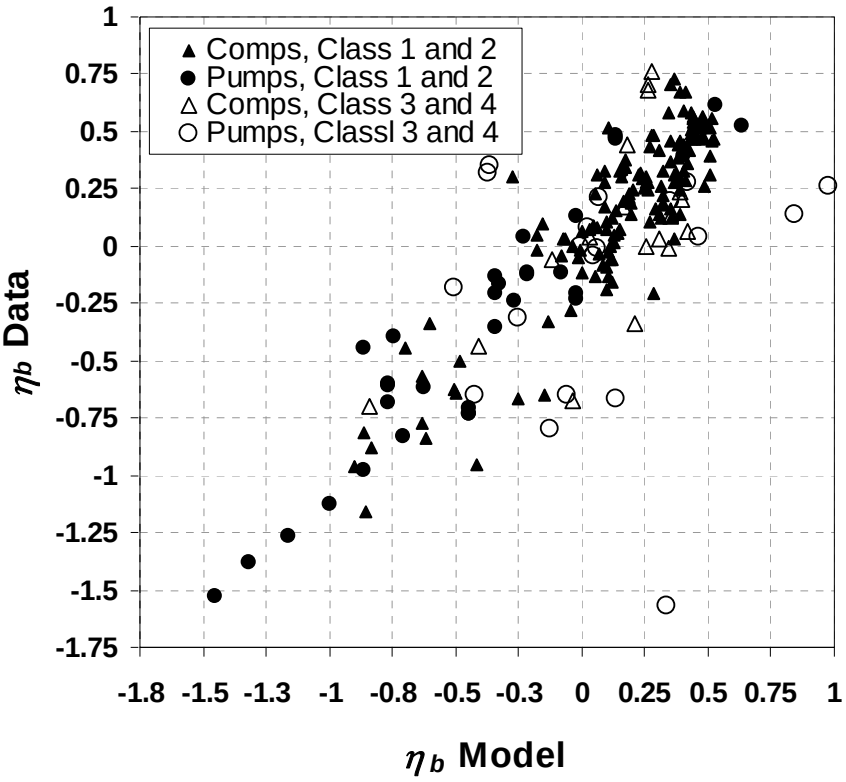

Figure 4-4: Regression results for the combined η_b model

4.2.2 η_b Model for Compressors Only

The combined model was used as a basis for developing models for specific machine types. The basic equation form and variables remained the same, but the

coefficients and exponents were allowed to vary. The η_b model for compressors only, as presented in Equation 20, uses only one less variable than the combined model. However, it is a much simpler expression. The R^2 of the compressor only model is approximately 0.83 and the standard error is nominally 0.144.

$$\eta_{b,comp} = k_1 \cdot {}^{L}\!/_{D} - k_2 \cdot A2/A1 - k_3 \frac{\left(Ro_{w2i,R2}\right)}{\left({}^{B2}\!/_{R2t}\right)^{0.252}} - k_4 \, {}^{ClrR}\!/_{B2} - k_5 \left(\frac{\left({}^{L}\!/_{D}\right)}{\left({}^{A2}\!/_{A1}\right)^{0.367}} \right) + k_6 \cdot \ln\left(Ro_{C2i}\right) + k_7 \quad \textbf{(20)}$$

Figure 4-5 compares the model performance to the test data. The class 1 and 2 data, solid black dots, are well matched and more scatter is seen in the lower quality data, represented by the open circles.

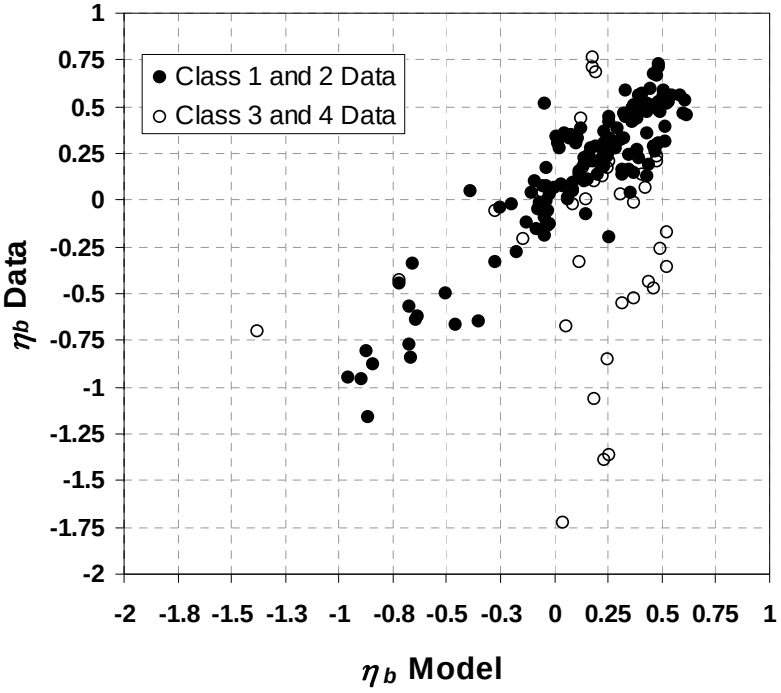

Figure 4-5: Regression results for the η_b compressor specific model

This difference in match quality is a result of the weighting that was applied to the data. The same weighting was used for the compressor only model as was used for the combined model. Data weighting was necessary to prevents the uncertainly in the low quality data from biasing the final model.

4.2.3 η_b Model for Pumps Only

The number of pump cases was relatively small, thus it was important to have the pump specific model based on the combined η_b model to ensure that it was statistically sound. The η_b model for pumps only, as expressed in Equation 21, is much simpler than the combined model. However, Equation 21 predicts η_b with similar accuracy as Equation 19.

$$\eta_{b,pump} = k_1\sqrt{L/D} - k_2 \cdot A_2 / A_1 - k_3 \cdot Ro_{w2pi,R2}^{k_4}\left(B2/R2t\right)^{k_5} - k_6 \cdot Clr_R/B_2 - k_7\left(\frac{\left(L/D\right)^{k_8}}{\left(A2/A1\right)^{k_9}}\right) + k_{10} \cdot \ln\left(Ro_{C2i}\right) + k_{11} \quad \textbf{(21)}$$

The most notable change between the η_b model for pumps and the combined and compressor only models is the change in sign of the exponent associated with B_2/R_{2t} in the third term. The model matched the test data with an R^2 of approximately 0.87 and a mean standard error of nominally 0.16. This is an improvement from the combined model where the standard error for pump cases was about 0.18.

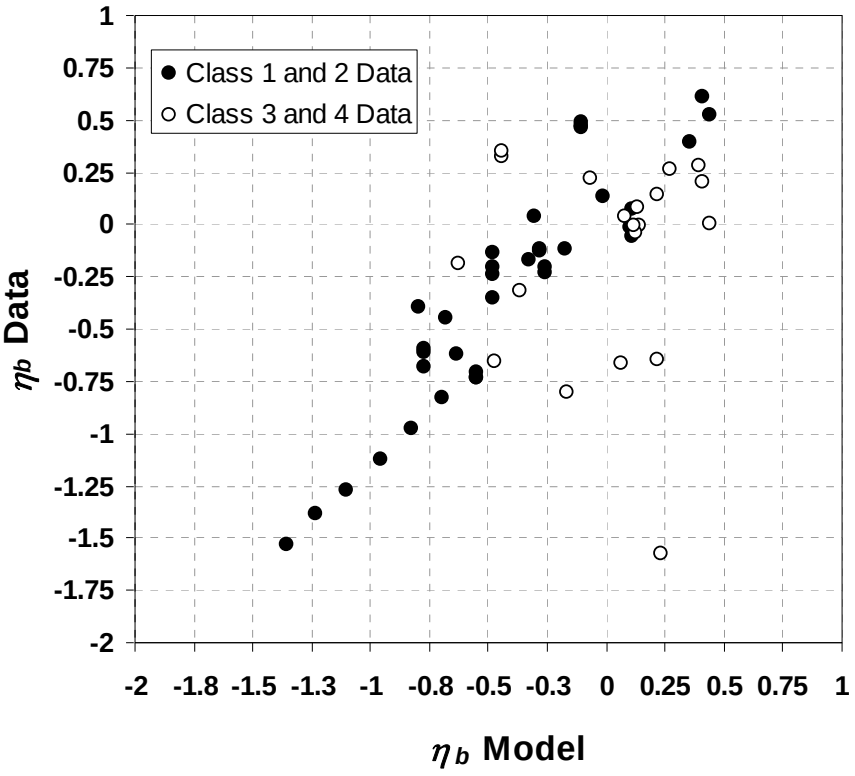

Figure 4-6: Regression results for the η_b pump specific model

4.3 Models for χ

4.3.1 χ Model at BIP

The model for χ was developed following the same procedure used for the other variables. The final model developed consists of six different variables organized into four separate terms, as shown in Equation 22.

$$\chi_{BIP} = \frac{1}{k_1\sqrt{Rot_{W1}} + k_2\sqrt{Ro_{W2}} - k_3 \cdot AR_{12}^{-0.2} + k_4} - \frac{k_5\left(\frac{A2}{A1}\right)^{k_6}}{\ln\left(1.1 + NS^{k_7}\right)} + k_8\left(\frac{Clr}{B2}\right) - k_9 \qquad (22)$$

The associated non-dimensional variables that have not been previously defined are given in Table 4-4. Three of the six variables are geometry based, and three are flow based.

Table 4-4: Variables used in modeling χ

Name	Definition
AR_{12}	Density * Pressure at impeller exit / (Density * Pressure at impeller inlet)
Rot_{W1}	Inlet blade height * Shaft speed / Inlet relative tip velocity

The final model yields an R^2 of approximately 0.69 with a mean standard error of nominally 0.09. Figure 4-7 shows the predictive model, Equation 22, compared to the BIP values of χ deduced from the database. Level 1 and 2 data are shown with solid dots and level 3 and 4 data are represented with open circles. While χ may theoretically range from 0 to 1, no cases in the database had a value greater than 0.95 or smaller than 0.01. So, when utilized as a predictive model, the expression is constrained to produce results within 0.01 and 0.95. The upper constraint is rarely encountered, while in practice the lower constraint does occasionally limit the model prediction. The lower constraint limits the prediction more frequently for pumps than compressors. Most of the scatter in the model prediction shows the actual value of χ is under-predicted, which could lead to an optimistic prediction of performance. A constant of 0.05 could be added to the model to produce a more conservative performance estimate.

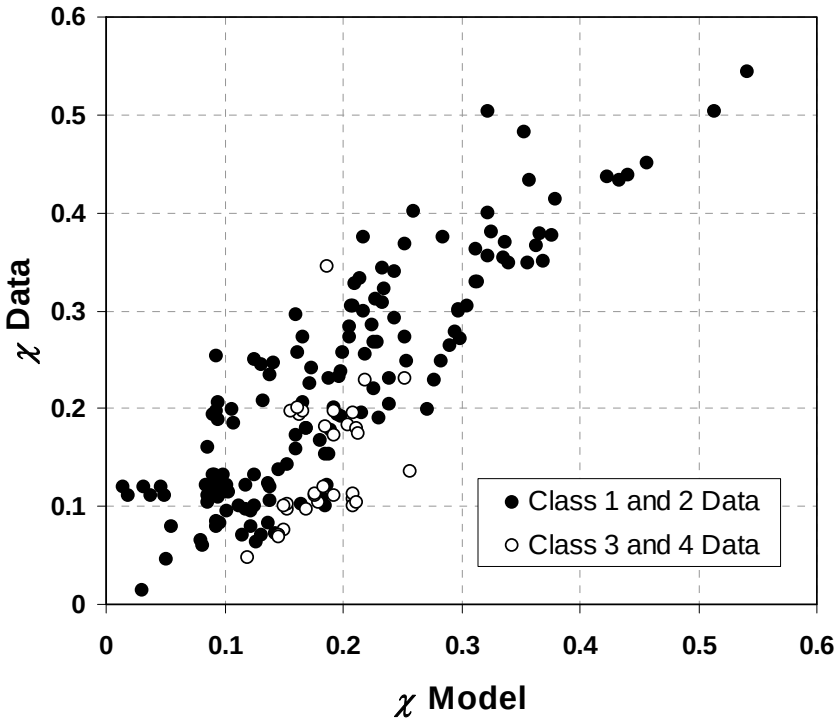

Figure 4-7: Regression results for the χ–BIP model

4.3.2 χ Model for Off-BIP Conditions

The off-BIP models were developed in an attempt to more accurately represent the loss mechanisms in an impeller. The complete development approach of the off-BIP χ model was detailed in section 2.3.1. Equation 23, shown below and presented earlier as Equation 15, was developed in the previously described manner using all available traverse data. The model increases the value of χ at off-BIP conditions as the inlet blade tip incidence, I_{It}, varies from the BIP value.

$$\chi = \chi_{BIP} + k_1(I_{1t} + \Delta I_{BIP})^2 - k_2\left(\exp\left(k_3 \cdot MR_2^5\right) - 1\right) \quad \textbf{(23)}$$

4.4 δ_{2p} Model at BIP

The final model for δ_{2p} at the BIP was also developed using the traverse data as described in section 3.2. The final developed expression is shown in Equation 24. It combines the BIP and off-BIP models presented earlier, Equations 12 and 14, respectively, into a single expression. It predicts the database values of $\delta_{2p,}$ Figure 4-8, with and R^2 of approximately 0.96 and represents the data with a mean standard error of nominally 1.10.

$$\delta_{2p} = -k_1 \exp\left[-k_2 \cdot (-\sin(\beta_{2b}))^{k_3}\right] - k_4 \exp(-k_5 \cdot S_2) - \exp\left(k_6 \cdot MR_2^5\right) + 2 \qquad \textbf{(24)}$$

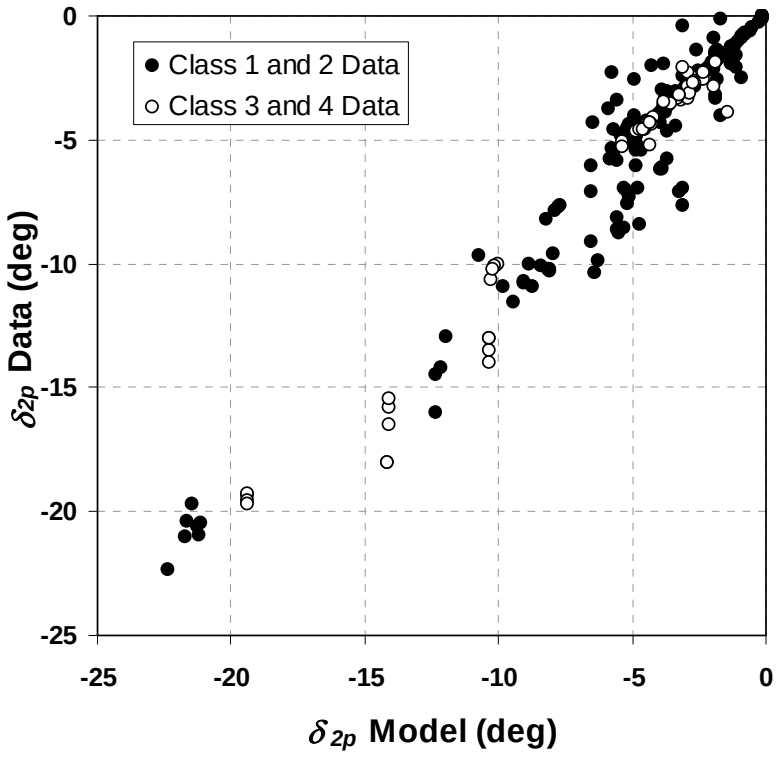

Figure 4-8: Regression results for δ_{2p} model compared to database values identified using EasyControl

The δ_{2p} model represents the test data more accurately than do the models for η_a, η_b or χ. This is expected since the bulk of the test data included in the database does not include traverses and required the value of δ_{2p} to be constrained in order to find a unique solution. As discussed in section 2.2.8, Equation 24 was used as the constraint when processing class 2 or lower level test data. The model is naturally a good representation of the deduced data since it was used as a guide in selecting a δ_{2p} in most cases.

4.5 Impeller Recirculation Loss (IRL)

Losses due to flow recirculation at the inlet or exit of the impeller must be correctly accounted for if the overall performance of the impeller is to be accurately modeled. Most well designed impellers have very little impeller recirculation loss (IRL) at the design point. All compressors and pumps will develop some recirculation at sufficiently high levels of incidence at off-design conditions. The actual magnitude of impeller recirculation loss cannot be correctly deduced unless all of the other losses are accurately modeled. Using the off-BIP models, Equations 23 and 24, produces a more accurate match of the actual impeller performance and consequently the calculated impeller recirculation loss is also more accurate.

Currently, no models exist for predicting the impeller recirculation loss. Most engineers assume a common loss profile for all machines that is representative of past experience. A set of models that can be used to predict the impeller recirculation loss has been developed in this work, and are presented below. These models were developed based on the understanding of how χ and δ_{2p} vary off-BIP as described by the traverse data. The impeller recirculation loss is modeled using two piecewise parabolas defined

by three control points, as shown in Figure 4-9. *PHIr* is the ratio of the mass flow at each control point to the flow rate at $C_{pa,i} = 0$, Equation 25. *Wbf* represent the magnitude of the impeller recirculation loss at each corresponding control point. The suffixes *Y*, *X* and *D* indicate the control points at the high, low and nominal and mass flow points, respectively. While a parabola may not be the best representation of the actual loss distribution in a machine, this approximation was made since there was insufficient data to better support any other theories.

$$PHIr = {}^{M}\!/_{M_{Cpai=0}} \tag{25}$$

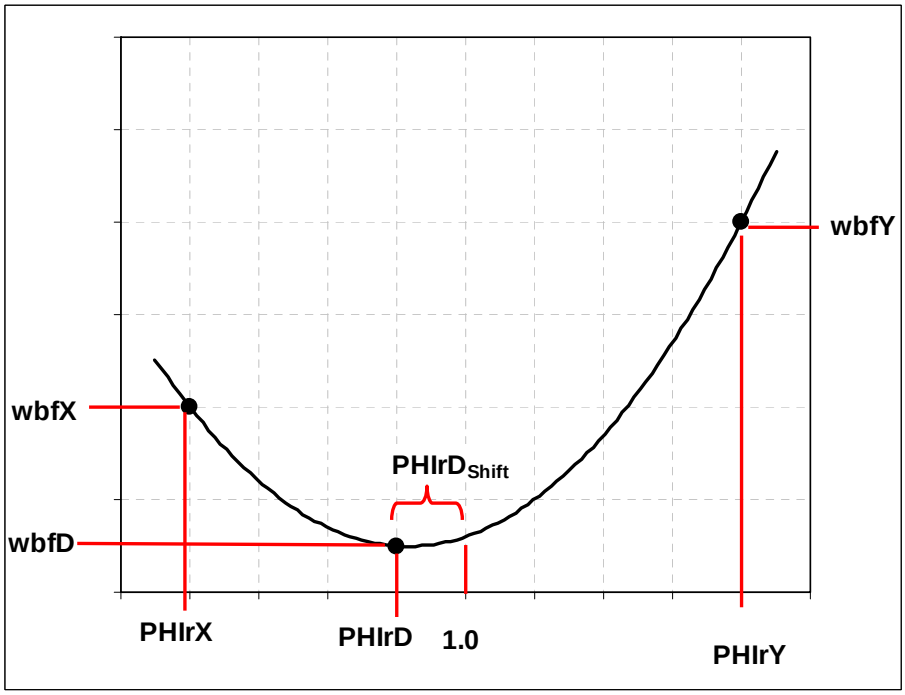

Figure 4-9: Graphical representation of variables used to define the IRL bucket

Accordingly, the point of minimum loss is assumed to be at *PhirD*. *PhirD* is approximately 1, where $C_{pa,i}$ and tip incidence are approximately *0*, although there may be a few percent variation. Equation 26 was developed following the same linear regression procedure detailed earlier, to model the point of minimum loss, *PhirD*. It contains three separate independent variables, Ro_{w2pi}, R_{1h}/R_{1t}, and exit solidity (S_R), defined in Equation 27. Figure 4-10 shows how the model for *PhirD* compares to the test results.

$$PHIrD = -k_1 \cdot Ro_{W2pi,R2}^{k_2} + k_3 \cdot \left(R1h/R1t\right)^{k_4} + k_5 \cdot Ro_{W2pi,R2} + k_6 \cdot S_R^{k_7} + k_8 \quad \textbf{(26)}$$

$$S_R = -\sin\left(\beta_{2b}\right) \quad \textbf{(27)}$$

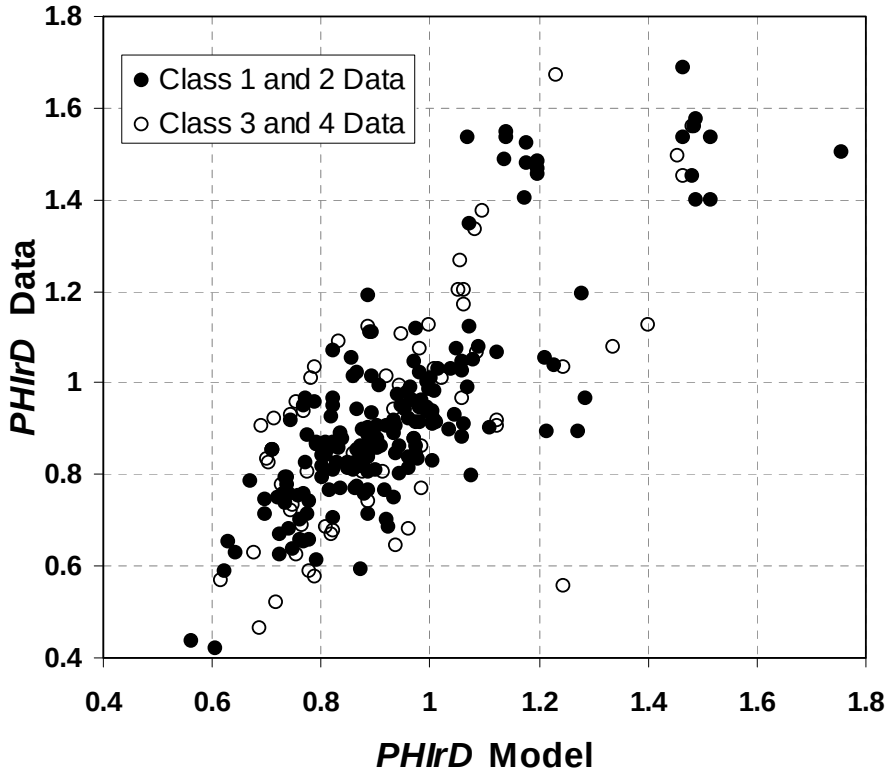

Figure 4-10: Regression results for *PHIrD*

Level 1 and 2 data are shown with solid dots and the class 3 and 4 data are shown with open circles. The data were weighted following the same procedure as was used for the other cases. The final model for *PhirD* is shown below in Equation 26, and the only previously undefined non-dimensional variable, S_R, is defined in Equation 27.

WbfD, or the level of minimum impeller recirculation loss, is set by the designer and should be near zero for most cases. Two empirical models were developed to predict the values of *wbfX* and *wbfY* at the specified setting of *PHIrX* and *PHIrY*, respectively. The model for *wbfX* is shown as Equation 28 and the individual terms in the expression are arranged in order of decreasing significance. The most important factors in the model are the rotation number, $Rot_{CAI,}$ and the difference between user specified value of *PHIrX* and *PHIrD*. The models for *wbfX* matched the test data with a mean standard error of nominally 0.09.

$$wbfX = k_1 \cdot Rot_{CA,i} + k_2 \cdot \left(PHIrX - PHIrD\right)^2 + k_3 \cdot S_1 - k_4 \cdot AS_1 - k_5 \cdot AR_a - k_6 + wbfD \quad \textbf{(28)}$$

The model for *wbfY*, Equation 29, predicts the magnitude of the impeller recirculation loss at high flow rates. It is very similar to the model developed for *wbfX*.

$$wbfY = k_1 \cdot Rot_{CA,i} + k_2\left(PHIrY - PHIrD\right)^2 - k_3 \, {}^{R1h}\!/_{R1t} - k_4 \cdot S_1 + k_5 + wbfD \quad \textbf{(29)}$$

The most significant terms in the model are the rotation number, Rot_{CAI}, and the difference between user specified value of *PHIrY* and *PHIrD* as was the case in Equation 28. The model for *wbfY* matched the test data with a mean standard error of nominally 0.03.

One additional application of the model for *PHIrD* (Equation 27) is in predicting the value of I_{BIP} used in the off-BIP χ model (Equation 15). While *PHIrD* represents the point where the impeller recirculation loss is a minimum, I_{BIP} is the location of the minimum value of χ for a given speedline. Although *PHIrD* is defined as the ratio of the flow rate at point of minimum impeller recirculation loss to design flow rate, and I_{BIP} is expressed in degrees incidence, they each model the same point of minimum loss. Therefore, Equation 30 can be used to calculate I_{BIP} from the predicted or model value of *PHIrD*.

$$I_{BIP}(\text{deg}) = \beta_{1b} - \tan^{-1}\left(PHIrD \cdot \frac{C_{M1t}}{\left(U_{1t} - C_{\theta 1t}\right)} \right) \qquad \textbf{(30)}$$

Figure 4-11 compares the deduced value of I_{BIP} to the inlet tip incidence at *PHIrD*, I_{PHIrD}. Some discrepancy exists between the value of I_{PHIrD} and I_{BIP} since they were calculated independently of each other within EasyControl. *PHIrD* was selected to match the IRL bucket while I_{BIP} was optimized to satisfy the objectives shown in Table 2-3. For most cases the comparison is very good, but some error can be seen at the extreme high and low values. This error arises since I_{BIP} was loosely constrained to be between –3 and +6° of incidence when calculated in EasyControl. This constraint was

set to ensure that no irrationally large offset values were deduced from the test data. This same constraint was used when predicting I_{BIP} from the *PHIrD* model, Equation 26.

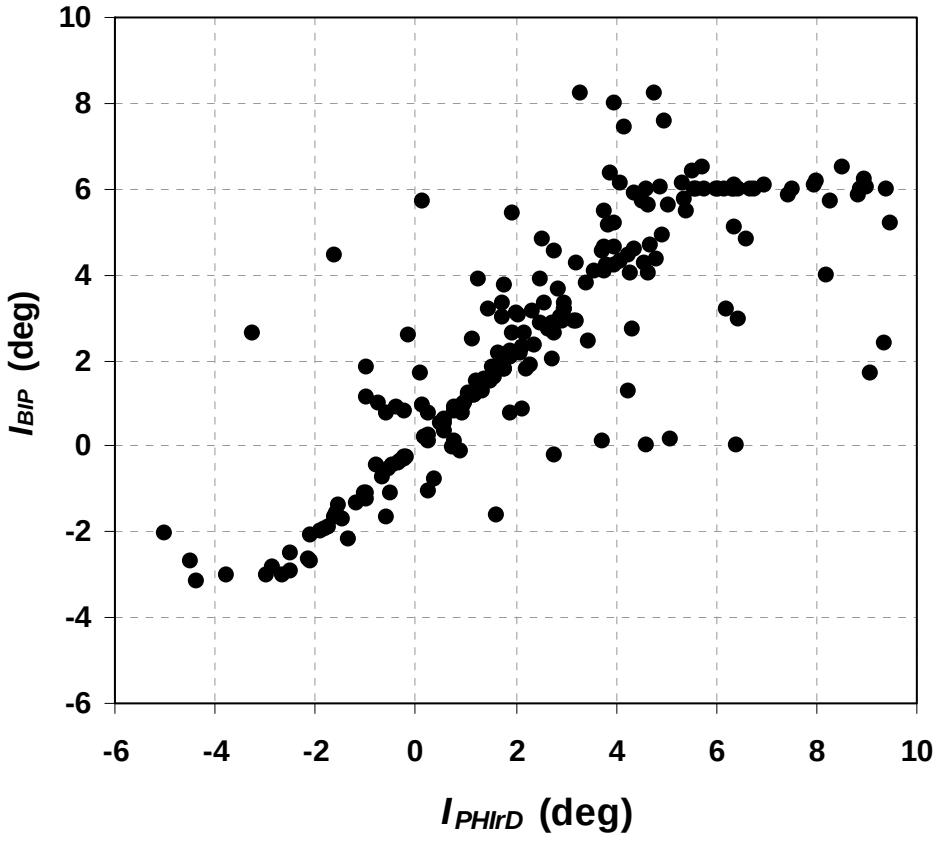

Figure 4-11: Inlet tip incidence at *PHIrD*, I_{PHIrD}, compared to I_{BIP}

4.6 Skin Friction

To make a performance prediction of a complete stage, the losses in the vaneless diffuser space must also be calculated. The Time-Cyclic diffuser model [22], and most others, requires the user to specify a model for the skin friction at the diffuser wall. An empirical model to predict the skin friction on the wall in a vaneless diffuser was

developed from the database. The resulting model for skin friction in a vaneless diffuser, Equation 31, is structured similar to classical expressions of c_f corresponding to flow over a flat plate. The model is applicable for any length diffuser processed with the time cyclic model. It can also be used with the Stantiz model, provided the diffuser is sufficiently long to have well mixed flow. Equation 31 shows the final model for diffuser skin friction derived from both pump and compressor tests.

$$c_f = \frac{k}{\mathrm{Re}_x^{0.3}} \tag{31}$$

It was recognized that the exponent in the denominator of Equation 31, of 0.3, is approaching what is commonly assumed in models of laminar flow, 0.5, and that a value of 0.15 – 0.2 would be more traditional for turbulent flows. This value was set solely based on the available test data and was not intended to imply anything about the flow structure entering the diffuser, although it is believed to be turbulent for most cases included in this research. Where the Reynold's number, Re_x, is defined in Equation 32. The velocity component is defined as the average of the inlet and exit diffuser velocities, C_{2m} and C_5.

$$\mathrm{Re}_x = \frac{\left(C_{2m} + C_5\right) \cdot s}{2 \cdot \nu} \tag{32}$$

The radial position, R_5, is used to calculate the approximate flow path length, s, shown in Equation 33. To estimate the flow path length also requires that the inlet flow angle, α_{2m}, be specified, Equation 34.

$$s = \frac{(R_5 - R_2)\sqrt{1 + b^2}}{b} \tag{33}$$

$$b = \frac{1}{\tan(\alpha_{2m})} \tag{34}$$

In traditional models of skin friction in turbulent flow over a flat plate the numerator is a constant. For diffuser data it was found that use of a constant numerator does not allow all of the test data to be matched sufficiently well. Figure 4-12, shows the local skin friction calculated in the vaneless diffuser as a function of R_5 for several different compressors. The legend details the case name given to each compressor when it was added to the database, followed by the shaft speed in rev/min. For example, the general distribution in c_f that results indicate that each case is in general similar, and somewhat approximated by Equation 32. The magnitude of c_f for each case can be more accurately matched by varying the numerator, k, for each specific case.

A change in the value of k shifts the c_f curve, predicted with Equation 31, up or down proportionally. Equation 35 predicts how k varies for different machines based on several additional terms that characterize the flow entering the diffuser. Seven variables are used in the final model.

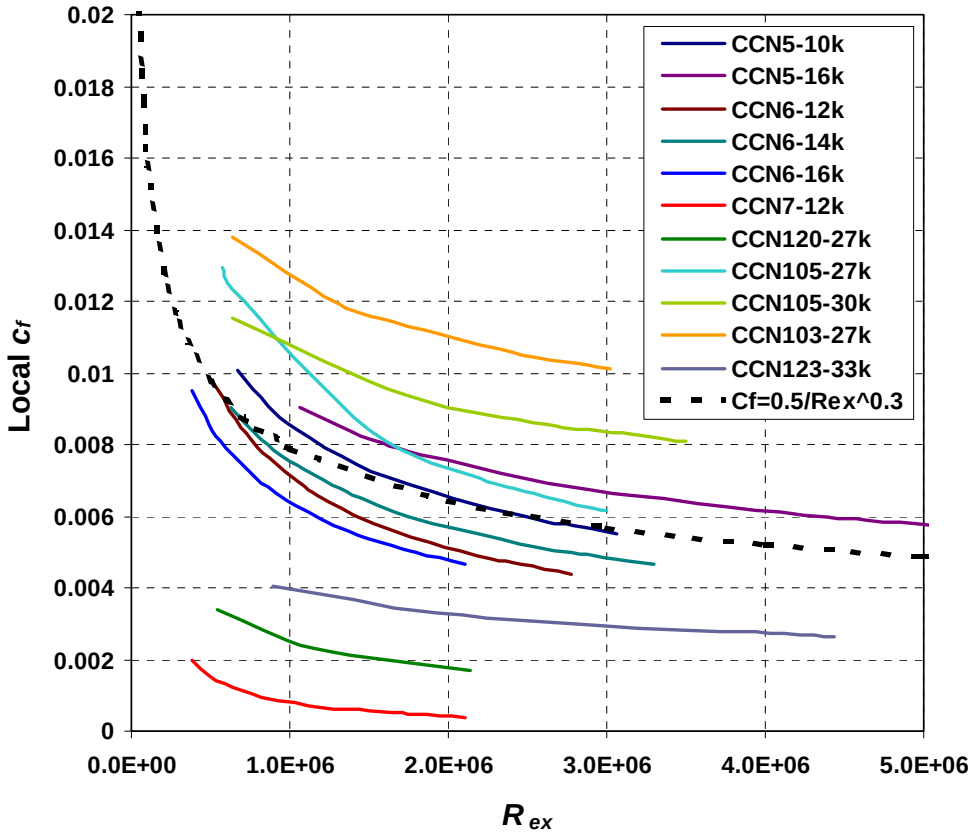

Figure 4-12: Calculated skin friction in the vaneless diffuser of several different centrifugal compressors

The most important variables in predicting the value of k are the impeller exit aspect ratio, AS_2 and s/b_2. The rotation number, Rot_{CA}, the secondary flow area ratio, ε, tip clearance to exit blade height ratio, $Clr/B2$, and the Mach number at the diffuser inlet, M_{2M}, are also included in the model.

$$k = k_1 \cdot AS_2^{\,k_2} \cdot \left(s/b_2\right)^{k_3} + k_4 \cdot Rot_{CA} - k_5 \cdot \varepsilon^{k_6} + k_7 \cdot \left(Clr/B2\right)^{k_8} - k_9 \cdot S/B2 + k_{10} \cdot M_{2m}^{k_{11}} - k_{12} \qquad (35)$$

Since class 3 and 4 data does not include a measured pressure at the impeller exit, P2, the impeller performance cannot be separated from the diffuser. Without a measured P2 the value of skin friction cannot be accurately deduced from the test data. To avoid the error of building the model on inaccurate data, cases without a P2 were not included in the regression analysis. Figure 4-13 shows the results for both sets of data. The model for k matches the Level 1 and 2 test data with an R^2 of approximately 0.75. The error in matching the low quality data is much larger, but the model still predicts reasonable values for all cases in the database. The lack of a P2 in the low class data is a critical weakness when developing models.

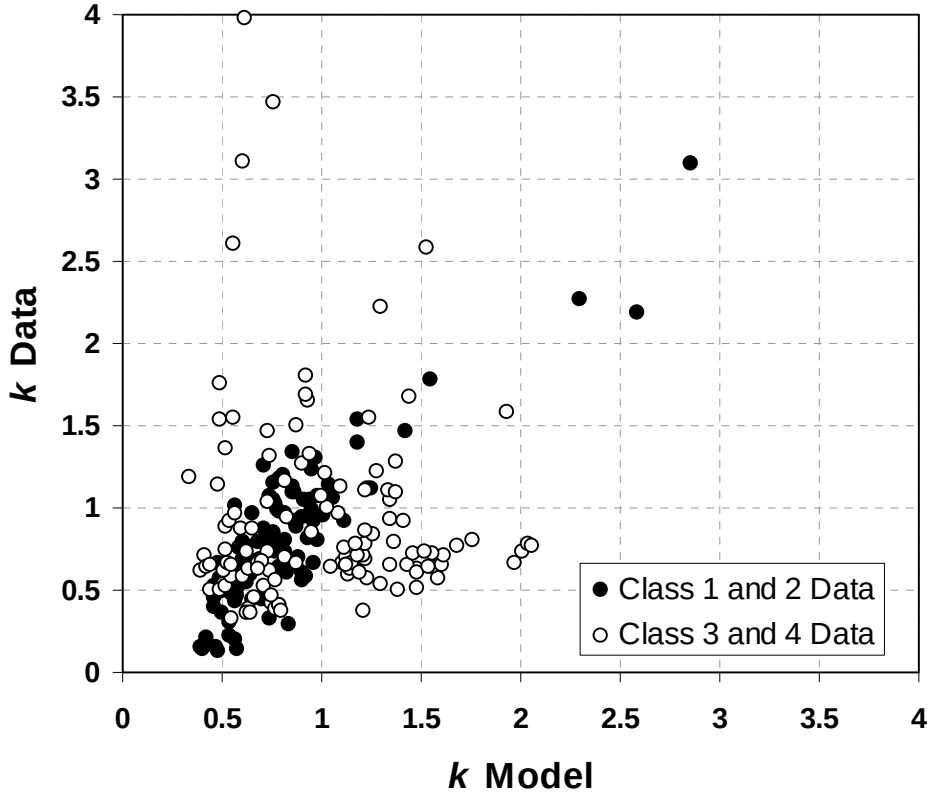

Figure 4-13: c_f Regression model results

4.7 Validation of Predictive Equations

4.7.1 Impeller Diffuser Ratio, DR_2

A first validation that should be performed is to ensure that the system of predictive equations can accurately calculate the actual diffusion ratio (DR_2) at the BIP. Predicting a correct value of DR_2 is critical to accurately modeling the stage efficiency and pressure or head rise. Figure 4-14 shows the value of DR_2 calculated from the models developed during this project compared to the actual values obtained from the measured test data.

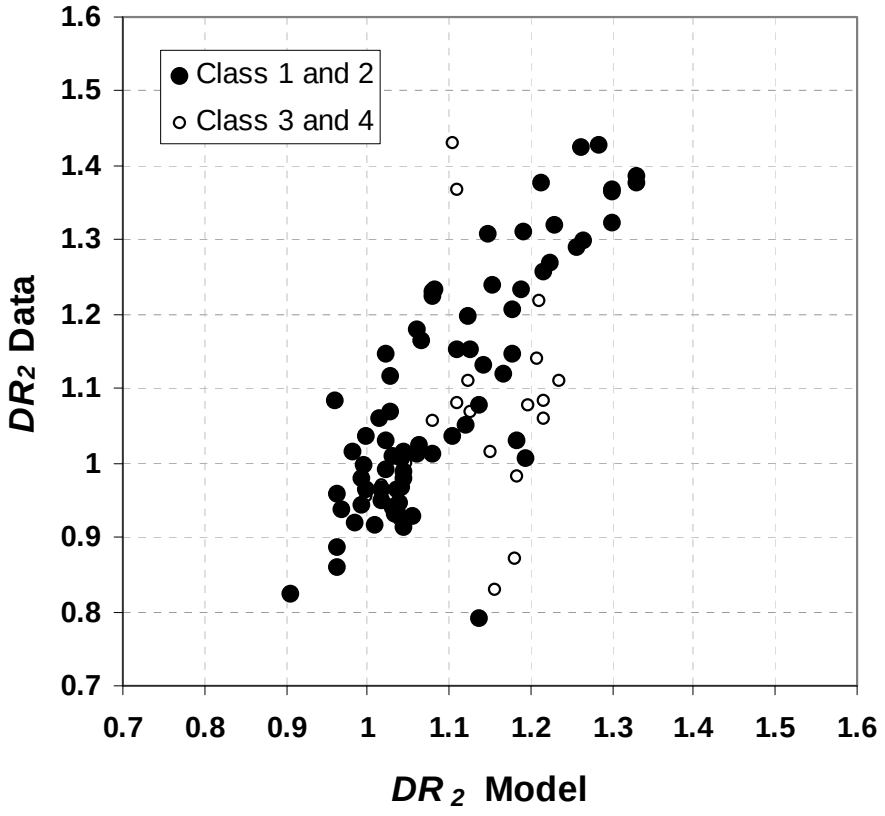

Figure 4-14: Predicted DR_2 compared to measured values

The models produce a reasonable match of DR_2 within the range 0.9 to 1.35. The predicted value of DR_2 matched the measured value with an R^2 of approximately 0.7 and a mean standard error of nominally 0.06. The level 1 and level 2 data is well predicted for almost all cases. The class 3 and 4 data show significantly more scatter, and make up the bulk of the outliers.

4.7.2 Comparison to State-of-the Art

Current state-of-the-art (SOA) modeling uses a combination of the Enhanced TEIS model to predict η_a and η_b, and single variable empirical models for χ and δ_{2p}, Figure 2-6. Predictions made using SOA modeling have been compared to those made with the models developed during this study. Table 4-5 summarizes the accuracy of the separate modeling approaches for predicting the TEIS and Two-Zone modeling parameters. Table 4-5 contains a row for each of the TEIS and Two-Zone modeling parameters, η_a, η_b, χ and δ_{2p}. The two columns compare the average error in predicting the modeling parameters for the database cases using the newly developed predictive models compared to the current SOA models.

For the TEIS parameters a significant improvement was realized using the new models compared to the older Enhanced TEIS models. The average error for η_a was reduced from 0.127 to 0.088 or approximately 30%. An even greater improvement was made for predicting η_b. The SOA models produced an average error of 0.616, and with the new model the average error is only 0.162. This corresponds to a 70% reduction in prediction error. One reason that such a dramatic increase in the prediction capability of η_b was realized is because the older Enhanced TEIS model uses a single value of η_b to

model an entire stage. The new model, Equation 19, allows the value of η_b to vary with speed and flow characteristics to better match the test data.

Table 4-5: Performance of the new models compared to SOA predictions

	Average Error	
	SOA models	New Models
η_a	0.127	0.088
η_b	0.616	0.162
χ	0.080	0.081
δ_{2p} (deg)	2.00	1.13

While the Enhanced TEIS model seemed to produce sensible predictions for some cases, in others it performed very poorly. This is likely because it was developed based on a significantly smaller dataset, thus the resulting models may be unstable if any of the input parameters are outside of the validated range. A much larger and more diverse database was used in developing the new models that increases the statistical confidence in the resulting equations.

Using the SOA method for calculating δ_{2p} according to exit blade angle, the average prediction error was only 2º. While this is generally an acceptable level of error, the new model further reduced it to just above 1º on average. A much less noticeable improvement was made in modeling the χ at the BIP. The new model for χ was no more accurate than the simple model based only on specific speed. There are several possible explanations for why an improvement was not seen. First, for most cases the simple model predicts a value of χ equal to 0.2 and the average value of χ found in the test data is 0.21 with a standard deviation of only 0.12. Since there is not much range in the bulk of the test data the simple model can adequately predict it for most cases.

Second, the values of χ used in building Equation 26 were deduced from the test data using EasyControl. Only in cases with traverse data could a value of χ be accurately determined. In all other cases, the majority of the database, the solution was constrained using the model for δ_{2p}, Equation 12, to allow a unique solution to be found. Consequently any error in the δ_{2p} model will increase the error in predicting χ. Fortunately the overall performance prediction is dominated by η_a and η_b. So some error in χ can be tolerated without significantly reducing the accuracy of the overall performance prediction.

4.7.3 Prediction Performance and Comparisons

The cases in the original database have been re-analyzed using the new models for η_a, η_b, χ, δ_{2p}, *IRL* and c_f to verify that they perform as intended when solved together inside the meanline code. The performance comparisons were made using the meanline codes Compal and Pumpal. The models for η_a, η_b, χ, δ_{2p}, *IRL* and c_f were solved simultaneously and the resulting modeling coefficients were used by the meanline code to predict the performance. An iterative approach was necessary; since, as the modeling coefficients changed, so did some of the model inputs. For example, the equation for χ includes the dimensionless specific speed, *NS*. The specific speed is a function of head rise, which is strongly dependent on η_b. Therefore, different values of η_b correlate to a different prediction of χ. So, the variables in the individual models had to be carefully selected to ensure that the final system of equations would converge. The validation cases demonstrated that the models converged quickly and reliably for all types of machines. Validation cases included those used in the initial model building since the

resulting prediction of each individual variable will change based on difference in the flow parameters calculated with these variables.

Following this approach, performance predictions were made for all of the machines in the original database, and a few additional cases that were not used in model building. The combined pump and compressor model was used to predict η_a and η_b for all cases, unless otherwise noted. The results of several of these tests are presented in this section. The same basic performance parameters were evaluated in the validation effort as were considered in the overlay and compare procedure used to deduce the modeling variables. This included DR_2, which illustrates how well η_a and η_b have been predicted. Power, stage efficiency and pressure ratio are also presented since they are usually design goals. The rotor efficiency is also shown to differentiate the performance of the models for the impeller compared to any downstream elements.

The first case, Figure 4-15, is an open centrifugal impeller that was included in the original database. A cartoon cross-section of the stage is shown in the lower right pane. The impeller is shown in red, and the diffuser is shown in blue. The reduced test data is shown as solid symbols and lines. The model prediction is displayed with dashed lines and open symbols. The models do an adequate job of matching the important design parameters and they produce a good match of the overall machine performance. The models matched the measured DR_2 curve, which indicates that the prediction of η_a and η_b is accurate. The trend in stage pressure ratio with flow rate is well captured, although the predicted magnitude is about 2.5% low. Stage power is also predicted reasonably well at the low speeds with error becoming more apparent at the higher

speeds. Some error exists in the prediction of stage efficiency at the off design conditions, but the peak value is predicted within 1% of the measured value.

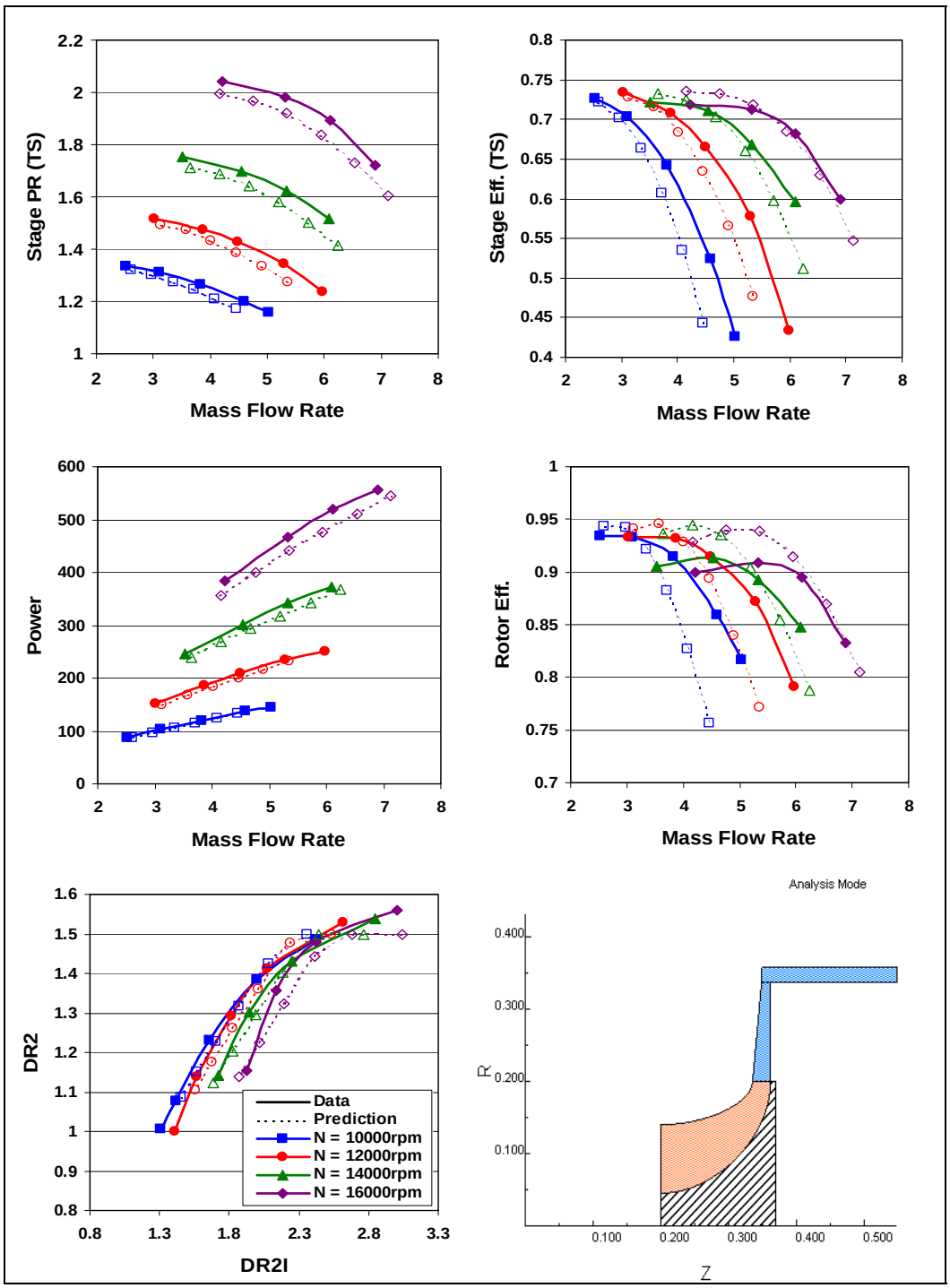

Figure 4-15: Performance prediction of a radial compressor case that was included in model building

Figure 4-16 contains four additional plots detailing additional measures of stage performance. In the lower right pane the predicted impeller pressure ratio is shown to match the test data very well. The prediction of impeller recirculation loss follows the general trend of the test data. The data for the higher speedlines shows that the IRL is 2-3 points above zero at the minimum. The model assumes that each speedline has a minimum at zero. This difference contributed to the error in the predicted rotor efficiency seen in Figure 4-15.

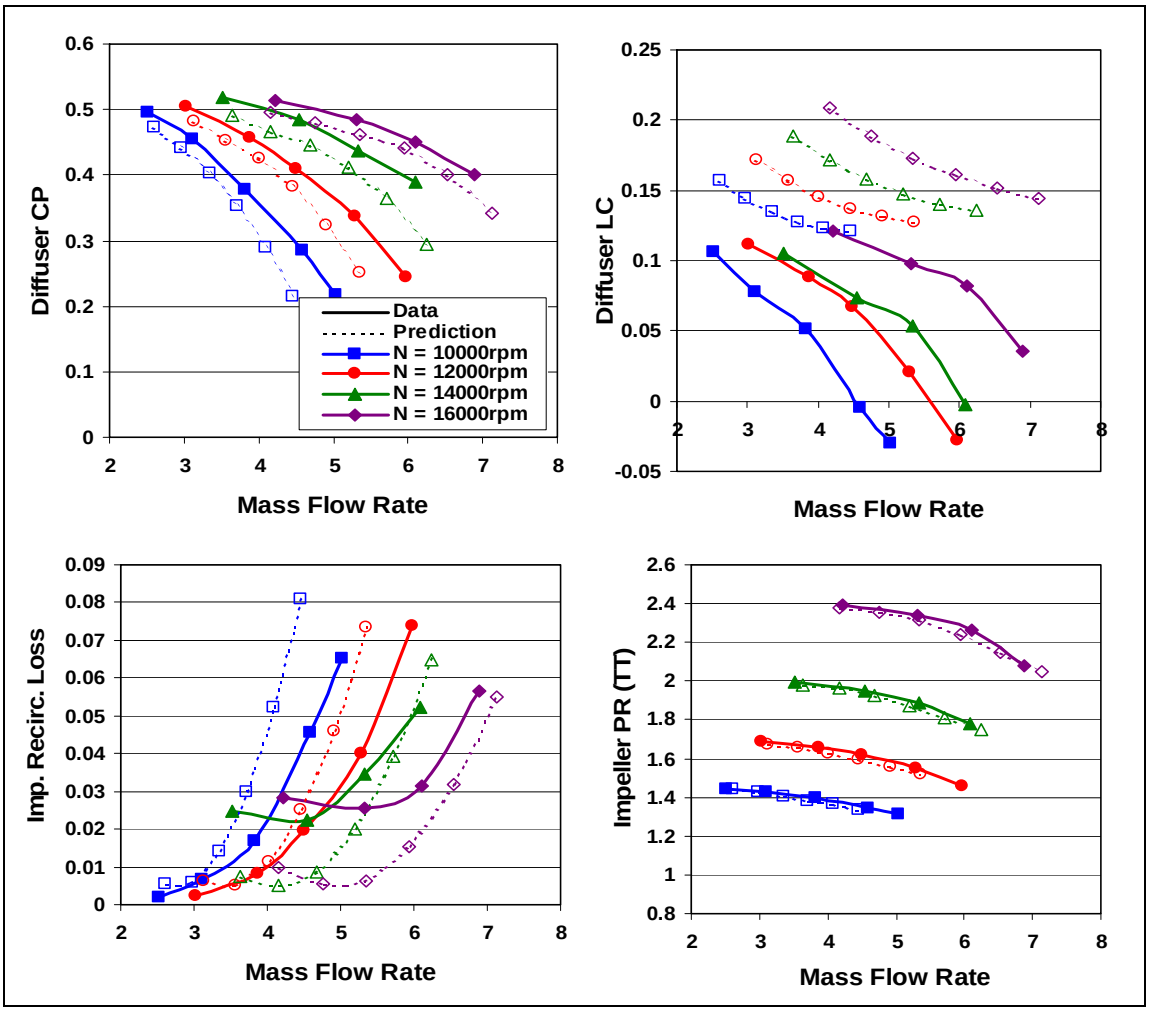

Figure 4-16: Additional performance calculations of a radial compressor case that was included in model building

The upper right and left panes show the diffuser loss and pressure recovery coefficient, *LC* and *CP*, respectively. *LC* is defined as the total pressure drop through the diffuser divided by the inlet total pressure minus the inlet static pressure. *CP* is defined as the static pressure rise through the diffuser divided by the inlet total pressure minus the inlet static pressure. For this case the diffuser losses are slightly over-estimated, resulting in an under-prediction of the stage pressure ratio. Some error exists in the prediction of LC and CP, which are based on a constant c_f value, although this modeling coefficient may vary with flow.

The second case considered for comparison is also a centrifugal impeller that was included in the database used for model development. Figure 4-17 shows the same set of plots that were presented for the previous validation case. Again, the reduced test data is shown as solid symbols and lines while the model prediction is displayed with dashed lines and open symbols. From the plot of DR_2 and $DR_{2I,}$ in the lower left, we can determine that η_a has been accurately predicted since the slope is approximately correct. It is also evident that η_b has been slightly over predicted since the predicted value of DR_2 is higher than the test data indicates. The error in η_b appears to be most significant for the lower speedlines. However the magnitude of error is relatively small, less than 0.05, so the overall performance prediction is still quite accurate. The upper left plot, in Figure 4-17, show that the overall stage pressure ratio data was well matched for all operating speeds by the new models. This would not have been possible without allowing η_b to vary between speedlines, as the new η_b model allows. The combined model for η_b has shown that it typically produced results that follow the observed trend of decreasing η_b at off-design speeds. In the upper right pane is a plot of stage efficiency vs. flow rate. The

position of peak efficiency is accurately modeled, but the magnitude is underestimated by 2% to 4%.

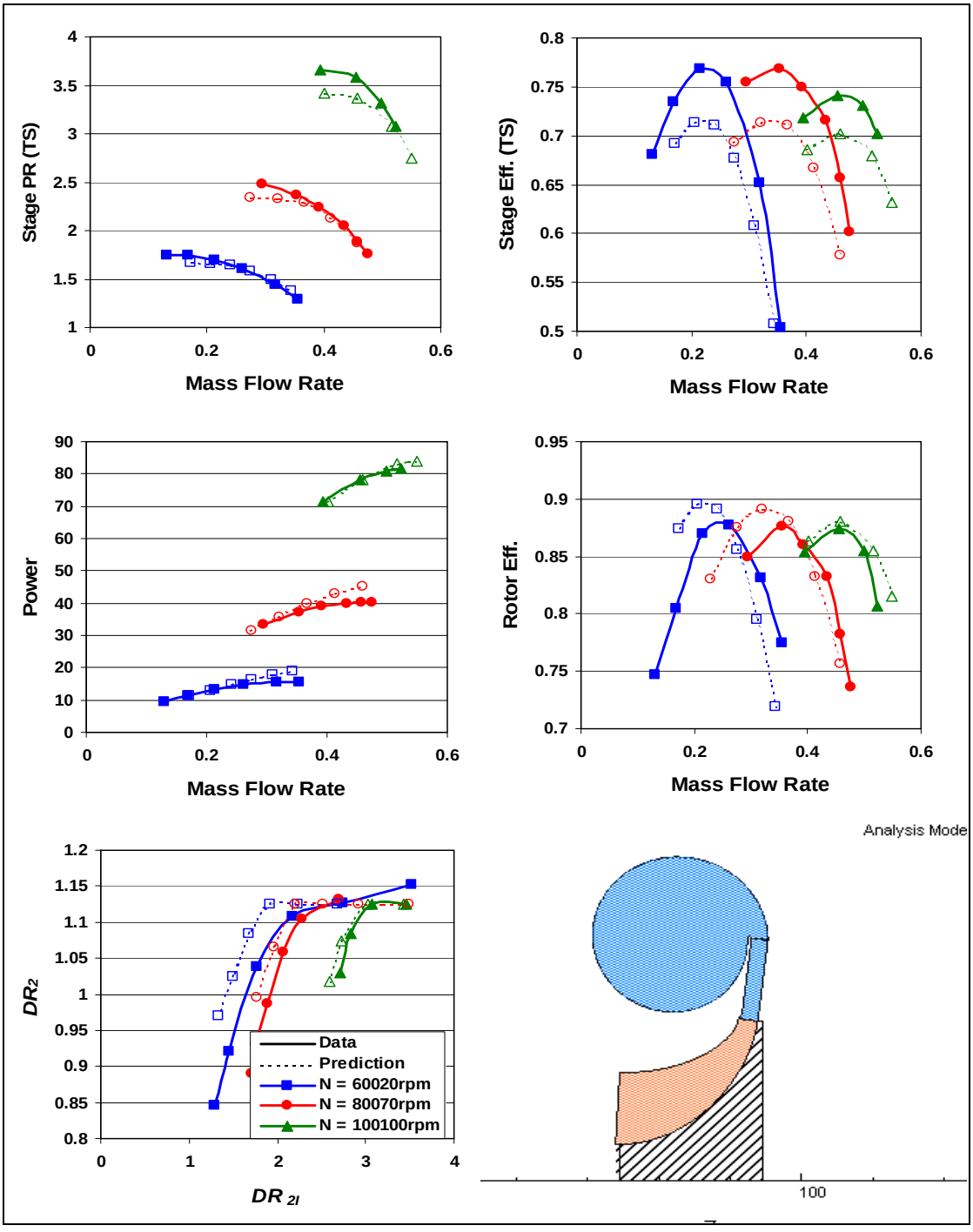

Figure 4-17: Prediction of a radial compressor performance for a case included in model building

Although stage efficiency is under-predicted, the rotor efficiency is over-predicted. Figure 4-18 shows plots of four additional performance parameters that help identify the cause of the error in prediction of stage performance. In the lower left pane the impeller recirculation is shown. In this case, the minimum point on the model bucket closely matches the flow rate where the minimum losses in the data were measured and the magnitude of the losses is correct.

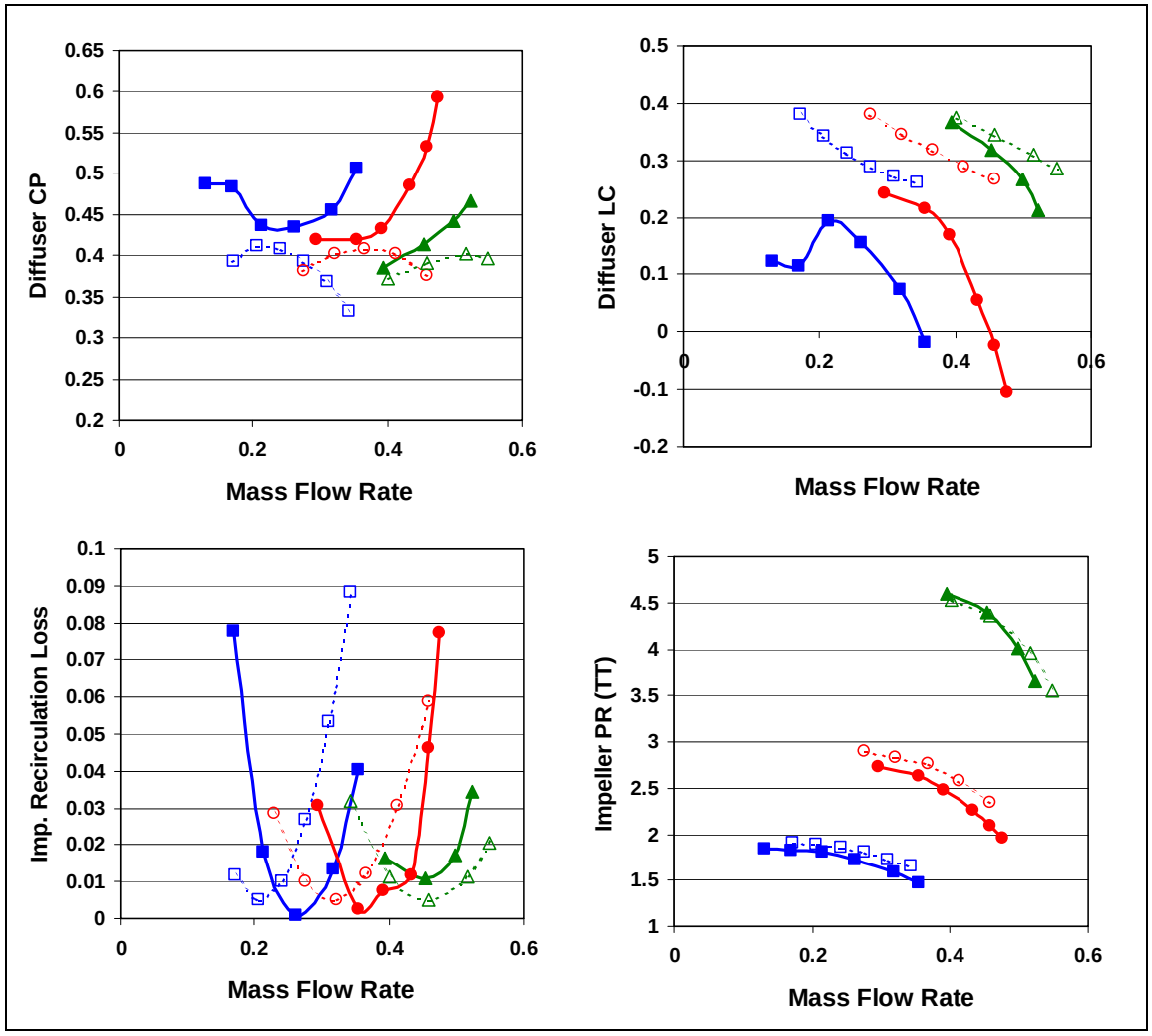

Figure 4-18: Additional predictions of the performance of a radial compressor case included in model building

In the lower right pane the impeller pressure ratio is plotted. The model prediction over-predicts the pressure ratio by about 5%, which is similar to the error in prediction of DR_2. In the upper left pane is a plot a diffuser pressure recovery, *CP*, and in the upper right pane is shown the corresponding loss coefficient, *LC*. The *LC* is significantly over-predicted, due to the model over prediction of c_f, which results in a low prediction of stage efficiency.

Figure 4-19 shows the combined models prediction for a covered pump. This case was included in the database and was used in model building. The same set of variables as those shown for the first two cases are shown again here. Although in this case, the stage pressure ratio plot has been replaced with a plot of total dynamic head, *TDH*, a common measure of pump performance. Again the data is shown with solid lines and the prediction with dashed lines. In the lower left is a plot of DR_2 vs DR_{2I}. Since the model matched the slope and magnitude of the DR_2 curve we can assume that η_a and η_b were accurately predicted. The DR_{stall} value was set manually to match the test data at high values of DR_2. The peak stage and rotor efficiency is predicted within about 1% of the actual value, but the model slightly under-predicts the level of efficiency at low flow. The upper left plot shows that the slope of the head rise curve, *TDH*, is well matched and only about 5% error at the highest and lowest flows. The predicted power, middle plot on the left, shows the correct magnitude, but the slope of the curve does not exactly match the measured data. This error corresponds to the error in the predicted rotor efficiency of off-BIP conditions.

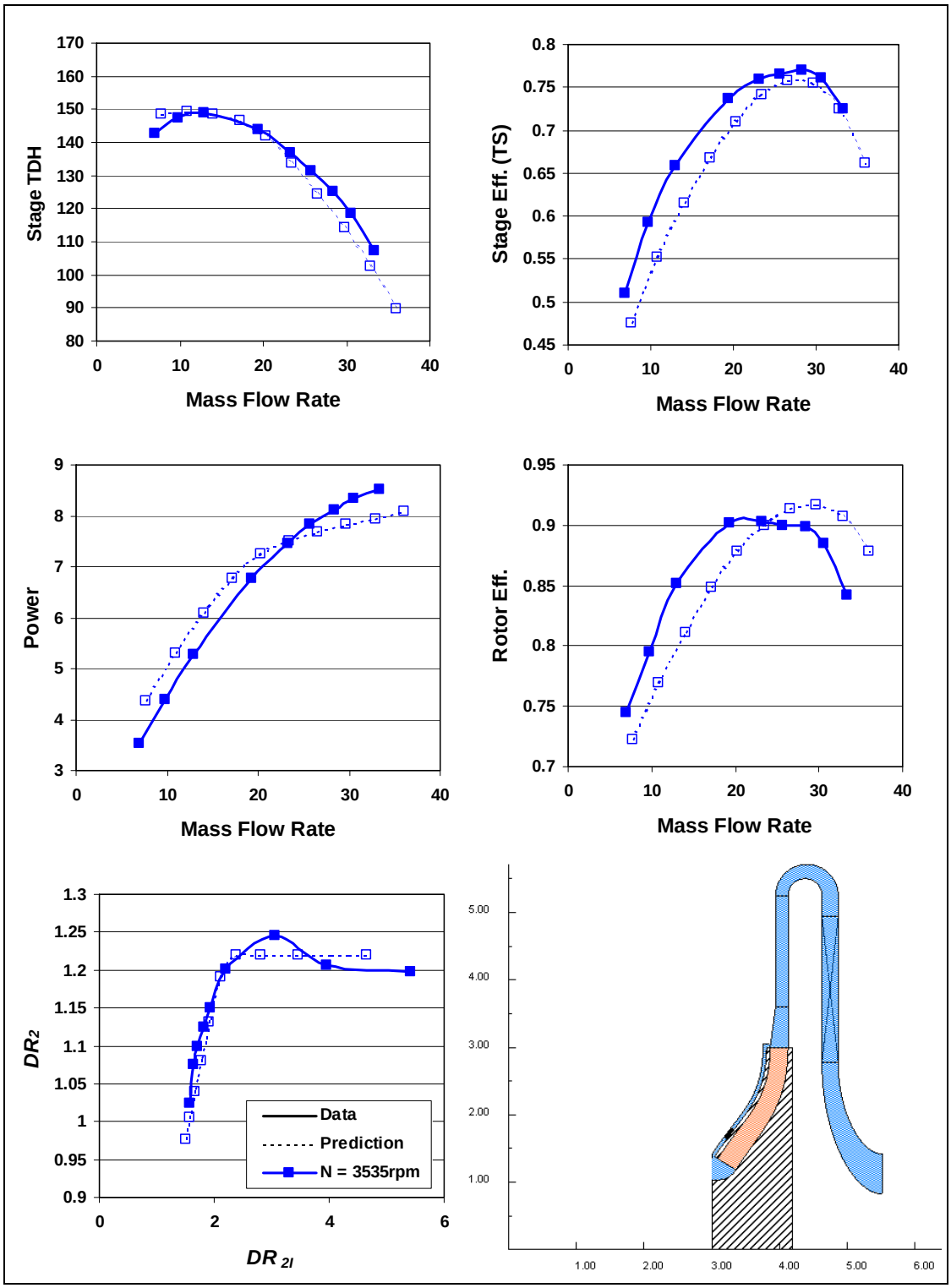

Figure 4-19: Performance prediction of a radial pump case that was included in model building

As with the other validation cases, four additional plots of stage performance are included in Figure 4-20. The impeller head rise is matched within 10% of the test data. The diffuser *CP* and *LC* are calculated from the impeller exit to the entry of the 180º bend. The losses in the first diffuser are slightly over estimated, resulting in an under-prediction of the stage total-to-static efficiency, seen in the upper right pane of Figure 4-19. The magnitude of the impeller recirculation loss is well modeled, lower left pane, but the bucket is shifted slightly to higher flow than seen in the test data. This shifts the predicted peak rotor efficiency to a higher flow rate too.

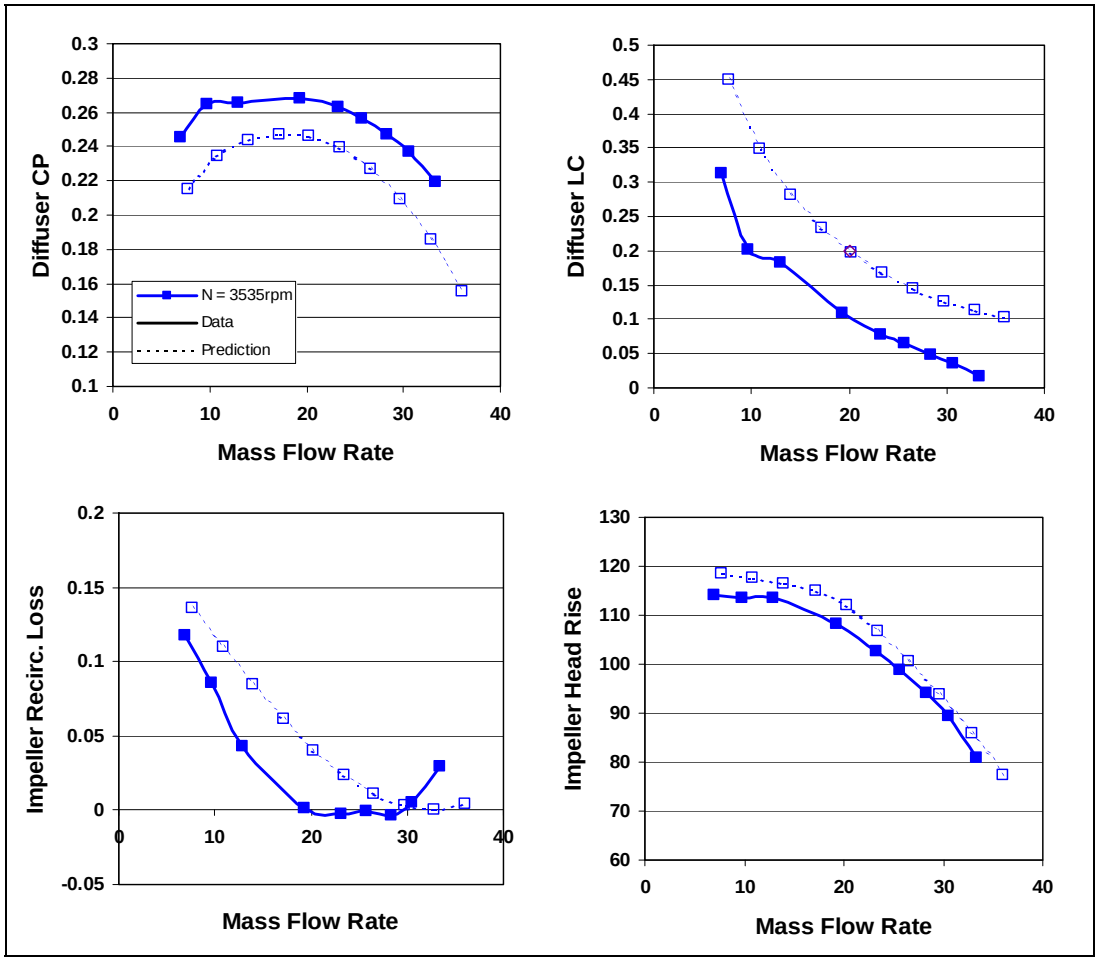

Figure 4-20: Additional performance predictions of the radial pump shown in Figure 4-19

The case compared in Figure 4-21 was not included in the database from which the models were developed. This case is an unshrouded radial compressor with a specific speed of 0.97 and was tested with an unpinched vaneless diffuser and a collector. Data from three separate speedlines has been reduced and compared to model predictions. The plot of DR_2 vs. DR_{2I} shows that the models significantly under-predict the level of DR_2. Since the slope of the DR_2 data is accurately matched, the prediction of η_a is approximately correct. While the slope is correct the magnitude of DR_2 is incorrect, which implies that the prediction of η_b is low. The error in η_b seems to increase with increasing speed, and the error in DR_2 is greatest at the highest speedlines. The models yield a prediction of the peak rotor efficiency that is within 1% of the measured value for all but the lowest speedline. The error in predicted stage efficiency is slightly worse than for the rotor alone. While the peak efficiency is well matched at the middle speedline, it is off by +2% and -2% at the low and high speedlines, respectively. At the low and mid speedline the pressure ratio, shown in the upper left, is predicted within 5% but the error is much larger at the highest speedline due to the error in η_b at for these points.

The model prediction of four additional performance measures are shown in Figure 4-22, and compared to the measured data. In the upper right and left panes, respectively, the diffuser *CP* and *LC* are shown. The data for this case shows much higher losses than the model predicted. One possible reason that the losses are larger than predicted is because the diffuser is unpinched, which is not common and was not a layout that was included in the database that the c_f model was developed from. The impeller recirculation loss is compared to the test data in the lower left pane. Again, the magnitude is approximately correct, but the minimum point is not well predicted.

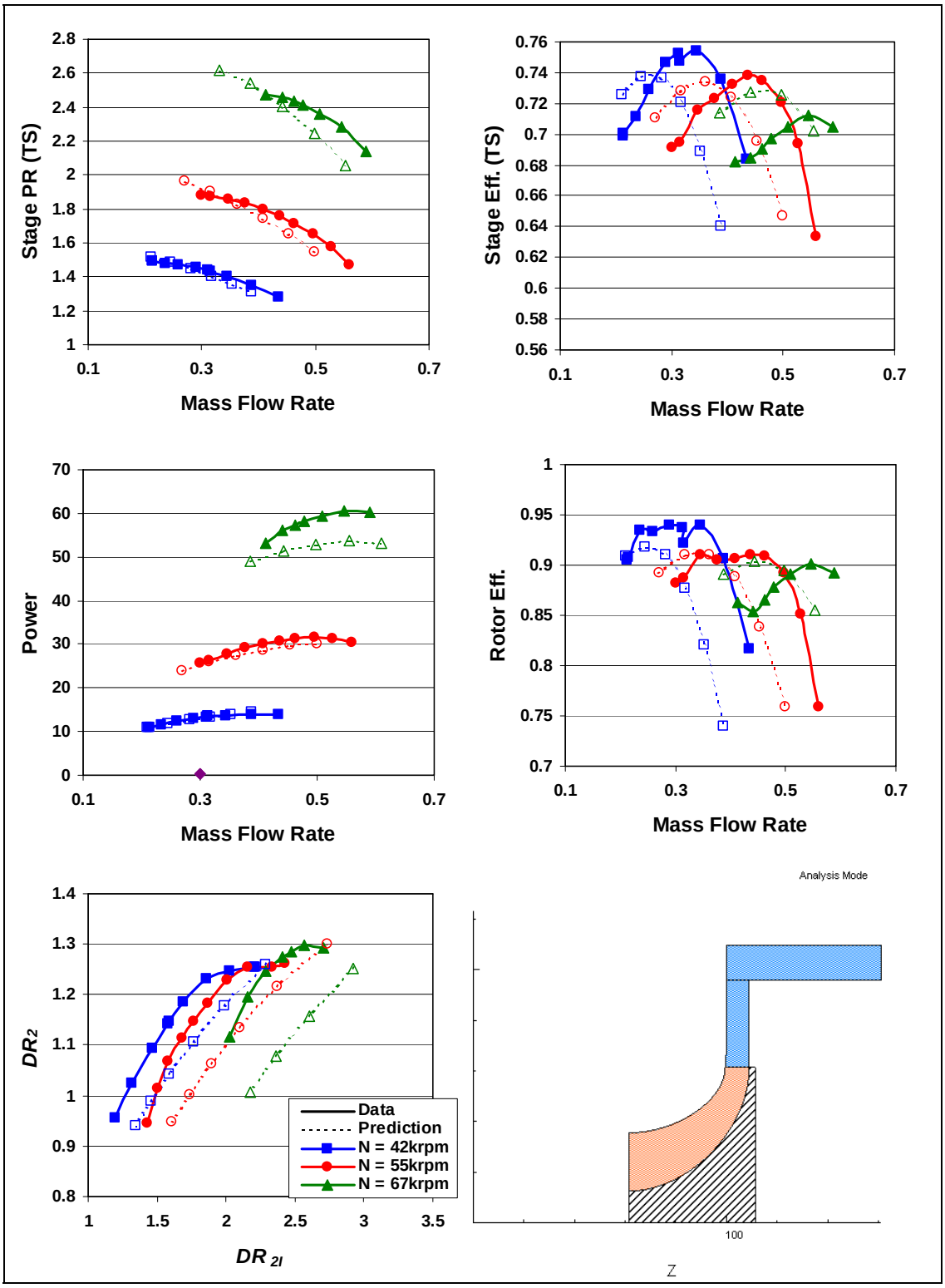

Figure 4-21: Performance prediction of a radial compressor case that was not included in original database

The last comparison plot shown in Figure 4-22, impeller pressure ratio, is shown in the lower right pane. For the lower two speedlines the model produces and acceptable prediction of the pressure rise. For the highest speedline the error becomes much larger. This same trend can be seen in the plot of DR_2 vs. DR_{2i}, show in the lower left of Figure 4-21. The error in DR_2 is directly due to errors in the prediction of η_a and η_b, which are most severe at the highest speed.

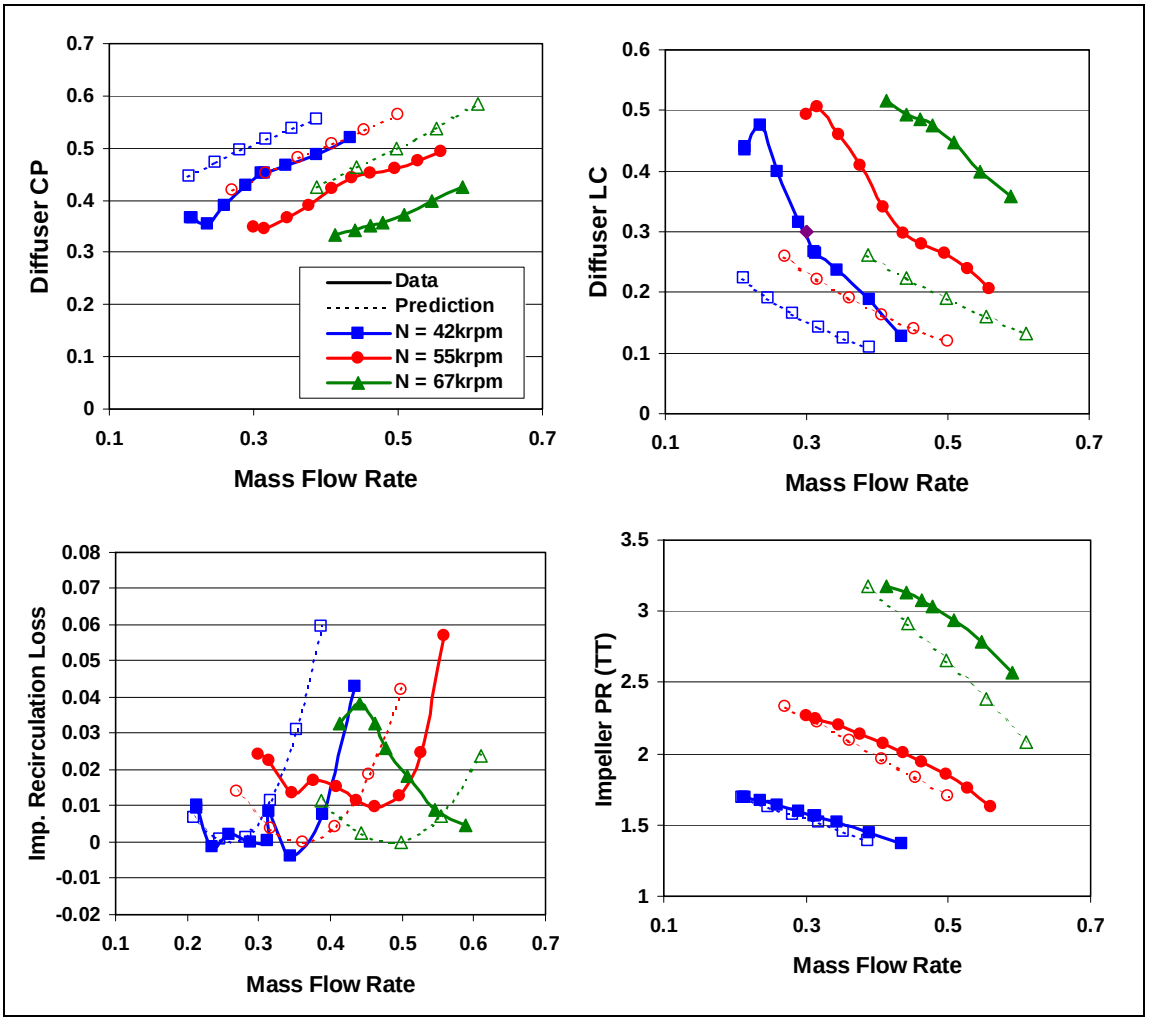

Figure 4-22: Additional performance calculations for a radial compressor case that was not included in original database

The Enhanced TEIS models were also run on this case to evaluate their performance, in comparison to the new models. The Enhanced TEIS models produced a prediction that under-estimated the design point efficiency by more than 20%, and the pressure ratio by 30%. This compares to an error from the new models of 5% and 4% for the stage efficiency and pressure ratio, respectively. In this case, the new models are a significant improvement over the Enhanced TEIS model and produce a much more accurate estimate of the stage performance.

The results of the initial validation effort confirmed two important facts about the models. First, it was shown that the system of equations can be solved simultaneously and will consistently converge to yield valid predictions of the model coefficients. This required that the variables in the individual models be sufficiently independent from each other that small changes in one would not result in large variations in another while converging to a solution. Second, it was shown that when applied together, the models can estimate the performance of a wide variety of machines, including some not included in the original dataset more accurately than with previous models. At this time only the combined models have been studied in detail, but the pump and compressor models should converge equally well since they rely primarily on the same variables.

5 Conclusions and Recommendations

5.1 Conclusions

Empirical models to predict the TEIS and Two-zone modeling parameters have been developed based on test data for a wide range of centrifugal pumps and compressors. The test data were provided by ConceptsNREC, and a large portion of the cases was both designed and tested by them. The test data were then reviewed and classified according to the type and quality of measurements collected. A weighting factor was associated with the different classifications. Regression models were developed using the weighting factor so that matching the performance of the high quality data, where there is less uncertainty, was given higher priority. For the TEIS parameters, η_a and η_b, the new models are 30% and 70%, respectively, more accurate than the current state-of-the-art models, as detailed in Table 4-5. One enhancement that allowed improvement on current state-of-the-art predictions was to allow the TEIS modeling parameters to vary with individual speedlines. This greatly improved the quality of match for off-design compressor speedlines.

Several contributions were also made to improve the modeling of the Two-Zone parameters. First, it was recognized that unique values of χ and δ_{2p} could not be identified using only static pressure data. The actual values of χ and δ_{2p} can only be

determined based on impeller exit traverse data. From the traverse data, both BIP and off-BIP values of the two-zone parameters were identified. For the first time, data were available showing how χ and δ_{2p} vary at off-design conditions. Based on this data, models were developed to account for the off-BIP variation in χ and δ_{2p}. Modeling the off-BIP variation allows the losses in the impeller passage to be more accurately defined, instead of simply assuming all the additional off-BIP losses were due to recirculation.

Based on the results of the off-BIP χ and δ_{2p} correlations, a model was developed to define the impeller recirculation loss bucket. Until now the impeller recirculation loss was estimated using a default bucket profile that was applied to all cases. The impeller recirculation loss models predict a bucket shape that is dependent on the specific geometry and flow of the machine being analyzed. A model was also developed to identify the flow rate, or incidence, where the losses are a minimum. Accurately predicting this point of minimal losses allows the point of peak rotor and stage efficiency to be correctly estimated.

Finally, an improved model was developed to predict the skin friction in the vaneless diffuser. This model was developed based on the results of detailed diffuser measurements that were matched in the meanline code using an advanced time-cyclic calculation. The time cyclic model can accurately calculate the properties in a vaneless diffuser in the entry region where the flow is not mixed. With this model, and the new c_f correlation, good prediction of any length vaneless diffuser can be made.

The combined set of models developed by this project specify all of the modeling parameters necessary to predict the performance of an impeller and can be applied to a wide range of cases. The current state-of-the-art models still require several parameters

to be defined by the user and are applicable to such a small range of cases that they cannot be effectively used in engineering design.

5.2 Recommendations

All of the models developed for use in predicting stage performance exceeded the accuracy of the state-of-the-art models with the exception of χ*–BIP*. To improve the accuracy of this prediction even further, a wider base of cases should be collected to base the regression model on. This should include primarily traverse data so that the Two-Zone parameters can be accurately modeled. It would also be desirable to include cases where the measured χ value is large. Most of the traverse cases available currently have χ values in the range of 0.2. Low specific speed cases with traverse data may indicate higher values and give greater range to the database.

This work has laid the foundation for additional work in applying the TEIS and Two-Zone models to other vaned elements. Some preliminary work was done at ConceptsNREC to explore the application of the TEIS and Two-Zone models to various diffuser vanes. This was further explored in another thesis project conducted in parallel with this study by Bitter at Brigham Young University (BYU) [28]. This work approached processing the data and modeling various diffuser vanes in a similar manner to that presented in this thesis. The conclusion of this work also produced complex mathematical models to predict, η_a, η_b, χ and δ_{2p} based on geometric and flow variables to represent the flow in the diffusers. To simplify the task of modeling the diffuser, the performance of the rotor was assumed to be fixed at a level deduced from vaneless

diffuser tests. The merits of Bitter's work cannot be fully realized until further work is done to account for impeller-diffuser interactions.

It would also be valuable to further examine the physical phenomena that govern the structure of the models used to predict the TEIS and Two-Zone modeling parameters. A continued effort should be made to add additional cases to the data and further validate the existing models and improve them if necessary. The most valuable test data to collect would be traverse data that can be used to deduce all of the relevant modeling parameters.

6 References

1 Japikse, D., 1996, *Centrifugal Compressor Design and Performance*, Concepts ETI, Inc., Wilder, VT, USA.

2 Japikse, D., 2001, "Enhanced TEIS and Secondary Flow Modeling for Diverse Compressors," TM 810, ConceptsNREC, Wilder, VT.

3 Whitfield, A., Baines, N. C., *Design of Radial Turbomachines,* Longman Scientific & Technical, John Wiley & Sons, Inc., New York.

4 Dixon, S.L., 1998, *Fluid Mechanics and Thermodynamics of Turbomachinery*, *Fourth Ed.*, Butterworth-Heinemann, Boston.

5 Japikse D, Baines N. C., 1994, *Introduction to Turbomachinery,* Concepts ETI, Inc., Norwich, VT, and Oxford University Press, Oxford, England.

6 Rodgers, C., 1980, "Efficiency of Centrifugal Compressor Impellers," AGARD Conference Proceedings. No. 282, Centrifugal Compressors, Flow Phenomena and Performance, Brussels, May 7-9, pp. 22-1 – 22-14.

7 Eckardt, D., 1975, "Instantaneous Measurements in the Jet-Wake Discharge Flow of a Centrifugal Compressor Impeller," Journal of Engineering for Power. pp. 337-345.

8 Dean, R. C., Senoo, Y., 1960, "Rotating Wakes in Vaneless Diffusers," Journal of Basic Engineering. pp. 563-574.

9 Johnson, M. W., Moore, J., 1980, "The Development of Wake Flow in a Centrifugal Impeller," Trans. ASME Journal of Engineering for Power. **102**: 382-390.

10 Japikse, D., 1985, "Assessment of Single- and Two-Zone Modeling of Centrifugal Compressors, Studies in Component Performance: Part 3," ASME Paper No. 85-GT-73.

11 Wiesner, F. J., 1967, "A Review of Slip Factors for Centrifugal Impellers," Trans. ASME, Journal of Engineering for Power. pp. 558-572.

12 Dean, R. C., 1972, "The Fluid Dynamic Design of Advanced Centrifugal Compressors," Creare, Technical Note 153.

13 Frigne, P., van den Braembussche, R., June 1978, "One-Dimensional Design of Performance Maps for Centrifugal Compressors Taking into Account Flow Separation in the Impeller," Von Karman Institute for Fluid Dynamics, Turbomachinery Department, Technical Note 129.

14 Japikse, D., 1984, *Turbomachinery Diffuser Design Technology*, Concepts ETI, Inc., Wilder VT, USA.

15 Japikse, D., 2003, Personal Communication, March 7.

16 Japikse, D., Oliphant, K., Pelton, R., 2004, "Optimization in Turbomachinery Data Reduction," ISROMAC-10, Honolulu, Hawaii.

17 Compal, 2007, Concepts ETI.

18 Daily, J. W., Nece, R. E., 1960, "Chamber Dimension Effects on Induced Flow and Frictional Resistance of Enclosed Rotating Disks," Trans ASME Journal of Basic Engineering. **82**, pp. 217-232.

19 Stanitz, J. D., 1952, "One-Dimensional Compressible Flow in Vaneless Diffusers of Radial or Mixed-Flow Centrifugal Compressors, Including the Effects of Friction, Heat Transfer and Area Change." NACA Technical Note 2610.

20 Traupel, W., 1977, *Thermische Turbomaschinen*, Springer-Verlag, Volumes I and II.

21 Dean, R. C., Jr., and Senoo, Y., 1960, "Rotating Wakes in Vaneless Diffusers," Journal of Basic Engineering, pp. 563-570.

22 Dubitsky, O., Japikse, D., 2005, "Vaneless Diffuser Advanced Model," ASME Paper No. GT-2005-68130.

23 Montgomery, D.C., Runger, G.C., Hubele, N.F., 1998, *Engineering Statistics*, John Wiley & Sons, Inc., New York.

24 Eckardt, D., Trultzsch, K.-J., Weimann, W., 1977, "Radialverdichter: Vergleichende Stromungsuntersuchungen an drei Radialverdichter-Laufradern mit konventionellen Messverfahren," Forschungsberichte Verbrennungskraftmaschinen, Heft 237, Vorhaben Nr. 182. In GERMAN

25 Eckardt, D., 1977, "Untersuchung der Laufradstromung in hochbelasteten Radialverdichterstufen Rad A, beta2s = 60 degrees.," Forschungsberichte Verbrennungskraftmaschinen, No. 227. In GERMAN

26 Eckardt, D., 1978, "Untersuchung der Laufradstromung in hochbelasteten Radialverdichterstufen Rad B, beta2s = 50 degrees," Forschungsberichte Verbrennungskraftmaschinen No. 243. In GERMAN

27 Koza, J.R., 1992, *Genetic Programming: On the programming of Computers by Means of Natural Selection*, MIT Press, Cambridge, MA.

28 Bitter, J., 2007, "One-Dimensional Modeling of Centrifugal Flow Vaned Diffusers, MS Thesis," Brigham Young University, Provo, UT.